Addressing Beyond Standard Model physics using cosmology

Akshay Ghalsasi

A dissertation
submitted in partial fulfillment of the
requirements for the degree of

Doctor of Philosophy

University of Washington

2017

Reading Committee:

Ann Nelson, Chair

Andreas Karch

Matt McQuinn

Program Authorized to Offer Degree:
Physics

•

University of Washington

Abstract

Addressing Beyond Standard Model physics using cosmology

Akshay Ghalsasi

Chair of the Supervisory Committee:
Professor Ann Nelson
Physics

We have consensus models for both particle physics (i.e. standard model) and cosmology (i.e. ΛCDM). Given certain assumptions about the initial conditions of the universe, the marriage of the standard model (SM) of particle physics and ΛCDM cosmology has been phenomenally successful in describing the universe we live in. However it is quite clear that all is not well. The three biggest problems that the SM faces today are baryogenesis, dark matter and dark energy. These problems, along with the problem of neutrino masses, indicate the existence of physics beyond SM. Evidence of baryogenesis, dark matter and dark energy all comes from astrophysical and cosmological observations. Cosmology also provides the best (model dependent) constraints on neutrino masses. In this thesis I will try address the following problems **1)**Addressing the origin of dark energy (DE) using non-standard neutrino cosmology and exploring the effects of the non-standard neutrino cosmology on terrestrial and cosmological experiments. **2)** Addressing the matter anti-matter asymmetry of the universe.

TABLE OF CONTENTS

LIST OF FIGURES

LIST OF TABLES

ACKNOWLEDGMENTS

First I would like to thank my advisor Ann Nelson for giving me a chance. She was always open to listening to my often non-sensical ideas and patiently explain why they couldn't work. She always answered all of my questions although I cant claim to have understood all the answers. Most of my knowledge of phenomenology and cosmology and indeed this thesis is due to her.

I would also like to thank Matt McQuinn for working with me and being patient even when I was unproductive. He was always available to talk to and answer questions. Most of my astronomy and astrophysics knowledge is due to him.

I would also like to thank the particle theory group as a whole. It is doubtless the most easy going and supportive set of people I have come across. I would like to thank the professors of the group for teaching me particle physics both in classes and by guiding me for my journal club talks. I would like to the postdocs especially David Mckeen for being a great collaborator and always patiently explaining things to me. Most of my projects would have taken a lot longer had it not been for his work and guidance. I would like to thank my fellow grad students Bridget Bertoni and Seyda Ipek for being supportive and Derek Horkel and Christoph Uhlemann for the fun times.

These six years would have been a lot harder had it not been for my group of friends. The merry nights at college inn, the great conversations and the road trips will always be remembered. I would also like to thank my roommate Oliver for countless stimulating conversations about politics, philosophy, physics and technology.

Finally and most importantly I would like to thank my parents. Without their sacrifice and inspiration none of this would have been possible.

DEDICATION

to my parents

Chapter 1

INTRODUCTION

1.1 Standard Model of Particle Physics

All of the known observable matter in the universe is comprised of quarks, leptons and their bound states. The quarks and leptons (the fermions) interact via the strong, the weak and the electromagnetic force (the gauge bosons) whose force carriers are the gluons, the W and Z bosons and photons respectively. The Higgs boson is responsible for the mass of quarks and leptons. The Standard Model (SM) of particle physics is a consistent quantum field theory that includes the fermions, the gauge bosons, the higgs boson and their interactions.

SM of particle physics was 'born' in 1897 with the discovery of electron by J.J.Thompson. In 1905 Einstein proposed that the electromagnetic fields were not classical waves as suggested by Maxwell's theory of electromagnetism but were in fact quantized. The quantization of light was conclusively proven by Compton in 1923, thus discovering the photon. The neutrino was first postulated by Pauli in 1930 to explain the broad distribution of electron energies in beta decays. It was directly observed in mid 1950's. In 1936 cosmic ray experiments to search for the Yukawa's meson (pion) discovered the muon (the heavier partner of electron). In 1964 Gell-Mann and Zweig independently proposed the quark model to classify the all the hadrons (baryons and mesons) as 'colorless' bound states of quarks carrying 'color charge'. In 1974 the fourth flavor of quarks (the charmed quark) was discovered after discovering the J/ψ meson which is a bound state of charm anti-charm quarks. Most of the other heavier hadrons comprised of the charm and bottom quarks as well as the tau lepton and its associated neutrino were discovered in the later part of the 1970's. The top quark which is extremely heavy compared to other quarks wasn't discovered until 1995. The W and Z bosons which were postulated by the electroweak theory of Glashow-Salam-Weinberg

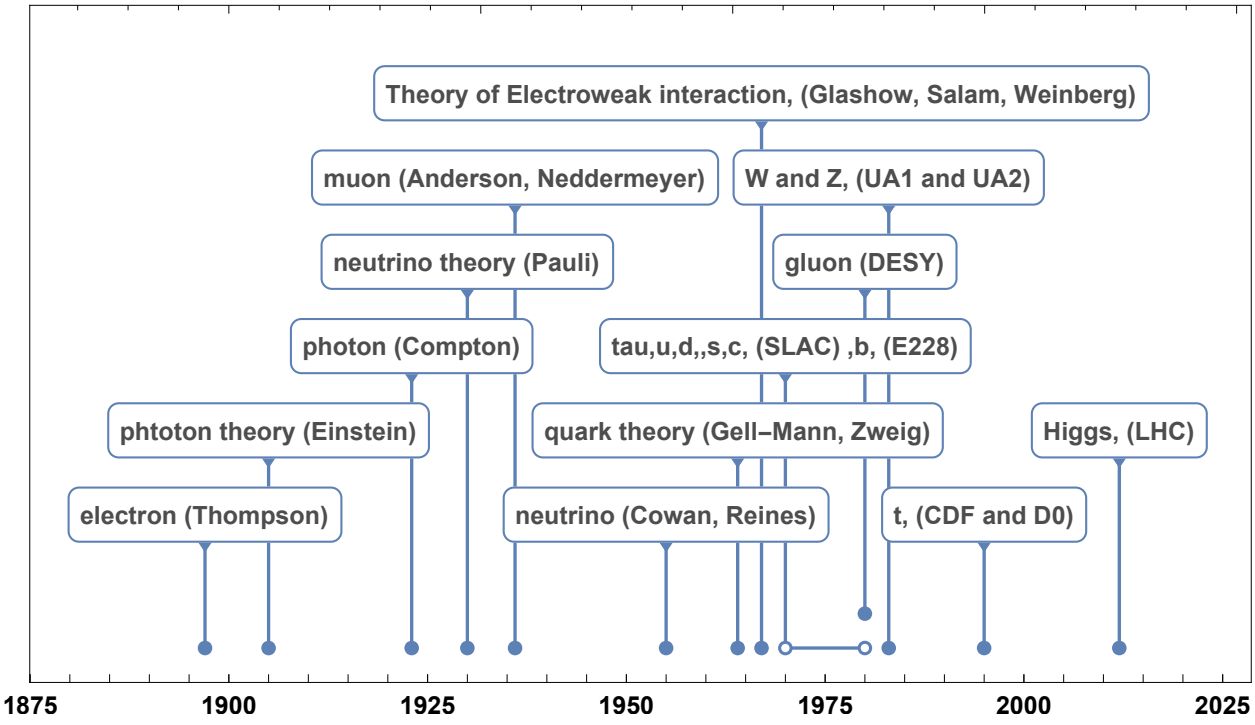

Figure 1.1: Standard Model history

were discovered in 1983. The discovery of the Higgs boson at the Large Hadron Collider at CERN in 2012 finally completed the SM of particle physics. The time-line of the history of the Standard Model is represented in Fig. 1.1. For an entertaining history of the SM see [1].

The SM provides a description for most of the phenomenon we observe and hence understanding it is the first stepping stone towards understanding the universe. The SM also provides a framework using which we can model beyond Standard Model (BSM) physics. In the following section we will briefly detail the SM and its interactions. For more details the curious readers should consult [2].

SM Interactions

The quarks in the SM participate in the strong and electroweak interactions, whereas the leptons and the higgs boson only participate only in the electroweak interactions. The

following Table 1.1 gives the SM fermions and the gauge interactions they are charged under . The SM Lagrangian is invariant under the gauge group $SU(3)_c \times SU(2)_L \times U(1)_Y$. The $SU(3)_c$ gauge group is responsible for strong interactions while $SU(2)_L \times U(1)_Y$ is responsible for electroweak interactions. Since all the fermions in SM interact with the electroweak gauge bosons, and all except the neutrino interact with the Higgs boson we will first start by talking about the electroweak gauge and Higgs sector.

Field \ Gauge	$SU(3)_c$	$SU(2)_L$	$U(1)_Y$
$\mathrm{Q} = \begin{pmatrix} u \\ d \end{pmatrix}$	3	2	1/6
U	$\bar{3}$	2	-2/3
D	$\bar{3}$	2	1/3
$\mathrm{L} = \begin{pmatrix} \nu \\ e \end{pmatrix}$	1	2	-1/2
E	1	1	1
G^{α}_{μ}	8	1	0
W^{α}_{μ}	1	3	0
B_{μ}	1	1	0
$\phi = \begin{pmatrix} H + v \\ \phi^{+} \end{pmatrix}$	1	2	-1/2

Table 1.1: The SM fields and their gauge charges under $SU(3) \times SU(2) \times U(1)$ gauge group.

- **Electroweak gauge and Higgs Sector**

Let us consider a scalar Higgs field Φ which transforms as (1,2,-$\frac{1}{2}$) under the SM gauge group, i.e. it is a singlet under SU(3) transformations, a doublet under SU(2) transformations and carries a U(1) charge of $-1/2$. The corresponding Lagrangian is given by

$$\mathcal{L} \;=\; -\frac{1}{2}\left(D_\mu\Phi\right)^\dagger\left(D_\mu\Phi\right) \;+\; \frac{1}{4}\lambda\left(\Phi^\dagger\Phi - \frac{1}{2}v^2\right)^2 \;-\; \frac{1}{4}F^{a\mu\nu}F^a_{\mu\nu} \;-\; \frac{1}{4}B^{\mu\nu}B_{\mu\nu} \tag{1.1}$$

where $D_\mu = \partial_\mu - i\left[g_2 A^a_\mu T^a + g_1 B_\mu Y\right]$ is the gauge covariant derivative with A^a_μ being the SU(2) gauge fields and B_μ being the U(1) gauge field. The $F^{a\mu\nu}F^a_{\mu\nu}$ and $B^{\mu\nu}B_{\mu\nu}$ terms are kinetic terms for the gauge fields and $\frac{1}{4}\lambda\left(\Phi^\dagger\Phi - \frac{1}{2}v^2\right)^2$ is the Higgs potential $V(\Phi)$.

It is clear from the Higgs potential that the Higgs boson has a minimum at $|\Phi| = \frac{1}{\sqrt{2}}v$. Thus the Higgs field gets a vacuum expectation value (vev) which we can chose to be

$$\Phi(x) \;=\; \frac{1}{\sqrt{2}}\begin{pmatrix} v + H(x) \\ 0 \end{pmatrix} \tag{1.2}$$

where H is what we call the Higgs boson i.e. the perturbations of the Higgs field around its vev. Plugging in the expectation value for the Higgs field into the kinetic term for the Higgs field we generate a mass term for our gauge fields given by

$$\mathcal{L}_m \;=\; -\frac{v^2}{8}\begin{pmatrix} 1, 0 \end{pmatrix}\begin{pmatrix} g_2A^3_\mu - g_1B_\mu & g_2(A^1_\mu - iA^2_\mu) \\ g_2(A^1_\mu + iA^2_\mu) & g_2A^3_\mu - g_1B_\mu \end{pmatrix}^2\begin{pmatrix} 1 \\ 0 \end{pmatrix} \tag{1.3}$$

We can then redefine the gauge fields such that $W^\pm_\mu = \frac{1}{\sqrt{2}}\left(A^1_\mu \mp iA^2_\mu\right)$, $Z_\mu = cos(\theta_w)A^3_\mu - sin(\theta_w)B_\mu$ and $A_\mu = cos(\theta_w)A^3_\mu + sin(\theta_w)B_\mu$. Here $\theta_w = tan^{-1}(g1/g2)$ is the weak mixing angle. Plugging the redefined fields in 1.3 and expanding we get that

$$\mathcal{L}_m = -M^2_W W^{+\mu}W^-_\mu - \frac{1}{2}M^2_Z Z^\mu Z_\mu \tag{1.4}$$

Thus by choosing a vev the Higgs field undergoes a spontaneous symmetry breaking (SSB) [1] which breaks the $SU(2)_L \times U(1)_Y$ gauge symmetry to $U(1)_{em}$ (electromagnetic)

[1] Its called SSB because the Lagrangian is still invariant under the original $SU(2)_L \times U(1)_Y$ symmetry but the physics is no longer symmetric since the Higgs boson chose a vev.

gauge symmetry.

The $W^{\pm}$ are the W bosons and have a mass of $M_W = g_2 v/2$ and Z^{μ} is the Z boson with mass $M_Z/cos(\theta_w)$. A^{μ} is the photon and is the massless gauge boson of the remnant $U(1)_{em}$ symmetry.

There are other contributions to the symmetry-broken Lagrangian that can be derived by expanding the higgs potential and the redefinition of the kinetic gauge boson terms in the Lagrangian. We will however skip that derivation and interested readers can consult [2]. Next we move to leptons which only experience electroweak interactions.

- **Lepton Sector**

  The SM leptons are fermions which are charged under electroweak interactions but are singlets under $SU(3)_c$ color charge. There are three generations of leptons, the electron, muon and tau and their corresponding neutrinos. The SM fermions can be described by considering two left handed Weyl fermion fields L and E, where L is a $SU(2)_L$ doublet and carries SM gauge charge (1,2,-$\frac{1}{2}$) and E is a SU(2) singlet with SM gauge charge (1,1,-1). The lepton (for a single flavor) Lagrangian is then given by

$$\mathcal{L} = iL^{\dagger j}\bar{\sigma_{\mu}}\left(D_{\mu}L\right)_j + iE^{\dagger}\bar{\sigma_{\mu}}\left(D_{\mu}E\right) - y\epsilon^{ij}\Phi_i L_j E - \left(y\epsilon^{ij}\Phi_i L_j E\right)^{\dagger} \tag{1.5}$$

  where D_{μ} is the appropriate gauge covariant derivative depending on the gauge symmetry each lepton field is charged under, y is the Yukawa coupling that couples the fermion fields to the Higgs field and ϵ^{ij} is the Levi-Civita symbol where the index refer to the component of the doublet fields. Note that the Lagrangian is gauge invariant.

  The lepton doublet L is given by

$$L = \frac{1}{\sqrt{2}} \begin{pmatrix} \nu \\ e \end{pmatrix} \tag{1.6}$$

  where ν is the Weyl neutrino field and e corresponds to the the Weyl electron field. After the higgs boson undergoes SSB and picks up a vev (Eq. 1.2) we get mass term for

the electrons from the Yukawa terms in the lepton Lagrangian given by Eq. 1.5. The mass term is given by $yveE$. Since there is no corresponding right handed neutrino field ($SU(2)_L$ singlet) in the SM, the neutrinos in SM are massless.

Expanding the kinetic terms in the Lagrangian 1.5 and redefining them in terms of W bosons, Z boson and the photon, we get that the electrons couple to all the gauge bosons while the neutrinos only couple to the W and Z bosons. The coupling with the photon is given by the electric charge whose generator is defined as $\mathcal{Q} = T_3 + Y$ where $T_3 = \frac{\sigma_3}{2}$ is a generator of the $SU(2)_L$ gauge group and Y is the hypercharge. Taking the neutrino as an example $T_3|\nu\rangle = \frac{1}{2}|\nu\rangle$ since it is the upper component of the doublet L. The hypercharge of neutrinos is the same as the hypercharge for L i.e. $-\frac{1}{2}$. Thus $\mathcal{Q}|\nu\rangle = 0$ and hence neutrinos carry no electric charge and don't interact with photons. Electrons on the other hand carry charge $\mathcal{Q}|e\rangle = -1$ and have electromagnetic interactions. For details consult [2]

- **Quark Sector**

  The quark sector is phenomenologically the richest sector in the SM. SM quarks can be described by introducing three Weyl fields, Q,U,D having gauge charges (3,2,$\frac{1}{6}$), ($\bar{3}$,1,-$\frac{2}{3}$) and ($\bar{3}$,1,$\frac{1}{3}$) respectively. Note that the quark fields unlike leptons transform under the fundamental representation of $SU(3)_c$. There are three generations of quarks, however for illustrative purposes we will start with one generation. The Lagrangian for quarks is given by

$$\mathcal{L} = iQ^{\dagger\alpha i}\bar{\sigma_\mu}\left(D_\mu Q\right)_{\alpha i} + iU^{\dagger\alpha}\bar{\sigma_\mu}\left(D_\mu U\right)_\alpha + iD^{\dagger\alpha}\bar{\sigma_\mu}\left(D_\mu D\right)_\alpha \tag{1.7}$$

$$- \left(y^{'}\epsilon^{ij}\Phi_i Q_{\alpha j} D^\alpha + h.c.\right) - \left(y^{''}\Phi_i^\dagger Q_{\alpha i} U^\alpha + h.c.\right) \tag{1.8}$$

$$- \frac{1}{4}G^{a\mu\nu}G^a_{\mu\nu} - \frac{g^2\theta}{32\pi^2}\tilde{G}^{a\mu\nu}G^a_{\mu\nu} \tag{1.9}$$

  where D_μ are the appropriate covariant derivatives, α are the color indices. The $G^{a\mu\nu}G^a_{\mu\nu}$ are the gluon kinetic terms and $\tilde{G}^{a\mu\nu}G^a_{\mu\nu}$ is the CP violating part of the QCD Lagrangian. The Lagrangian above is gauge invariant.

Since Q is a SU(2) doublet we can write it as $Q = \frac{1}{\sqrt{2}} \begin{pmatrix} u \\ d \end{pmatrix}$. Applying the charge operator $\mathcal{Q} = T_3 + Y$ on the up(down) type quark fields (u,U)(d,D) gives us a charge magnitude of $\frac{2}{3}(\frac{1}{3})$. After the Higgs fields gets a vev, the quarks get their masses from the Yukawa terms in the Lagrangian. Adding the flavor indices back we get the quark masses to be

$$\mathcal{L}_m = -\frac{v}{\sqrt{2}} d_{\alpha I} y^{'}_{IJ} D^{\alpha}_{J} \; - \; \frac{v}{\sqrt{2}} u_{\alpha I} y^{''}_{IJ} U^{\alpha}_{J} + h.c. \tag{1.10}$$

where (I,J) = 1,2,3 are generation indices. Note that the Yukawa couplings don't have to be diagonal. In order to define quarks in their mass basis we can redefine our quark fields by making unitary transformations on the quarks in the generation space given by $d_I = \mathcal{D}_{IJ} d_J$, $D_I = \bar{\mathcal{D}}_{IJ} D_J$, $u_I = \mathcal{U}_{IJ} u_J$ and $U_I = \bar{\mathcal{U}}_{IJ} U_J$ where $\mathcal{D}, \bar{\mathcal{D}}, \mathcal{U}, \bar{\mathcal{U}}$ are unitary matrices. This transforms the Yukawa couplings $y^{'} \rightarrow \mathcal{D}^T y^{'} \bar{\mathcal{D}}$ and $y^{''} \rightarrow \mathcal{U}^T y^{''} \bar{\mathcal{U}}$. There is enough freedom in the unitary transformations to diagonalize the Yukawa couplings and make their entries real thus defining a mass basis for the quarks.

The unitary transformations mentioned above leave all the kinetic terms in the Lagrangian unchanged except for the kinetic terms that couple up type quarks to down type quarks, i.e. the kinetic terms involving the charged current interactions of quarks with the $W^{\pm}$ bosons. As an example consider the kinetic term $u^{\dagger \alpha I} \bar{\sigma}^{\mu} W^{+\mu} d_{\alpha I}$ which comes from expanding the first kinetic term in the Lagrangian given by Eq. 1.7. After the unitary transformations of the quark fields described above the transformed term becomes $u^{\dagger \alpha I} \bar{\sigma}^{\mu} W^{+\mu} V_{IJ} d_{\alpha J}$ where $V = \mathcal{U}^{\dagger} \mathcal{D}$ is a general 3×3 unitary matrix. A complex unitary matrix can be defined by nine real parameters. We can use the generational phase rotations, $\mathcal{D}_I = e^{i\alpha_I} D_I$ and $\mathcal{U}_I = e^{i\beta_I} U_I$, which do not affect the mass or other gauge coupling terms to get rid of five of the nine parameters, making the first row and column of the 3×3 unitary matrix real. The remaining four parameters can be parameterized by rotation angles $\theta_{1,2,3}$ and a complex phase δ_i. Thus V which

is also known as the Cabibo-Kobayasi-Maskawa (CKM) matrix can be written as

$$V = \begin{pmatrix} c_1 & s_1c_3 & s_1s_3 \\ -s_1c_2 & c_1c_2c_3 - s_2s_3e^{i\delta} & c_1c_2s_3 + s_2c_3e^{i\delta} \\ -s_1s_2 & c_1s_2c_3 + c_2s_3e^{i\delta} & c_1s_2s_3 - c_2c_3e^{i\delta} \end{pmatrix} \tag{1.11}$$

where $c_i(s_i) = cos(\theta_i)\,(sin(\theta_i))$

The presence of complex phase indicates that charged weak interactions violate CP symmetry. The CP violation is experimentally observed in Kaon and B meson oscillation and decay. For details consult [1].

So far we have only talked about the electroweak interactions in SM. However quarks also have strong interactions which makes the quark sector phenomenologically very rich. Asymptotic freedom of the $SU(3)_c$ gauge interactions implies that free quarks cannot exist at low energies. Quarks instead bind to form colorless mesons or hadrons. We will not delve further into the strong interactions aspect of quarks. Interested readers should refer to any modern field theory textbook for further information.

1.2 Problems with SM

The SM of particle physics is a consistent quantum field theory which has been phenomenally successful in describing most of the observations in terrestrial experiments. An example of the success of the SM can be illustrated by calculating the corrections to the fine structure constant α to 1 part in 10^8[3]. However it does have empirical and philosophical problems when it come to explaining some terrestrial, astrophysical and cosmological observations. Here we enumerate the problems with SM.

1. **Massive Neutrinos** As we saw in the previous section, neutrinos in SM are massless. However atmospheric and solar neutrino oscillation experiments indicate that the neutrinos must have masses with the atmospheric mass splitting $\Delta m^2_{atm} \approx 10^{-4}\,\mathrm{eV}^2$ and

a solar mass splitting of $\Delta m^2_\odot \approx 10^{-3}\,\mathrm{eV}^2$. Assuming the lightest neutrino is massless and assuming a normal hierarchy this puts a lower bound on the sum of neutrino masses $\Sigma\, m_\nu \geq 0.04\,\mathrm{eV}$. Current terrestrial bounds on neutrino masses are $m_{\nu,e} \leq 2\,\mathrm{eV}$ while cosmological bounds assuming standard neutrino cosmology are $\Sigma\, m_\nu \leq 0.3\,\mathrm{eV}$. Later in this thesis we will explore non-standard neutrino cosmology in Chapters 2 and 3 which can evade cosmological bounds.

The standard way of giving SM neutrinos mass is introducing a sterile neutrino (N) with gauge charges (1,1,0) i.e. it does not interact with any gauge bosons. We can then write the neutrino mass terms as $\left(y\Phi^{\dagger i} L_i N + h.c.\right) + m_N NN$ where the first term is the standard yukawa mass term, while the second term is a majorana mass term for sterile neutrinos. The neutrino mass matrix then becomes

$$M = \begin{pmatrix} 0 & m_D \\ m_D & m_N \end{pmatrix} \tag{1.12}$$

where the Dirac mass $m_D = yv$ after the Higgs boson acquires a vev. Assuming $m_N \gg m_D$ and diagonalizing the mass matrix we get that the mass of the mostly active neutrino is $m_\nu \approx \frac{m_D^2}{m_N}$ and the mass of the mostly sterile neutrino is $\approx m_N$. This mechanism for neutrino masses is known as the see-saw mechanism, since as the sterile neutrino becomes heavier the active neutrino becomes lighter and vice-versa.

2. **Dark Matter** Dark matter (DM) makes up 26% of the energy density of universe today and has been observed only through its gravitational interactions. It is not known to have any SM interactions, hence the name dark matter. It was postulated that heavy neutrinos could act as hot dark matter. However observations of cosmic microwave background and structure in the universe rule that out. Hence SM at present cannot explain DM and any explanation of DM has to be BSM. We briefly mention some of these in Sec. 1.3.1 and we will describe thermal WIMP DM and constraints on it in Sec. 1.3.2.

3. **Baryogenesis** There are more baryons in the universe than anti-baryons. The initial baryon asymmetry required to explain the present day baryon number density is approximately one part in a billion and the production of this asymmetry is known as baryogenesis. Sakharov conditions state that any model of baryogenesis must have i)CP violation ii)Baryon number violation and iii) Departure from thermal equilibrium.

   Initially it was thought that electroweak baryogenesis could occur in SM since the SM satisfies the first two Sakharov conditions. It has CP violation in the quark sector as we demonstrated in the previous section. Although the SM Lagrangian has no baryon number violation, non perturbative processes known as sphalerons do violate baryon and lepton number in SM. However since the Higgs potential and its thermal corrections are well understood and they do not show a first order phase transition there can be no baryogenesis in the SM itself.

   We will discuss popular model of baryogenesis in Sec. 1.3.2. We will also present a new model of baryogenesis in Ch.4.

4. **Dark Energy** Dark Energy constitutes about 69% of the energy density of the universe today. The easiest explanation for dark energy is a cosmological constant. We can do a naive calculation of the SM contribution [2] to the cosmological constant by considering the contribution to the zero point energy by a scalar field which is given by

$$\rho_{DE} = \frac{\Lambda^4}{16\pi^2} \tag{1.13}$$

   where Λ is the cut off of the theory. Choosing $\Lambda = M_{pl} \approx 10^{18}\,\text{GeV}$ we get $\rho_{DE} \approx 10^{107}\,\text{eV}^4$ which is about 120 orders of magnitude larger than than the observed value of $\rho_{DE} \approx 10^{-10}\ \text{eV}^4$. Thus the naive calculation in SM massively overestimates the the DE in the universe. We will discuss DE in more detail in Sec. 1.3.1. The MaVaNs models we discuss in Chapters 2 and 3 are also a models of DE.

5. **Inflation** In order to explain the flatness and horizon problems of the universe it is postulated the universe underwent a rapid exponential expansion at early times. The

most plausible paradigm of inflation is slow roll inflation in which a scalar field rolls slowly down an almost flat potential. However the only scalar field in the SM is the Higgs boson and the Higgs potential does not satisfy conditions needed for slow roll inflation. Hence inflation needs a BSM solution.

We will discuss inflation in more detail in Sec. 1.3.2.

6. **Strong CP problem**

   As mentioned in Eq. 1.7 the strong interactions violate CP unless $\theta = 0$. Since SM does not set the value of θ, we expect the SM to have CP violation. However trying to measure the amount of strong CP violation by measuring the neutron EDM moment [4] constrains $|\theta| < 2 \times 10^{-10}$.

   The most popular way to solve the strong CP problem is to promote the θ parameter to a field called axion. The axion is a pseudo goldstone boson of a broken Peccei-Quinn symmetry [5, 6, 7]. The axion dynamically relaxes to zero after chiral symmetry breaking. The axion solution is attractive because in addition to solving the strong CP problem it can act as DM. For axion cosmology review see [8].

7. **Gravity** Although the SM explains the strong and the electroweak forces it does not explain gravitational force and gravity is not emergent from SM.

8. **Flavor hierarchy** The mass (or equivalently Yukawa coupling) hierarchy for leptons exceed three order of magnitudes with electron mass, $m_e = 0.5\,\mathrm{MeV}$ and tau mass $m_\tau = 1.7\,\mathrm{GeV}$. The hierarchy in the quark sector is even more extreme with the up and down quark, $m_{u,d} \simeq \mathcal{O}\,\mathrm{MeV}$ and the top quark mass $m_t = 172\,\mathrm{GeV}$. SM does not explain the large spread of masses or the origins of the Yukawa couplings.

9. **Naturalness (Hierarchy Problem)** The largest mass scales in the SM are related to the weak scale of $\approx 100\,\mathrm{GeV}$. We know the SM should hold until energies of

$M_{pl} \approx 10^{18}\,\text{GeV}$ beyond which we need a fundamentally different theory. We expect there to be new particles between the weak and Planck scale in order to solve problems with baryogenesis, DM and inflation and we expect these particles to couple to SM and the Higgs boson. Radiative corrections from these couplings contribute to the Higgs mass at the scale proportional to the scale at which the new particles enter. The naturalness/hierarchy problem then is the question why are the weak and Planck scale so separated.

The most attractive solution to the hierarchy problem is supersymmetry (SUSY). If SUSY is exact each boson gets a fermion as their superpartner with the same mass. The fermionic and the bosonic contributions to the radiative corrections of the Higgs boson mass cancel exactly no matter the scale at which the new physics enter. However since SUSY is not an exact symmetry the corrections to the Higgs mass is proportional to the scale of SUSY breaking $m_H^2 \propto m_{SUSY}^2$. If m_{SUSY} is close enough to the weak scale i.e. $\mathcal{O}\,\text{TeV}$, there is no naturalness problem. Supersymmetry is a vast field and the interested reader should look at this excellent review [9].

Examples of other popular solutions to the Heirarchy problem are extra dimensions [10, 11, 12], composite Higgs [13] models and using dynamics in the early universe [14].

10. Other potential observational discrepancies

Although SM is phenomenally successful in describing observations, few anomalies exist. None of these anomalies exceed the 5σ 'gold standard' required to confirm new physics. We will mention the few credible anomalies that have been observed.

Short baseline neutrino oscillation experiments are consistent with a sterile neutrino with eV mass. See Chapter 2 for more.

Muon gyromagnetic ratio g_μ is measured to be larger than SM predictions [15].

1.3 Standard Model of Cosmology (ΛCDM)

As we saw in the previous section, the SM of particle physics is incomplete and most of its empirical shortcomings come from inconsistencies with cosmological and astrophysical observations. Any consistent beyond standard model (BSM) description of particle physics which addresses the shortcomings of the SM must confront cosmological observations and fit in a consistent cosmological history. Thus a good understanding of cosmological history is prerequisite in understanding the nature of reality. The ΛCDM model of cosmology provides a consistent framework within which we can verify and constrain our particle physics models. I will start by giving a brief overview of cosmology followed discussing the energy content of the universe. I will end with detailed discussion of the timeline of the universe.

In order to get a sense of scale of how big the observable universe is let us start with our solar system. The distance between earth and sun is about 5×10^{-6} parsec (pc). Our sun is one star out of 100 billion in our Milky Way galaxy which has a diameter of about 30 kpc. Our galaxy is just one within about 100 billion galaxies in the observable universe [2] which has a size of about 15.6 Gpc. The universe is also about 14.8 billion years old.

We know have a good understanding of how it all came to be and we will start by giving a brief account of the history of the universe. In the beginning our universe underwent a rapid exponential expansion in a process known as inflation. At the end of inflation, the energy density of the universe came to be dominated by radiation[3]. As the universe continued to expand (although no longer exponentially) and cool it developed an asymmetry between baryons and anti-baryons and formed a dark matter relic density. As the universe cooled to temperature below an MeV the protons and neutrons combined to form heavier elements (mostly Helium). Throughout this period the universe was a plasma of charged particles and photons. As the universe cooled further the dark matter began to collapse gravitationally to form deeper potential wells. As the baryons followed the dark matter into

[2] distance to the surface of last scattering

[3] Here radiation refers to all particles with a thermal description with T > m

the potential wells, their temperature and pressure increased and were pushed back out. This oscillatory behavior imprinted correlations of temperature in the baryon photon plasma. At temperatures of around an eV the universe became neutral after the electrons combined with the nuclei to form atoms. The photons in the plasma traveled unimpeded after that carrying the information of photon temperature correlations with them which can be observed today. As the universe cooled further the dark matter formed deeper wells into which the atoms collapsed, cooled and formed dense objects like galaxies, stars and eventually planets and life itself. We have included a schematic of the history of the universe in Fig. 1.2. We will discuss the constituents of the universe and its history in much greater detail in the following sections but we will start with some prerequisite definitions.

The universe is isotropic and homogeneous on large scales. Thus instead of using the full Einstein equations to describe the evolution of the metric of the universe we can boil them down to the Friedmann-Robertson-Walker (FRW) equations. The FRW metric is given by $ds^2 = -dt^2 + a^2(t)\,dx^2$. Here a is the scale factor of the universe i.e. it controls the size of the universe and is only a function of time. The FRW equation that we will be that governs the dynamics of the scale factor is given by

$$\left(\frac{\dot{a}}{a}\right)^2 = H^2 = \frac{8\pi\rho G}{3} \tag{1.14}$$

where ρ is the energy density of the universe and is a function of the scale factor and H is the Hubble expansion rate. In order to understand how the scale factor of the universe behaves through its history we need to understand the composition of the energy density of the universe. In the following section we will discuss the constituents of the energy density of the universe and the epochs in the cosmic history in detail.

1.3.1 Constituents of the energy density of the universe

The present day universe is made up of about 69 % DE, 26 % DM and 5 % baryons. Neutrinos and photons make up for the remaining 0.1 %. We only consider a flat universe i.e. there is no contribution to the energy density of the universe due to its curvature. For a flat universe

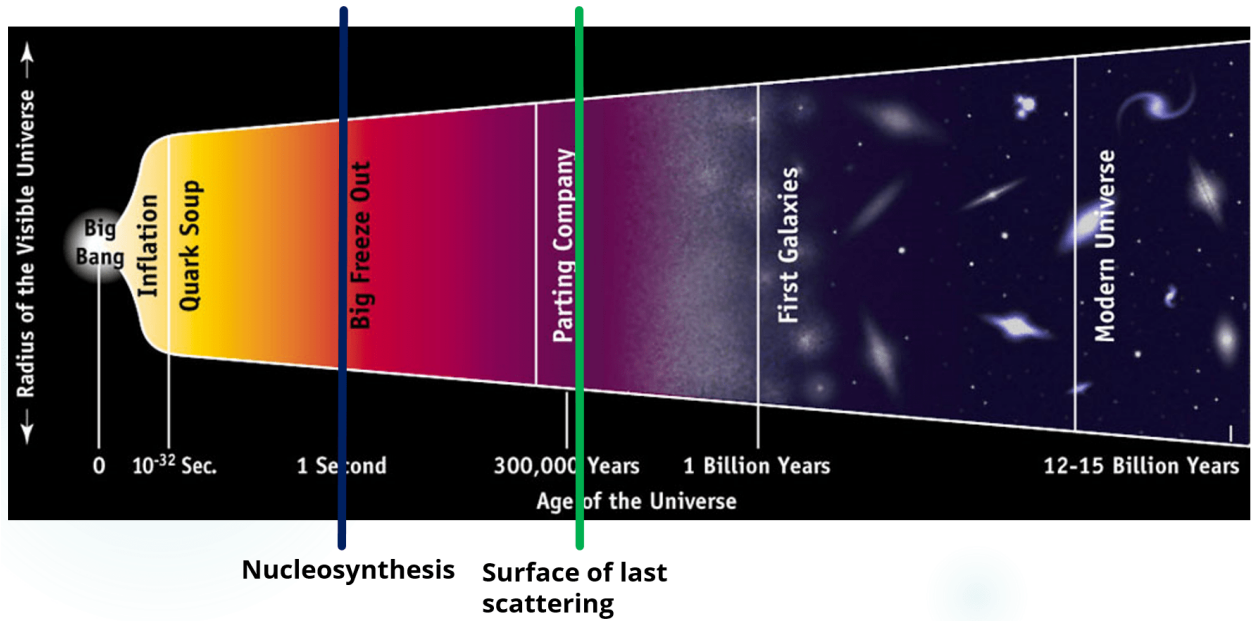

Figure 1.2: Timeline of the Universe.

$\sum_i \Omega_i = \frac{\rho_{i,0}}{\rho_c} = 1$[4], where $\rho_c = \frac{3H_0^2}{8\pi G}$ is the critical energy density of the universe. Even though the energy density of the universe is dominated by DM and DE today, it was dominated by photons and neutrinos earlier in the history of the universe. In Fig 1.3 we plot the relative energy density due to each component as a function of photon temperature (or equivalently redshift $1 + z = \frac{T_\gamma(a)}{T_\gamma(a_0)}$).

1. **Photons**

   In 1964 Penzias and Wilson discovered that the universe was bathed in a background bath of photons. Modern experiments confirm that these photons have an almost perfect black body spectrum with a temperature of $T_{\gamma,0} = 2.72K = 1.7 \times 10^{-4}$eV[16]. This is consistent with the fact that the photons were in thermal equilibrium with the baryons (mostly protons and electrons) until the temperatures became low enough to form hydrogen atom making the universe transparent to the photons. Since the

[4]The 0 subscript stands for present day values

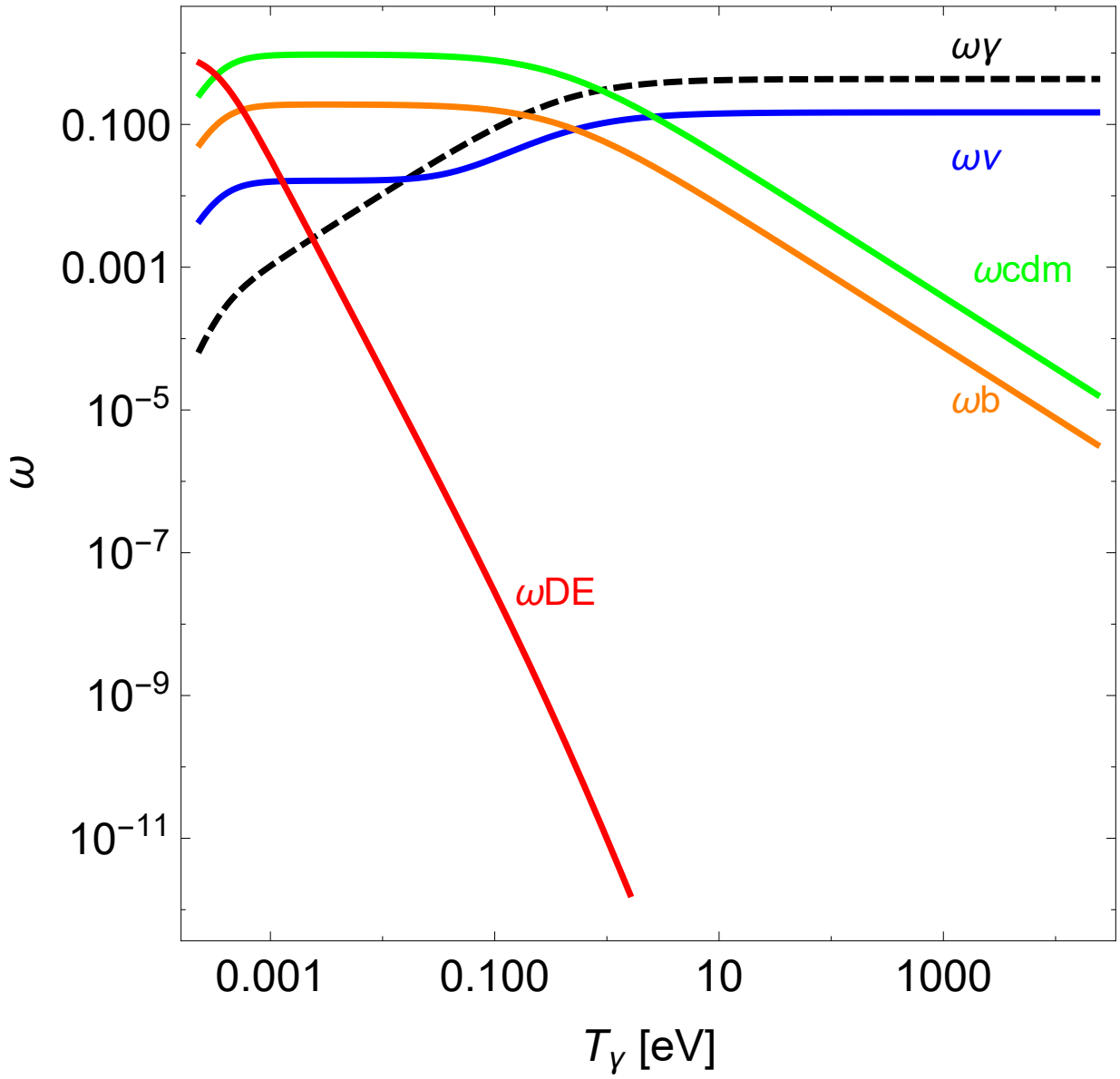

Figure 1.3: relative energy density, $\omega_i = \rho_i/\rho_{tot}$ of photons, neutrinos, baryons, DM and DE. As we can see the universe is DE dominated today but was matter dominated for 2×10^{-4}eV $\lessapprox$ T$_\gamma$ $\lessapprox$ 1eV and radiation dominated for $T_\gamma \gtrapprox$ 1eV.

photons have a perfect thermal distribution, $f_\gamma(p) = \frac{1}{e^{p/T}-1}$, we can calculate their energy density given by

$$\rho_\gamma = g_\gamma \int \frac{d^3p}{(2\pi)^3} \frac{p}{e^{p/T}-1} = \frac{\pi^2}{15} T_\gamma^4 \tag{1.15}$$

where $g_\gamma = 2$ counts the degrees of freedom (polarization states) of the photon. The photon maintains its thermal spectrum as the universe expands. Since the universe expands, the photon number density goes down as $\frac{1}{a^3}$. However energy of each photon also decreases since their wavelength gets stretched as $\frac{1}{a}$. Thus the energy density of photons is proportional to $\frac{1}{a^4}$ [5]. Comparing this to Eq. 1.15 we get that $T_\gamma \propto \frac{1}{a}$ i.e. as the universe expands the photons get cooler [6]. Hence we use the temperature of photons as a proxy for the scale factor.

Plugging $T_{\gamma,0}$ into Eq. 1.15 we get that $\rho_\gamma = 1.5 \times 10^{-16}\text{eV}^4$ which gives us $\Omega_\gamma = \frac{\rho_\gamma}{\rho_{cr}} = 6 \times 10^{-5}$. Even though photons make a tiny fraction of the energy density today it scales as $\frac{1}{a^4}$ and quickly dominates the energy density in the early universe above $T_\gamma \gtrapprox 1\text{eV}$.

2. **Neutrinos**

Neutrinos are extremely light and act as radiation through most of the cosmic history. At extremely high temperatures $T >$ MeV the weak interactions through which neutrinos are created and annihilated are rapid i.e. $\Gamma_{weak} > H$ and keep the neutrinos in thermal equilibrium with the photon and baryon plasma. As the universe temperature drops below an MeV the weak interactions become slower than the Hubble expansion rate and the neutrinos fall out of thermal equilibrium. Hence by the time electrons and positrons annihilate the electrons are already out of thermal equilibrium, and the annihilations only end up heating the photons and not the neutrinos. Thus even though the neutrinos today have a thermal distribution, they are colder than the photons. The

[5] for a more rigorous derivation see [17]

[6] This is only valid when there is no entropy production

ratio of neutrino and photon temperature is given by $\frac{T_\nu}{T_\gamma} = \left(\frac{4}{11}\right)^{1/3}$. Analogous to the photons we can use the fact that $f_\nu = \frac{1}{e^{p/T_\nu}+1}$ we can calculate the number density of neutrinos as a function of neutrino temperature

$$n_\nu = g_\nu \int \frac{d^3p}{(2\pi)^3} \frac{1}{e^{p/T_\nu}+1} = g_\nu \frac{3\zeta(3)}{4\pi^2} T_\nu^3 \tag{1.16}$$

where $g_\nu = 3$ are the neutrino degrees of freedom [7].

Unlike the photons the cosmic neutrino background is not at present detectable since the neutrinos interact extremely weakly and the cosmic neutrinos are extremely cold. However we can detect the presence of cosmic neutrinos through the effect their energy density has on nucleosynthesis and the CMB (See 4). The CMB and nucleosynthesis measurements are both consistent with SM neutrinos with three flavors [16]. The best constraints on neutrino mass assuming standard neutrino cosmology state that $\Sigma m_\nu \leq 0.3\,\text{eV}$. If we saturate the bound by assuming degenerate neutrinos of mass $m_{\nu,i} 0.1\,\text{eV}$ each we get that $\rho_\nu = m_\nu n_\nu$ and $\Omega_\nu = \frac{\rho_{nu}}{\rho_c} = 4 \times 10^{-3}$.

3. **Baryons** The energy density of the baryonic component [8] is harder to measure since unlike CMB photons and neutrinos they don't have a thermal description in the present-day universe. However in the early universe when the temperature of the universe was larger than the hydrogen binding energy, the baryons and photons formed a strongly coupled plasma. Sound waves in this strongly coupled plasma left their imprints as anisotropies in the CMB. Measurement of these anisotropies indicates $\Omega_b = 0.05$ [16]. We will look at CMB anisotropies in more detail in 1.3.2.

   Since protons and neutrons are much heavier than neutrinos, their energy density scales as matter in the late universe ($T < 0.1\text{MeV}$) i.e. $\rho_b \propto \frac{1}{a^3}$.

4. **Dark Matter** As we briefly discussed in Sec. 1.2, DM has no known SM interactions

[7] Only 3 and not 6 because only left handed chirality neutrinos are thermalised

[8] baryons refers to all the nuclei and electrons

with SM particles and only interacts through its gravitational force. Evidence of DM was first found by studying the galactic rotation curves [18] i.e. stellar velocities in the gravitational potential of their host galaxy. It was observed (see Fig 1.4a) that the stellar velocities became flat beyond a certain radius from the center of the galaxy instead of monotonically decreasing as predicted by assuming the observed baryons in the galaxy were the only source of the gravitational potential well.

The presence of DM has also been confirmed by observations of the bullet cluster and the anisotropies of CMB[9]. CMB anisotropies provide the best measurements of DM density, $\Omega_m = 0.26$. CMB and matter power spectrum measurements are consistent with the fact that DM matter behaved as cold dark matter in the late universe cosmology ($T < 0.1\,\mathrm{MeV}$)[10]. Thus $\rho_{DM} \propto \frac{1}{a^3}$ in the late universe.

Consistent DM BSM models are dime a dozen and span a mass range from $10^{-24}\,\mathrm{eV}$ for non thermal fuzzy DM [19] to few $M_\odot$ for primordial black holes [20] acting as DM. Popular models include non-thermal DM such as axions and sterile neutrinos [21, 22] and thermal DM such as Weakly Interacting Massive Particles (WIMPs). It is beyond the scope of this thesis to discuss the creation mechanisms and constraints on even the popular DM models. However since most of terrestrial experiments are directed at thermal WIMP scenarios we will discuss thermal DM in the WIMP context in 1.3.1.

5. **Dark Energy** If we calculate $\Omega = \frac{\rho_{total}}{\rho_{crit}}$, just based on the contributions of photons, neutrinos, DM and baryons we get that $\Omega \approx 0.3 \neq 1$. This would indicate that we do not live in a flat universe which would be theoretically unmotivated[11]. This theoretical bias indicated that there should be another form of energy density that is smooth i.e. does not cluster and is called dark energy (DE). Direct evidence of DE was found by

[9]Bullet cluster and CMB effectively rule out modified gravity as an explanation of galactic rotational curves.

[10]There is a caveat called small scale structure problem which we will briefly talk about in Sec. 1.4

[11]Inflation indicates that contributions from the curvature term to energy density should be negligible.

studying the luminosity of distant Type IA supernovae which act as standard candles [23, 24]. It was observed (see Fig 1.4b) that the higher the redshift of the supernovae (SNE), the smaller its luminosity was compared to expected luminosity in a universe with no DE. This indicated that the galaxies at high redshift were farther away from us and that the universe was not just expanding but accelerating in its expansion, indicating the presence of DE.

The general equation of state (EOS) for DE is given by $\rho_{DE} \propto a^{-3(1+\mathrm{w})}$ where w is called the EOS parameter. If the DE is just a cosmological constant $\mathrm{w} = 1$. In quintessence models of DE, such as the ones we will look at in Ch. 3, $\mathrm{w} \neq -1$. Measurement of the CMB anisotropies provide the best measurement of DE and assuming $\mathrm{w} = -1$, we get $\Omega_{DE} = 0.69$ [16].

In conclusion the ΛCDM model of cosmology provides a phenomenal consistency with cosmological observations and is considered the standard model of cosmology. In the next section we will use the ΛCDM model to describe the timeline of our universe.

1.3.2 ***Timeline of the universe***

Our universe is 14.8 billion years old. The cosmic history can be divided into two parts early universe cosmology, which includes inflation, baryogenesis, relic DM production and nucleosynthesis, and late universe cosmology which includes recombination and structure formation. Early universe cosmology is important to understand the first three minutes of the universe which set up the initial conditions of the universe. Late universe cosmology is important to understand how those initial conditions evolve and end up forming the galaxies we see today. Both epochs are important to constrain BSM physics.

Early Universe Cosmology

Early universe cosmology extends from the beginning of inflation to the the end of nucleosynthesis, and covers the first three minutes of the universe. Even though this represents

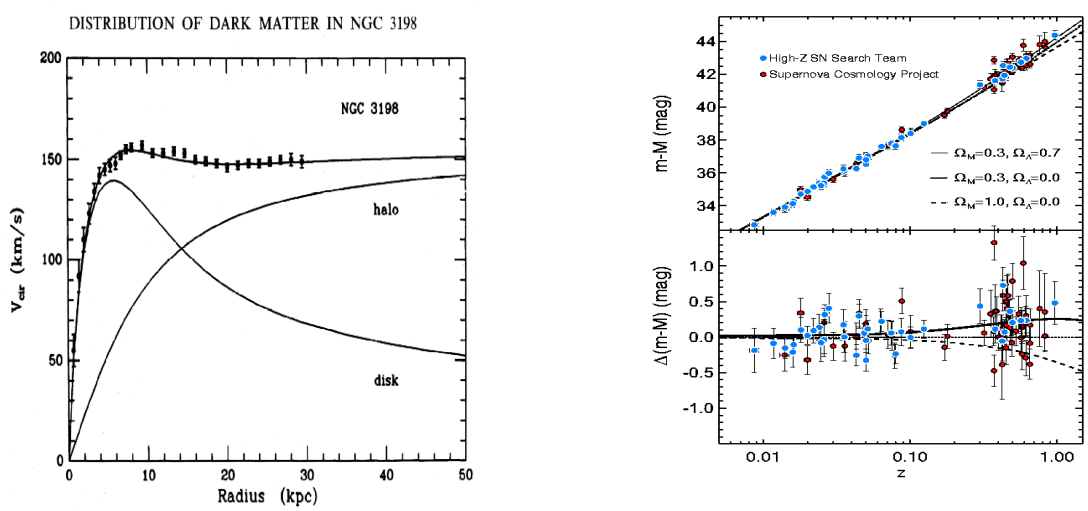

(a) Galactic rotation curves

(b) Supernovae luminosity as a function of z.

Figure 1.4: Evidence of dark matter and dark energy from 'local' observations. The figure on the left is the Stellar rotational velocities in Andromeda galaxy. The figure on the right are TypeIA SNE luminosities as a function of redshift. The CMB ultimately provides best constraints on both DM and DE

an extremely short time compared to the age of the universe, this era is extremely important for setting up the initial conditions that later evolve to form galaxies, stars and life itself. We will present this section chronologically starting with inflation and ending with nucleosynthesis. In each section I will briefly discuss each of the epochs and present a vanilla BSM model when required to explain them.

1. **Inflation** As we saw in the previous section, the universe is DE dominated today until about $z = 2$, matter dominated till about $z = 10^4$ and radiation dominated before that. Now we have good reason to suspect that before radiation domination the universe was dominated by a slowly varying vacuum energy. If we plug in $\rho \approx$ const. in Eq. 1.14 we get that $a(t) \propto e^{Ht}$ where the Hubble H is also approximately constant. This exponential growth of the scale factor is known as inflation.

   The strongest argument in favor on inflation comes from the horizon problem. The horizon is defined as the farthest distance a particle could have traveled from, to a given point since the beginning of the universe. Thus the horizon gives us a measure of the part of the universe that can possibly be in thermal contact at any given point of time.

   Before the epoch of recombination (last scattering) we know that the universe was hot and the baryons and photons formed a thermal plasma. We can then calculate the size of the horizon at last scattering, given by

   $$d_H(t_L) \;=\; a(t_L) \int_{t_*}^{t_L} \frac{dt}{a(t)} \tag{1.17}$$

   where t_* is the time at the 'beginning' of the universe. Assuming that there was no inflation and that the universe was radiation dominated at early times ($t_* = 0$), we get that $d_H(t_L) \approx \frac{1}{H_0(1+z_L)^{-3/2}}$ where $z_L = 1100$ is the redshift at the surface of last scattering. Since we know the distance to the surface of last scattering $d_A \approx \frac{1}{(1+z_l)^{-1}}$ we can calculate the angular distance of the horizon in the CMB today by $\theta \approx \frac{d_H}{d_A} \approx 1.6\,\text{deg}$. Thus if we assume that there was no inflation and the early universe was

only radiation dominated, the CMB should be a patchwork of $1.6\,\mathrm{deg}^2$ patches each having a different temperature. However the observed CMB has a remarkably uniform temperature of about $2.7K$. This is known as the horizon problem, which simply is the question: How do different parts of the universe that were never in causal contact have the same temperature.

Inflation solves the horizon problem by increasing the horizon size exponentially with the exponential increase in its scale factor. Including inflation the horizon size at last scattering is given by $d_H(t_L) \approx \frac{a(t_L)}{a_I H_I} e^{\mathcal{N}}$, where a_I, H_I are the scale factor and Hubble at the end of inflation and $\mathcal{N} = H_I(t_I - t_*)$ is the number of e-foldings. To encompass the entire observable universe into the horizon, d_H needs to be large enough to satisfy $e^{\mathcal{N}} > \frac{a_I H_I}{a_0 H_0}$. Assuming instantaneous reheating we get that $\mathcal{N} > 17$ for reheating temperature of $T_{rh} = 1\mathrm{MeV}$ and $\mathcal{N} > 62$ for GUT scale reheating ($T_{rh} = 10^{16}\mathrm{GeV}$).

The current paradigm of inflation is known as slow-roll inflation[12]. For slow-roll inflation consider the energy density of the universe dominated by an almost uniform scalar field (inflaton) ϕ with a potential $V(\phi)$. Since the inflaton is almost uniform, we can ignore the contributions to its kinetic energy coming from the spatial derivatives. The energy density and the pressure of the scalar field are then given by

$$\rho = \frac{1}{2}\dot{\phi}^2 + V(\phi) \tag{1.18}$$

$$p = \frac{1}{2}\dot{\phi}^2 - V(\phi) \tag{1.19}$$

The equation of motion of the scalar field in the expanding universe is then given by

$$\ddot{\phi} + 3H\dot{\phi} + V^{'}(\phi) = 0 \tag{1.20}$$

where $H\phi$ is the "Hubble friction" and $V^{'}(\phi) = \frac{\partial V}{\partial \phi}$. We can quantify the 'slow-rolling' of the inflaton field by two parameters ϵ and η known as the slow roll parameters. $\epsilon = \frac{\dot{H}}{H^2}$

[12]Slow roll inflation was proposed by Linde [25]. Earlier version of inflation proposed by Guth always ended up giving cold universes(See [26])

quantifies the change in the Hubble parameter in one Hubble time ($\frac{1}{H}$) and $\eta = \frac{\ddot{\phi}}{H\dot{\phi}}$ quantifies the change in $\dot{\phi}$ in one Hubble time. In order to get nearly exponential expansion we need to satisfy that the slow roll parameters $\epsilon, \eta \ll 1$. $\epsilon \ll 1$ gives us $\left|\frac{V'(\phi)}{V(\phi)}\right| \ll \sqrt{16\pi G}$ and $\eta \ll 1$ gives us $\left|\frac{V''(\phi)}{V(\phi)}\right| \ll 24\pi G$. Note that the slow roll parameters wont always be satisfied. If we consider a polynomial potential $V(\phi) \propto \phi^n$ the slow roll conditions are satisfied for $\phi \gg M_{pl}$. When the slow roll conditions are violated we consider the inflation to have ended. The scalar field is no longer supported by Hubble friction and rolls to its minima leading to reheating.

Even though the inflaton field in mostly uniform, there are random fluctuations in the inflaton field $\Delta\phi \simeq H$. These fluctuations which are small and are random gaussian in nature are responsible for the structure we see today.

We can observe these fluctuations in the CMB. Since the inflaton rolls down the potential as the universe expands, not all the modes have the same energy density in them and smaller modes which formed later have lower energy density. This manifests itself as 'spectra tilt' ($n_s = 1 - 4\epsilon - 2\eta$) in the scalar power spectrum $P_s(k) \propto k^{n_s - 1}$, with $n_s = 1$ representing a scale invariant spectrum [13]. The tilt in the tensor power spectrum can is given by $n_T = -2\epsilon$ whose imprint can be observed by the polarization of the CMB. The current constraints on inflaton potential based on CMB observations is given in Fig. 1.5a.

2. **Baryogenesis**

As we discussed in the previous sections 1.3.1,1.2 we have excess of baryons over anti-baryons in our universe. The excess can be quantified by comparing the excess baryon density with photon entropy $\eta = \frac{n_B - n_{\bar{B}}}{s_\gamma} \simeq 10^{-10}$. Since we believe the initial conditions of the universe dictate $n_B = n_{\bar{B}}$, baryogenesis needs to take place between the end of inflation and the beginning of nucleosynthesis. In order to achieve baryogenesis

[13] See [17] for in depth derivation

we need to satisfy the Sakharov conditions. **(1) Baryon number (B) has to be violated** since we have a universe with more baryons then anti-baryons. **(2) C and CP symmetries must be violated** since we have more matter than anti-matter in the universe.**(3)The B, C and CP violating processes should take place out of thermal equilibrium** to avoid the reverse processes from washing out any baryon asymmetry created. In this section we will discuss baryogenesis via the paradigm of baryogenesis via leptogenesis.

As we mentioned in previous section 1.2, the SM of particle physics does not satisfy the Sakharov condition[14]. The SM does not violate baryon number (B) or lepton number (L) at the Lagrangian level. However non-perturbative processes (sphalerons) violate conservation of both B and L currents[15]. However sphalerons violate the baryon and lepton number by equal amounts and the net baryon (lepton) number created by sphaleron processes is given by

$$\Delta B \,=\, \Delta L \,==3\times\int d^4x\frac{g^2}{32\pi^2}Tr\left(\tilde{F}F\right) \tag{1.21}$$

where $F(\tilde{F})$ are the field strength (conjugate) tensors of the $SU(2)_L$ group of the SM. The sphalerons are only active between temperatures of 100GeV $\lessapprox$ T $\lessapprox$ 10^{12}GeV. For $T < 100$GeV the gauge fields associated with $SU(2)_L \times U(1)_Y$ symmetry become massive on account of SSB and supress the sphaleron rate, whereas for $T > 10^{12}$GeV it can be shown that the sphaleron rate is smaller compared to the Hubble expansion rate, thus suppressing the baryon violating effects of the sphaleron.

Since sphalerons convert baryons to anti leptons and vice-versa we can achieve baryogenesis by starting with an initial excess of anti-leptons ($n_{L-\bar{L}} \neq 0$), which get converted to excess of baryons via sphaleron processes[16]. Assuming the SM three generations

[14]Although B is violated, the CP violation is not enough and there is no departure from thermal equilibrium.

[15]Sphalerons are essentially $SU(2)_L$ instantons at finite temperature.

[16]Processes that create equal initial excess of baryons and leptons do not give baryogenesis since the sphalerons which conserve B-L end up erasing the baryon and lepton excess at each others expense.

of quarks and one higgs doublet the excess baryon density at the end is given by $n_B = (28/79)n_{B-L}$ where n_{B-L} is the initial excess of lepton asymmetry over the baryon asymmetry[17].

There can be several ways of generating an initial lepton asymmetry, however the most attractive way is by introducing three generations of heavy (right handed) sterile neutrinos (N_i) which not only give the active neutrinos mass via see-saw mechanism (see Massive Neutrino in Sec 1.2), but also violate the lepton number via the Majorana mass term $m_{N,ij}N_iN_j$. Introducing three generations of sterile neutrinos also introduces CP violation in the neutrino mixing (PMNS) matrix in analogy to the CKM matrix discussed in Sec. 1.1. CP violating decays of the sterile neutrinos can create an excess of lepton asymmetry which can then be converted into baryons. For examples where sterile neutrinos have been used to achieve baryogenesis see [27].

Note that baryogenesis via leptogenesis needs fairly high reheating temperatures. For an example of baryogenesis at low reheating temperature $T_{rh} \leq 200$MeV see Ch. 4.

3. **Dark Matter relic density creation**

As already explained in the previous sections the SM does not explain DM and BSM models for DM are plentiful. In this section we will focus on the Weakly Interacting Massive Particles (WIMP) paradigm of thermal DM, since most terrestrial experiments are set up to detect WIMPs.

Let us assume a DM particle (X) which was in thermal equilibrium with SM particles at high temperatures ($T > m_X$) and that the DM particle can annihilate to SM particles ($X + X \rightarrow SM + SM$). The Boltzmann equation of the number of DM particles per co-moving volume a^3 is given by

$$\frac{d(na^3)}{dt} = -\left(n^2 - n_{eq}^2\right) a^3 \langle \sigma v \rangle \tag{1.22}$$

[17]For a rigorous derivation see [26]

where $n^2a^3\langle\sigma v\rangle$ is the annihilation rate of the DM particles and n_{eq} is the DM number density in thermal equilibrium equilibrium. At $T \gg m_X$ the annihilation and production rates of X are equal and $n = n_{eq}$. However after the temperature drops below m_X, the SM particles don't have enough energy to produce X. Thus at $T \ll m_X$ the annihilation term comes to dominate. As the DM particles annihilate their number density keeps decreasing until the annihilation rate drops below the expansion rate. At this time the DM partices no longer annihilate appreciably and their number density 'freezes' and decreases as $\frac{1}{a^3}$ till present time. We can numerically solve the differential equation given in Eq. 1.22. The temperature at which the DM freezeout happens is given by $T_f \approx m_X/20$ [18].

An analytical approximation to the solution of Eq. 1.22 gives the contribution of DM to the present day energy density to be

$$\Omega_M \;=\; 2.6 \times 10^{-10} \left(\frac{m_X}{\mathrm{GeV}}\right)^{0.05} \left(\langle\sigma v\rangle \mathrm{GeV}^2\right)^{-0.95} \tag{1.23}$$

where we have assumed a fermionic DM, and the relativistic degrees of freedom at freezeout to be $\mathcal{N} = 10$. As we can see, if the cross section is specified the DM density depends only weakly on its mass. However in general the cross section will depend on m_X. For fermionic DM annihilations to SM particles the cross section approximated as $\langle\sigma v\rangle = G_F^2 m_X^2$, where G_F is the effective Fermi coupling[19]. Assuming that weak interactions mediate the annihilations and that $m_X \leq m_W$ we get that $m_X \approx \mathcal{O}\,\mathrm{GeV}$ to get the correct DM relic density. This is known as the WIMP miracle where weak scale couplings and weak scale DM masses give the correct DM relic density.

Since WIMP DM annihilates to SM particles we can detect them through their interactions with SM particles (SM+X $\rightarrow$ SM+X) in laboratories. Several such 'direct detection' experiments have been conducted and the current bounds on DM interaction are shown in Fig. 1.5b. Note that these bounds rule out the vanilla DM scenario

[18]The freezeout temperature depends mildly on m_X

[19]Assuming weak interactions mediate the annihilation$G_F \approx 1/m_W^2$ for $m_X < m_W$

described above. However once can easily construct models with different mediators and DM couplings mostly to the heavy quarks and leptons to evade the direct detection constraints

4. **Primordial Nucleosynthesis**

The excess of baryons created during baryogenesis can be processed to form heavier nuclei in the early universe through primordial nucleosynthesis. Hydrogen is the most abundant element in the universe followed by Helium (He^4) which through primordial nucleosythesis makes up about 24 % of the baryons by mass. Primordial nucleosynthesis forms heavier elements like Lithium and Beryllium in small quantities. However in this section we will only discuss He^4 helium production. Primordial nucleosynthesis observations are in line with their SM predictions for the most part so we wont discuss any BSM physics in this section[20].

Finding the primordial helium abundance is equivalent to finding the number of neutrinos that survive until the temperature of universe drops enough to start synthesizing helium. At $T >$ MeV, the weak interactions keep the neutrons and protons in thermal equilibrium through the interactions($n + \nu \leftrightarrow p + e^-$), ($n + e^+ \leftrightarrow p + \nu$) and ($n \leftrightarrow p + \nu + e^-$). However since the neutrons are heavier than protons, the neutrons as a fraction of the nucleons in thermal equilibrium can be shown to be

$$X_n = \frac{n_n}{n_N} = \frac{\Gamma(p \to n)}{\Gamma(p \to n) + \Gamma(n \to n)} = \frac{1}{1 + e^{Q/T}} \tag{1.24}$$

where $Q = 1.3$MeV is the neutron-proton mass difference. As the temperature drops the weak interactions fall out of thermal equilibrium at $T \approx$ MeV and the neutron fraction at the end of thermal equilibrium is given by $X_n \simeq 0.16$. The neutrons continue to decay into protons as the temperature drops further. Thus the neutron fraction after thermal equilibrium is given by $X_n = 0.16 \times e^{-t/\tau}$ where $\tau = 886s$ is the neutron lifetime.

[20]Predictions for Lithium are larger than their observations.

Bound nuclei can form once the temperature of the universe drops below their binding energy per nucleon i.e. once they can no longer be dissociated by photons. Since He^4 has the highest binding energy per nucleon of the low atomic number isotopes of Deuterium (d), Tritium (H^3) and Helium 3 (He^3), we would expect He^4 to form first. However the number density of nucleons is low enough that only two body interactions are in equilibrium. Thus He^4 formation has to undergo a multi-step two-body process given by $p + n \rightarrow d + \gamma$; $d + d \rightarrow H^3 + p$ OR $d + d \rightarrow \mathrm{He}^3 + \mathrm{n}$; $d + \mathrm{H}^3 \rightarrow \mathrm{He}^4 + \mathrm{n}$ OR $d + \mathrm{He}^3 \rightarrow \mathrm{He}^4 + \mathrm{p}$. Thus He^4 formation needs deuterium formation as an intermediate process. However the deuterium binding energy is small and deuterium number density does not grow large enough to form He^3 and H^3 until the temperature drops to $T \simeq 0.1\mathrm{MeV}$ (assuming $\Omega_b h^2 = 0.02$). This is known as the 'deuterium bottleneck' and nucleosynthesis does not proceed until this temperature has been crossed. As soon as the deuterium bottleneck is crossed the remaining protons and neutrons immediately form helium. Since the neutrons have been decaying all the way along until then, the mass fraction of primordial helium (Y_p) is extremely sensitive to the time (and hence the temperature) at which the universe crosses the deuterium bottleneck. This temperature $T \simeq 1\,\mathrm{MeV}$ is reached at approximately $t \simeq 168s$. Thus the mass fraction of the Helium is given by

$$Y_p \;=\; 2 \times X_n \;=\; 2 \times 0.16 \times e^{-168/886} \;=\; 0.27 \tag{1.25}$$

where the factor of 2 comes from the fact that $A/(A - Z) = 2$ for He^4. Numerical calculations give $Y_p \simeq 0.24$ which is consistent with He^4 observations in metal poor regions of the universe[21].

Since Y_p is so sensitive to the time when the universe crosses $T \simeq 0.1\,\mathrm{MeV}$, it is extremely sensitive to number of relativistic species present during nucleosynthesis. Thermalized relativistic species in addition to the three relativistic neutrinos increase

[21]Metal poor regions are 'pristine' environments for primordial He^4 since stellar nucleosynthesis has not affected its prevalence.

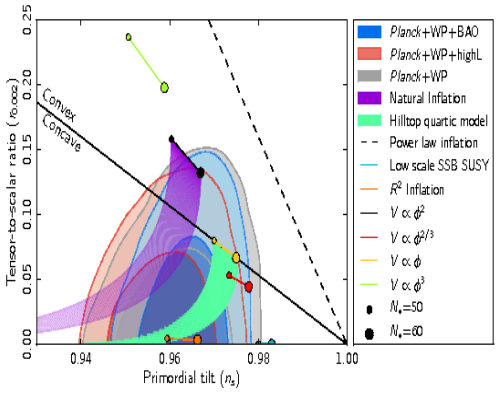

(a) CMB constraints on inflation [28]

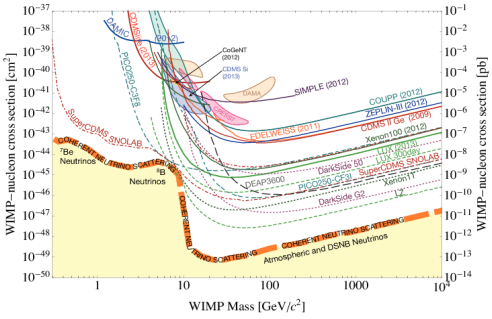

(b) WIMP nucleon interaction constraints [29]

Figure 1.5: Constraints of inflationary potentials from CMB showing 68% and 95% CL regions for the scalar spectral tilt and $r = \frac{n_T}{n_s}$ from Planck Collaboration on inflationary potentials on the left and constraints on WIMP-nucleon spin-independent cross section limits (solid lines) and projected constraints (dotted lines) on the right.

the Hubble H and modify the $H\,vs.\,T$ relation. He^4 observations are consistent with three relativistic neutrino species during nucleosynthesis.

Late Universe Cosmology

Late universe cosmology refers to the period after nucleosynthesis. In this era the inhomogeneities created by inflation, DM relic density production, baryogenesis and nucleosynthesis evolve over 14.8 billion year to form galaxies, stars and the structure we see today. This era of the universe includes the acoustic oscillations in the baryon-photon plasma which are observed in the cosmic microwave background and the growth of the DM perturbations. Since the CMB is presently our major source of constraining non-standard cosmologies and BSM physics a good understanding of this era is important.

Since we are interested in the evolution of inhomogeneities, let us start by defining them. The distribution of any density component can be parametrized as $f(x, t, p, \hat{p})$ i.e. its a function of of the comoving coordinate x, time t, momentum p and direction $\hat{p}$. The metric perturbations can be written as $g_{00} = -1 - 2\Psi(x, t)$ and $g_{ij} = a^2(t)\delta_{ij}(1 + 2\Phi(x, t))$, where Ψ can be interpreted as Newtonian gravitational potential and Φ is the perturbation to spatial curvature. Since the photons are parametrized only by the temperature, we can parametrize the photon perturbations as $f_\gamma(x, \hat{p}, t) = \frac{1}{e^{p/T(1+\Theta(x,\hat{p},t))}}$. Note that since the photons can 'stream' and are not isotropic, they are a function of the direction $\hat{p}$. The DM and baryon perturbations can be written as $n_{cdm,b} = n^0_{cdm,b}\,(1 + \delta_{cdm,b}(x, t, \hat{p}))$ where $n_{cdm,b} = \int d^3p\, f_{cdm,b}$ are the number densities. They can also in general have bulk velocity perturbations $v_{cdm,b}$.

The evolution of the distribution of every component can be written as $\frac{df}{dt} = C[f]$, where $C[f]$ is the collision term that captures the interactions of the component. The 0th order collisionless equations simply give the standard scale factor scalings for the energy density each components (e.g. $\rho_\gamma \propto \frac{1}{a^4}$). The interesting dynamics come from considering the first order equations including collisions. As an example let us consider the first order collision equation for photons

$$\frac{\partial\Theta}{\partial t} + \frac{\hat{p}_i}{a}\frac{\partial\Theta}{\partial x_i} + \frac{\partial\Phi}{\partial t} + \hat{p}_i\frac{\partial\Psi}{\partial x_i} = n_e\sigma_T\left(\Theta_0 - \Theta + \hat{p}v_b\right) \tag{1.26}$$

where n_e is the electron number density, σ_T is the Thompson cross section and Θ_0 is the photons temperature monopole. Parsing the equation the first two terms on the LHS account for the effects of photon "free streaming" whereas the third and fourth terms take into account the effect on photon temperature from gravitational potential wells. The right hand side comes from the photon compton scattering off electrons. As can be seen, if there is no bulk baryon velocity v_b the Compton scatterings enforce $\Theta_0 = \Theta$ is equilibrium i.e. makes the photon temperature uniform.

Taking the fourier transforms of the Boltzmann equations and replacing the time deriva-

tives with conformal time ($\eta = \int_0^t \frac{dt'}{a(t')}$) derivatives we get

$$\dot{\Theta} + ik\mu\Psi\Theta = -\dot{\Phi} - ik\mu - \dot{\tau}\left(\Theta_0 - \Theta + \mu v_b\right) \tag{1.27}$$

$$\dot{\delta}_{cdm} + ikv_{cdm} = -3\dot{\Phi} \tag{1.28}$$

$$\dot{v}_{cdm} + \frac{\dot{a}}{a}v_{cdm} = -ik\Psi \tag{1.29}$$

$$\dot{\delta}_b + ikv_b = -3\dot{\Phi} \tag{1.30}$$

$$\dot{v}_b + \frac{\dot{a}}{a}v_b = -ik\Psi + \frac{\dot{\tau}}{R}\left(v_b + 3i\Theta_1\right) \tag{1.31}$$

$$\dot{N} + ik\mu N = -\dot{\Phi} - ik\mu \tag{1.32}$$

$$k^2\Phi + 3\frac{\dot{a}}{a}\left(\dot{\Phi} - \frac{\dot{a}}{a}\Psi\right) = 4\pi G a^2\left(\rho_{cdm}\delta_{cdm} + \rho_b\delta_b + \rho_\gamma\Theta_0 + \rho_\nu N_0\right) \tag{1.33}$$

$$k^2\left(\Phi + \Psi\right) = -32\pi G a^2\left(\rho_\gamma\Theta_2 + \rho_\nu N_2\right) \tag{1.34}$$

where $R = \frac{3\rho_b}{4\rho_\gamma}$, μ is the cosine of the angle between the perturbation wavenumber $\vec{k}$ and photon direction $\hat{p}$ and N are the neutrino temperature perturbations analogous to Θ. In principle, this set of coupled differential equations along with the initial conditions dictated by inflation allows us to solve the evolution of perturbations numerically. However that does not give us an intuitive understanding of the evolution of these perturbations. In the following sections we will try to give an intuitive understanding of the matter power spectrum and the CMB.

We will begin by studying the evolution of dark matter perturbations.

5. Matter Power Spectrum and Structure Formation

In this section we will be looking at the evolution of matter perturbations δ_{cdm} through the cosmic history. Our final aim is to understand the matter power spectrum $P(k)$ in Fig. 1.6. Understanding the matter power spectrum will help us understand the evolution of DM halos and galaxies.

The matter power spectrum is the two point correlation function of matter perturbations $\langle\delta(\vec{k})\delta(\vec{k'})\rangle = 2\pi^3 P(k)\delta^3\left(\vec{k} - \vec{k'}\right)$ and describes the power in each fourier mode.

In order to gain a physical intuition lets look at the answer in Fig. 1.6 (see [30]). The primordial power spectrum has $P(k) \propto k^{n_s}$ where $n_s \simeq 1$. However the power spectrum today is not linear in k. In fact the $P(k)$ decreases as k increases for $k \gtrapprox 0.03h\text{Mpc}^{-1}$. In order to understand this let us consider the evolution of mode with wavenumber k. The mode k does not begin to evolve until it enters the causal horizon i.e. $k\eta = 1$. The simplest regime to consider is when k is small (large wavelength) and has not yet entered the horizon or entered the horizon recently. Such a mode has not grown much and hence preserves the original matter power spectrum scaling $P(k) \propto k$. This can be seen for $k \lessapprox 10^{-3}h\text{Mpc}^{-1}$ If however k is large (small scale), the mode enters the causal horizon early when the universe is still radiation dominated. Free streaming of radiation (photons and neutrinos) during radiation dominated era makes the gravitational potentials within the free streaming scale decay. Thus modes that enter the horizon during the matter dominated era do not grow efficiently until matter domination begins, suppressing their power. This can be seen for $k \gtrapprox 0.1h\text{Mpc}^{-1}$.

Let us try to quantify this slightly more. Instead of calculating the matter perturbations $\delta_{cdm}(k)$, we can calculate the the potential $\Phi(k)$. The evolution of the potential perturbations can be written as $\Phi(k) = \frac{9}{10}\Phi_p(k) \times T(k) \times D(a)$, where $\Phi_p(k)$ are the primordial perturbations set up at inflation. The factor $\frac{9}{10}$ is a suppression all modes experience when they cross matter radiation equality. $T(k)$ is defined to be the transfer function that calculates the evolution of each mode from deep inside radiation when the scale factor is $a \ll a_{eq}$ domination to deep inside matter domination $a_{late} \gg a_{eq}$. $D(a)$ is the growth function that describes the evolution of all modes for some $a > a_{late}$. We can relate the matter perturbation today to the gravitational potential today by using Poisson equation $\Phi = \frac{4\pi a^2 G \rho_{cdm}\delta_{cdm}}{k^2}$. The k scaling of the matter power spectrum can then be written as $P(k) \propto k \times T^2(k)$ where we have assumed $n_s = 1$.

Let k_{eq} be the scale that crosses the horizon at matter radiation. As we already mentioned large scales $k \ll k_{eq}$, enter the horizon when the universe is matter dominated.

It can be shown that Φ remains is constant during matter domination. Thus $T(k) = 1$ for $k \ll k_{eq}$ and $P(k) \propto k$. In the case where $k \gg k_{eq}$ we have to calculate the evolution of Φ through horizon crossing in radiation dominated era. Assuming the radiation perturbations are dominant i.e. $\rho_\gamma \Theta \gg \rho_{cdm}\delta_{cdm}$, we can show using equations 1.27 and 1.33 from that

$$\Phi(k) = 3\Phi_p \left(\frac{sin(k\eta/\sqrt{3}) - (k\eta/\sqrt{3})cos(k\eta/\sqrt{3})}{(k\eta/\sqrt{3})^3} \right) \tag{1.35}$$

where η is the conformal time (comoving horizon) as usual. As can be observed, if we ignore the oscillatory behavior $\Phi(k) \propto \frac{1}{k^2}$ today when $k\eta_0 \gg 1$. Thus $P(k) \propto \frac{1}{k^3}$ for $k \gg k_{eq}$. However our assumption $\rho_\gamma \Theta \gg \rho_{cdm}\delta_{cdm}$ is not valid throughout radiation domination. Including this effect we get $P(k) \propto \frac{ln(k/k_{eq})^2}{k^3}$ for $k \gg k_{eq}$[22]. Since we know the behavior of the matter power spectrum for $k \gg k_{eq}$ and $k \ll k_{eq}$, we can interpolate the results to approximate the powerspectrum. Though we wont quote the splined result here it is well consistent with the exact power spectrum plotted in 1.6.

Since after a_{late} all the modes scale by the same growth factor $D(a)$, the scaling of the power spectrum does not change. The growth factor is defined as $D(a) = \frac{a\Phi(a)}{\Phi(a_{late})}$ for $a > a_{late}$. Since the potentials dont drow during matter domination we can show $D(a) = a$ and in a universe with no DE we get the growth function today to be $D_0 = 1$. However since DE takes over at low redshifts we can show $D_0 = 0.7$ since DE will suppress the growth of structure (see [17]).

6. CMB and Recombination

As we have previously explained the cosmic microwave background is the radiation that last scattered at the epoch of recombination. The CMB is not completely isotropic but has fluctuations of $\mathcal{O}(10^{-5})$ in its temperature. This is to be expected since the seeds of this anisotropy are seeded during inflation as we have already discussed. However unlike

[22]This is tedious to calculate. See [17].

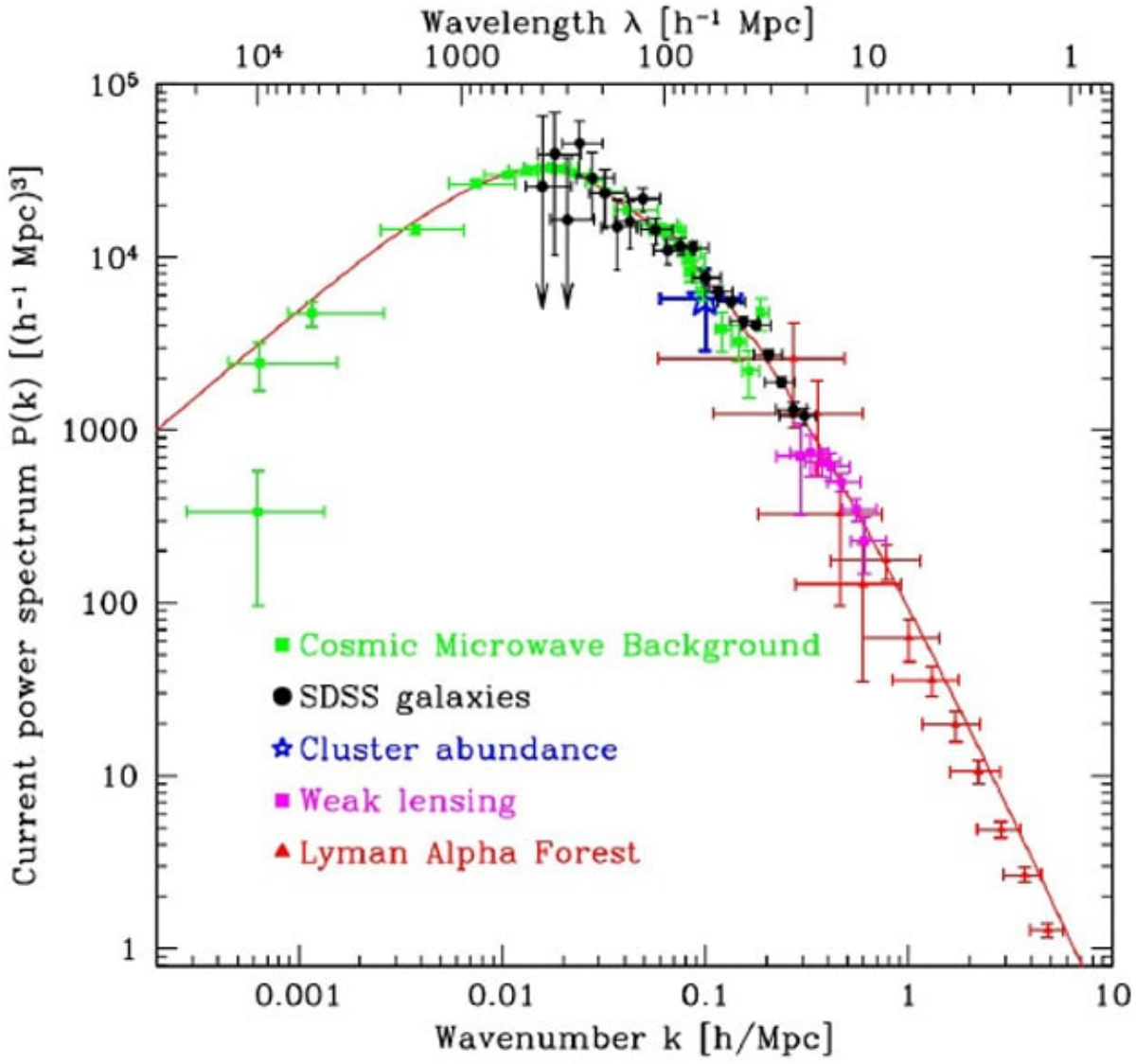

Figure 1.6: Matter power spectrum measurements and best fit ΛCDM model prediction

the inhomogeneities seeded during inflation which are random gaussian in nature, the anisotropies of the CMB are correlated. If we plot the two point correlation function of the cosmic microwave background, (see Fig. 1.7) we can see that there are correlations at about 1 deg, i.e. if you pick a random point in the sky there is a higher probability that the points 1 deg away from it have the same temperature. In this section we will address the dynamics that go into producing the temperature correlations show in Fig. 1.7 from initial conditions that have no correlations. We will present a relatively brief review with minimal derivation, for a full treatment see [17].

The shape of the CMB anisotropies (henceforth referred as CMB spectrum) correlation function is controlled by six parameters, Ω_b, Ω_{cdm}, H_0, A_s, n_s and τ, where A_s is the amplitude of the primordial inhomogeneities and τ is the optical depth at reionization[23]. In the discussion that follows we will only consider Ω_b, Ω_{cdm} and H_0 to simplify matters.

The basic picture is as follows. Before recombination the baryons and photons were tightly coupled plasma. The baryon-photon fluid collapses due to gravity, which causes the temperature and pressure to increase. This pushes the baryon, photon plasma back and these contractions and rarefactions are what gives us our 'wavy' CMB spectrum. This complicated dance involves interactions between DM, metric perturbations, photons, protons, electrons and neutrinos. Let us try to formalize these interactions as a set of coupled Boltzmann equations. We will not be explicitly deriving any of these but we will try to give a physical intuition.

After inflation the causal horizon size is much smaller than the size of the universe and most perturbation modes lie outside the causal horizon and don't evolve. As time goes along the causal horizon expands and the modes that enter the causal horizon begin evolving according to the Eqs. 1.27. Thus the first peak on the CMB spectrum corresponds to the mode that has recently entered the horizon and undergone maximal

[23]More parameters influence the neutrinos such as Σm_ν and N_{eff}. We will mostly ignore these for the discussion

contraction at the time of last scattering, the second peak corresponds to a mode that has undergone one contraction and one rarefaction at the time of last scattering, and so and and so forth. There is a clear damping of higher l modes. However if we ignore that damping, the third peak which is at maximum contraction at last scattering will be higher than the second peak which is at a rarefaction. Thus the contractions have an higher amplitude than the rarefactions an effect that can be attributed to the heavy baryons and is known as "baryon loading"[24]. This is exactly what is seen in the Boltzmann equations. Taking the Legendre transformation the photon Boltzmann equation and the baryon velocity equation, keeping only the monopole and dipole terms for the photon perturbation Θ we get that the photon monopole and dipole are given by[25]

$$\Theta_0(\eta) + \Phi(\eta) = (\Theta_0(0) + \Phi(0))\, cos(kr_s) + \tag{1.36}$$

$$\frac{k}{\sqrt{3}} \int_0^\eta d\eta^{'} \left[\Phi(\eta^{'}) - \Psi(\eta^{'})\right] \left(sin\left[k\left(r_s(\eta) - r_s(\eta^{'})\right)\right]\right) \tag{1.37}$$

$$\Theta_1(\eta) = \frac{1}{\sqrt{3}} (\Theta_0(0) + \Phi(0))\, sin(kr_s) + \tag{1.38}$$

$$\frac{k}{3} \int_0^\eta d\eta^{'} \left[\Phi(\eta^{'}) - \Psi(\eta^{'})\right] \left(cos\left[k\left(r_s(\eta) - r_s(\eta^{'})\right)\right]\right) \tag{1.39}$$

$$\tag{1.40}$$

where $\Phi(0), \Theta_0(0)$ are primordial perturbations, $r_s(\eta) = \int_0^\eta d\eta^{'} c_s(\eta^{'})$ is the sound horizon i.e. the distance the sound waves travel with the speed of sound $c_s = \sqrt{\frac{1}{3(1+R)}}$[26].

The above represents the forced harmonic oscillator that the monopole and dipole undergo. Now let us discuss the damping that is responsible for suppressing the peaks at higher l in Fig. 1.7. The photons and baryons are in a tightly coupled plasma.

[24]This is analogous to a weigh attached at the end of a hanging spring which favors the expansion of the spring from its original equilibrium position to the contractions.

[25]In the tightly coupled plasma only the monopole and dipole terms contribute. Higher order terms are suppressed because the optical length of the photon is small and shorter angular distances are already in thermal equilibrium

[26]A lot of assumptions went into deriving 1.36. Consult [17] for rigorous derivation

However the photons can still diffuse over the distance comparable to their optical depth. This diffusion leads to equalization of the temperatures at shorter distances (larger k). Including the diffusion damping the monopole and dipole terms are given by $\Theta_{0,1}(k,\eta) \rightarrow \Theta_{0,1}(k,\eta)e^{-L_D^2 k^2}$, where $L_D^2 \simeq \int_0^\eta \frac{d\eta'}{n_e \sigma_T a}$ is the length over which the photons diffuse. Note the higher the Compton scattering the smaller is diffusion length.

This derives the evolution of the modes up until recombination. However the anisotropies we observe today are on a sphere of the surface of last scattering. Thus we need to evolve the fourier modes until today by free streaming the photons from the surface of last scattering until today. We will just state the result in terms of the monopole and dipole moments of each of the mode

$$\Theta_l \simeq [\Theta_0(k,\eta^*) + \Psi(k,\eta^*)]\, j_l[k(\eta_0 - \eta^*)] + \tag{1.41}$$

$$3\Theta_1(k,\eta_*)\left(j_{l-1}[k(\eta_0-\eta^*)] - \frac{(l+1)j_l[k(\eta_0-\eta^*)]}{k(\eta_0-\eta^*)}\right) \tag{1.42}$$

where j_l are spherical bessel functions, and η_0, η_* are the conformal times today and at last scattering respectively. We can finally relate this to the two point correlation function plot that we have plotted in 1.7 as $C_l = \frac{2}{\pi}\int_0^\infty dk\, k^2 P(k) \left|\frac{\Theta_l(k,\eta_0)}{\delta(k,\eta_0)}\right|$, where $P(k), \delta(k,\eta_0)$ are the matter power spectrum and DM overdensity for mode k today respectively.

This is not the complete story. We made massive simplifications while stating the results above. We also ignored the early and late integrated Sachs-Wolfe effect (ISW). The early ISW effect comes from the fact that the gravitational potential wells are still decaying right after recombination which redshifts the photons streaming out of these potential wells. The late ISW effect is the same except its the DE that becomes dominant at low redshifts that is responsible for the decay of the potential wells. Overall the ISW effect increases the $C_l's$ at low $l's$.

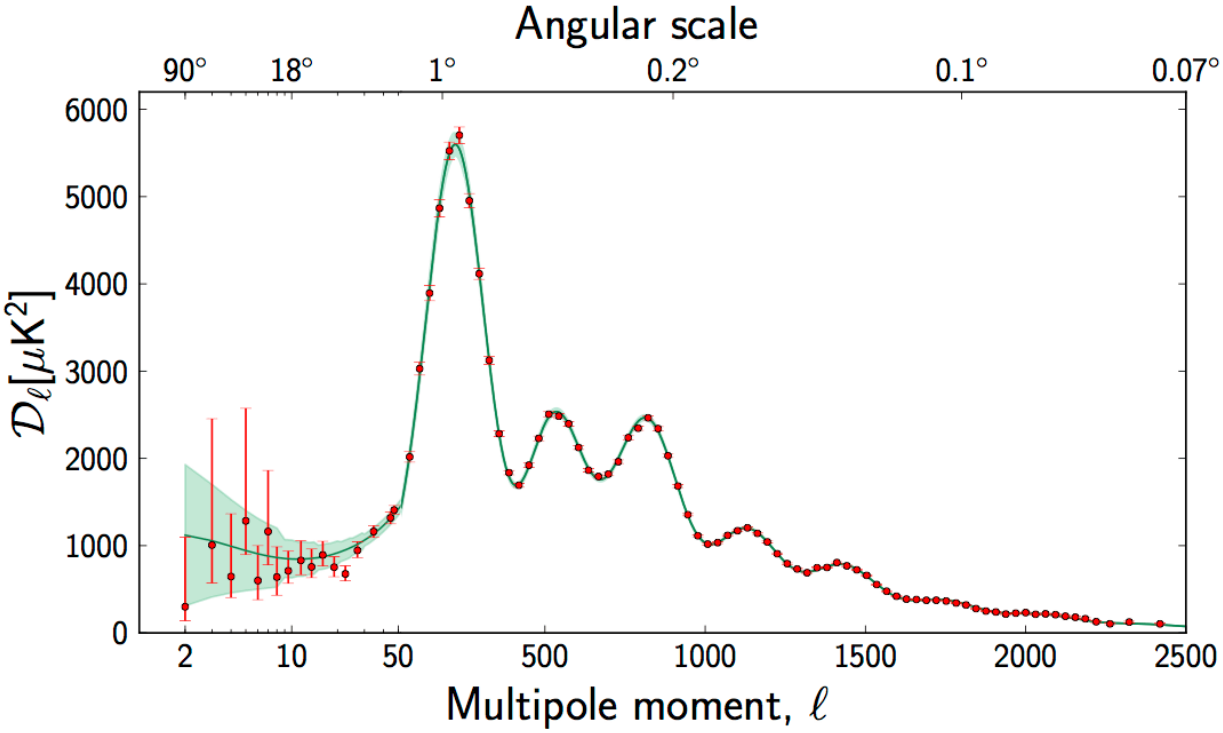

Figure 1.7: Planck 2015 CMB angular power spectrum

1.4 Problems with ΛCDM cosmology

The ΛCDM model of cosmology explains the vast majority of cosmological and astrophysical observations. However there are certain observational inconsistencies which may indicate the presence of interesting BSM physics or non-standard cosmology. Here I will list them briefly without refering to the proposed solutions. None of these anomalies are statistically significant to quantify an new physics.

1. **CMB anomalies** In the CMB power spectrum in Fig. 1.7, it can be seen that the measurements of low multipole modes ($l \leq 50$) are consistently smaller than their predicted value from the best fit to ΛCDM cosmology. This is called the low-l anomaly. Since cosmic variance is the major uncertainty for the low-l modes, the anomaly is not statistically significant. Other anomalies in the CMB is the large cold spot in the CMB temperature measurements and the hemispherical anomaly.

2. **Small scale structure problems** Small scale structure problems generally refer to DM not behaving exactly like cold dark matter at length scales smaller than the about the size of our galaxy. Of the small scale structure problems the core-cusp problem refers to the fact that the DM distribution in galaxy halos has a “cored" profile instead of the cuspy NFW profile predicted by DM structure formation simulations. Another small scale structure problem is the missing satellite problem which refers to the fact that we don’t observe the large number of satellite galaxies to our Milky Way galaxy as predicted by structure formation simulations. There is a vast literature on solving these problems by proposing alternate models of DM such as warm DM and self interacting DM. However baryonic feedback processes during structure formation which are not well understood can also resolve these anomalies. Thus they are not considered conclusive evidence of new physics.

3. H_0 **and** σ_8 **problems** The measurement of the present day Hubble constant H_0 from CMB is smaller than the “local" measurements of H_0 by about 2.5σ (see the H_0 dis-

cussion in [16]). This is known as the H_0 problem. We can quantify the amplitude of matter fluctuations within a size of radius R as

$$\sigma_R^2 = \frac{1}{2\pi^2} \int dk k^2 P(k,z) |W(kR)|^2 \tag{1.43}$$

where $P(k,z)$ is the linear matter power spectrum at redshift z and $W(kR)$ is a spherical top hat window function. A common way of reporting the amplitude of matter fluctuations is to report σ_8 which corresponds to the σ_R for R $= 8h^{-1}$Mpc. The value of σ_8 as derived from CMB measurements is about 2.5σ larger than the one derived from actual measurements of galaxy mass distribution function (see [31]). This is known as the σ_8 problem. Although the H_0 and σ_8 problem are not in principal related, trying to solve one problem typically exacerbates the other. In Ch. 3 we will show a solution to the σ_8 without significantly affecting the H_0 problem.

1.5 Layout

In the following chapters of this thesis we will address some of the problems with the SM and ΛCDM cosmology.

In Ch. 2 we address the problem of neutrino masses and the possibility of light (eV mass) sterile neutrinos with a unique neutrino mass mechanism known as Mass Varying Neutrinos (MaVaNs). We also point out the importance of conductiong terrestrial neutrino experiments which can act as a 'smoking guns' for scenarios with non-standard neutrino cosmology such as MaVaNs

In Ch. 3 we explore the cosmology of specific type of MaVaNs. We show by doing global fits to Planck CMB data, that we can reduce the σ_8 discrepancy by using MaVaNs.

In Ch. 4 we address the problem of baryogenesis. Our model includes hadronic bound states (mesinos) whose oscillations give CP violations (in exact analogy to Kaon oscillations in SM) and whose decays give baryogenesis. This model is novel since baryogenesis occurs at low temperatures ($T < 200$MeV) without involving large couplings of the new physics to SM.

Chapter 2

MASS VARYING NEUTRINOS: IMPLICATIONS FOR TERRESTRIAL EXPERIMENTS

Over the past twenty years, definitive evidence for neutrino oscillations from a host of experiments has revealed that neutrino masses are nonzero. Because neutrino masses cannot be accounted for in the standard model (SM), this is a clue to physics beyond the SM. Since oscillation experiments are only sensitive to the difference in (squared) masses, the overall mass scale is not known and only two mass differences have been conclusively established, the so-called solar and atmospheric mass splittings, $\Delta m^2_{\odot} \simeq 7.5 \times 10^{-5}$ eV^2 and $\Delta m^2_{\rm atm} \simeq 2.4 \times 10^{-3}$ eV^2. It has also been well established that the neutrino mixing matrix, characterizing the mismatch between weak interaction and mass eigenstates, involves large mixing angles, in stark contrast to the quark sector. While they may seem like an uninteresting example of new physics—we have seen other chiral fermions obtain masses in the SM—neutrino masses could differ in a fundamental way from other fermion masses. Because neutrinos are not charged under electromagnetism, their mass generation mechanism could involve Majorana masses, violating lepton number, while the nonzero charges of the other fermions requires their masses to be of purely Dirac form. To generate neutrino masses in a way that does not disturb the successful picture we have of electroweak symmetry breaking, new neutrino states that are uncharged under the electroweak gauge group (or "sterile" neutrinos, as opposed to the "active" ones that carry electroweak charge) are typically invoked. Since they are gauge singlets, mass terms for these sterile neutrinos need not involve Higgs fields, which means that the mass scale in the sterile neutrino sector is largely a free parameter. While there may be theoretical bias for this scale to be very large compared to the weak scale, it is entirely possible and self-consistent that it is within reach of current experiments.

Indeed, there are phenomenological reasons to consider a mass scale in the sterile neutrino sector as small as an eV. Alongside this standard three neutrino picture, there have been a number of experimental hints of neutrino oscillations characterized by a squared mass splitting of $\Delta m^2 \sim \mathcal{O}\,(1\text{ eV}^2)$ and a mixing angle $\theta \sim \mathcal{O}\,(0.1)$; these include short-baseline reactor experiments [32, 33], the flux of neutrinos from radioactive sources in gallium solar neutrino experiments [34, 35], and electron (anti)neutrino appearance in muon (anti)neutrino beams [36, 37]. To interpret these data in terms of neutrino oscillations requires an additional (sterile) neutrino around an eV and a large mixing angle with the active neutrinos. For detailed analyses, see, e.g., [38, 39]. It should be noted that there is generally tension between disappearance and appearance data, as a recent search for ν_μ and $\bar{\nu}_\mu$ disappearance at IceCube [40] shows, disfavoring the sterile neutrino interpretation of electron (anti)neutrino appearance data. However, a global fit including the IceCube results claims that a relatively large active-sterile mixing is allowed [41].

Additionally, progress in the direct search for neutrino masses has been ongoing. Searches using the endpoint in tritium β-decay currently limit the electron neutrino mass to less 2.05 eV at 95% CL [42]. The upcoming KATRIN [43] and Project-8 [44] experiments hope to probe masses down to about $0.1 - 0.2$ eV in the near future. Conceivably, the PTOLEMY experiment could use inverse beta decay to be sensitive to cosmological neutrinos [45, 46, 47].

In parallel with progress in neutrino measurements, cosmology has entered an era of impressive precision, enabling cosmological tests of physics beyond the standard model. We have direct observational evidence of the state of the Universe up to temperatures of a few MeV, corresponding to the time of neutrino decoupling and primordial nucleosynthesis (BBN). The precise picture of the Universe we now have at these temperatures and below allows for new physics below an MeV, even if weakly coupled, to be confronted with observation.

Because (active or sterile) neutrinos interact very weakly with the rest of the Universe after decoupling–acting as a form of non-interacting radiation until they become nonrelativistic when they begin to act like dark matter–their observational consequences are relatively

easy to understand. At early times, the cosmic microwave background (CMB), structure formation, and BBN are all sensitive to the energy density in neutrinos, which can be related to their masses and, in the case of sterile neutrinos, their mixing with the active neutrinos. The general agreement of these data with the standard cosmological picture based on three (essentially massless) neutrinos allows constraints to be placed on additional sterile neutrinos or on the masses of the active neutrinos. However, at late times, the neutrino energy density is the only SM component that can have nonstandard cosmology, which makes finding probes of this behavior crucial.

In the case of a single massive sterile neutrino that is fully thermalized at early times, an up-to-date fit to cosmological observations give an upper bound on its mass (assuming the light, mostly active neutrinos' masses are negligible) of 0.53 eV [48]. In the standard case of only three (active) neutrinos, the Planck analysis of only CMB data constrains the sum of the light neutrino masses to 0.675 eV [16]. Including further cosmological data improves the bounds to 0.3 eV [16, 49, 50, 51]. Note that these upper limits are all at 95% CL. Improved observations could allow values of the sum of the active neutrino masses as small as 0.06 eV to be probed [52]. Sterile neutrinos which are much lighter than an eV and have similar abundance to the active neutrinos are disfavored by the Planck determination of N_{eff} [16].

At first glance, the null results from cosmological analyses are in strong tension with the sterile neutrino interpretation of the short baseline anomalies. In addition, the projected reach in the limit on the sum of the neutrino masses in the standard three neutrino scenario coming from cosmology seems to imply that current laboratory searches will not be sensitive enough to see nonzero neutrino masses. However, these conclusions rely on the assumption of a standard cosmological history. Thus, one should view contemporary terrestrial experiments seeking to measure neutrino masses or to test the sterile neutrino solution to short baseline anomalies as nontrivial probes of cosmology. Some scenarios that allow for cosmological observations to be compatible with eV mass neutrinos include coupling the sterile (with respect to the SM) neutrinos to a new U(1) gauge boson [53, 54, 55, 56, 57, 58] or pseudoscalar [59, 48], allowing the sterile neutrinos to be chiral under a new gauge group [60, 61],

or the possibility of resonant conversions to lighter states at temperatures around a keV [62].

In this chapter we will focus on the reconciliation of eV mass neutrinos with cosmology via the dependence of the neutrino masses and mixing angles on the expectation value of a non constant light scalar field. This possibility was originally motivated to address the puzzle of dark energy [63, 64], but we will consider this possibility more generally, including the possibility of additional contributions to neutrino mass, the effects of neutrino clustering, and models which do not give dark energy. We will consider two scenarios. In § 2.2 we consider a MaVaN model containing a light scalar field with a logarithmic potential, and find parameters such that eV mass sterile neutrinos with sizable mixing angles are allowed today which were always heavy enough at earlier times so that these states were never populated in the early universe and have no observable effect on cosmology. In § 2.3 we consider a scenario which allows the observed, active neutrinos to have a mass which is today around an eV. Because the masses were much lighter at high redshift, cosmological observations indicate a much smaller mass. In § 2.4 we discuss a cosmologically viable supersymmetric MaVaN scenario which could allow eV mass sterile neutrinos to appear in terrestrial experiments.

2.1 Introduction to MaVaNs

2.2 The Model: Logarithmic Potential

2.2.1 A single active neutrino

We begin by describing a framework with one active flavor, and will discuss incorporating three flavors in § 2.2.2. We introduce an active (i.e. electroweak doublet) neutrino, ν, and a sterile (i.e. electroweak singlet) neutrino, N. After electroweak symmetry breaking, their masses are generated by

$$\mathcal{L}_{\rm mass} = -m_D \nu N - m_N N N + \text{h.c.} \tag{2.1}$$

As is well known, in the limit $m_D \ll m_N$, this leads to a light, mostly active neutrino, $\hat{\nu} = \nu + \theta N$, with a mass $m \simeq m_D^2/m_N$ and a heavy, mostly sterile neutrino, $\hat{N} = N - \theta \nu$,

with mass $M \simeq m_N$. (We use hats here and below to denote mass eigenstates.) The active-sterile mixing angle is $\theta \simeq \sqrt{m/M}$.

The short baseline reactor anomaly suggests oscillations between active (electron in this case) and sterile neutrinos with a mixing angle of $\mathcal{O}(0.1)$ and a squared mass splitting of $\mathcal{O}(1\ \mathrm{eV}^2)$. This can easily be accounted for by choosing $m \sim 0.01$ eV and $M \sim 1$ eV. This simple explanation of short baseline anomalies is in tension with cosmological observations because the heavy neutrino with a mass ~ 1 eV will be in thermal equilibrium at the time neutrinos decouple, due to its relatively large admixture of active neutrino [65, 66, 67, 68, 69, 70, 71, 72, 73, 74].

However, as mentioned above there are well-motivated scenarios where this conclusion does not hold. One of the simplest possibilities is when the sterile neutrino's Majorana mass depends on the value of a scalar field which we call A. Because the light neutrino mass is determined by the Majorana mass, it also depends on A, and therefore a finite density background of light neutrinos can give corrections to the potential for A. Since the density of neutrinos is determined by the temperature, these corrections can cause the value of A to vary with temperature (or, equivalently, time, as the Universe cools).

To see this, consider the contribution at a temperature T to the energy density from the light neutrino, whose mass $m(A)$ varies with the scalar field A,

$$\delta V(A,T) = 2 \times \int \frac{d^3p}{(2\pi)^3} \frac{\sqrt{p^2 + m^2(A)}}{e^{p/T}+1}. \tag{2.2}$$

The effective potential for A is given by its zero temperature scalar potential, V_0, and the contribution from the neutrino background,

$$V(A,T) = V_0(A) + \delta V(A,T). \tag{2.3}$$

We first consider a logarithmic scalar potential [63],

$$V_0 = \Lambda^4 \log\left(1 + \left|\frac{A}{\sigma}\right|\right), \tag{2.4}$$

with σ small compared to the range of relevant A values. We will discuss a quadratic potential in § 2.4 when we introduce the SUSY version of theory. Taking the light neutrino

to be relativistic, the full scalar potential at finite T is

$$V(A,T) = \Lambda^4 \log\left(1 + \left|\frac{A}{\sigma}\right|\right) + \frac{m^2(A)\,T^2}{24} + \mathcal{O}\left(m^4(A)\right). \tag{2.5}$$

We assume, quite generally, that the sterile neutrino mass has A-dependent and -independent terms,

$$m_N(A) = m_0 + \kappa A. \tag{2.6}$$

In this case, the light neutrino mass is $m_\nu(A) = m_D^2/(m_0 + \kappa A)$, resulting in an effective potential of

$$V(A,T) = \Lambda^4 \log\left(1 + \left|\frac{A}{\sigma}\right|\right) + \frac{m_D^4 T^2}{24\,(m_0 + \kappa A)^2}. \tag{2.7}$$

The first term tends to push the scalar field toward smaller values, while the second (the importance of which increases at high T) prefers larger values of A; the interplay of the two determines the value of A that minimizes the effective potential. At high temperatures, κA can be large compared to m_0. When this is the case, minimizing the effective potential results in $A \propto T$ so that the heavy (mostly sterile) neutrino tracks the temperature, $M \propto T$. The light neutrinos mass is therefore smaller at large temperatures, $m_\nu \propto T^{-1}$. At some temperature, κA becomes comparable to m_0. A then moves toward its minimum as determined by V_0 and the neutrino masses approach the temperature-independent values $M \simeq m_0$ and $m \simeq m_D^2/m_0$.

We illustrate this behavior in Fig. 2.1, showing the neutrino masses and A as functions of temperature for $\Lambda = 3.4 \times 10^{-2}$ eV, $m_D = 0.22$ eV, $m_0 = 1$ eV, and $\kappa = 10^{-6}$. Although the heavy neutrino's mass chosen to be 1 eV today, it is always large compared to the temperature so that its number density is exponentially suppressed and it has no cosmological impact. Correspondingly, the light neutrino mass grows until it reaches a present-day value of 0.05 eV around $T = 0.1$ eV. Since the active neutrino becomes non-relativistic after its mass becomes independent of temperature it will act as having a mass $m \simeq m_D^2/m_0 = 0.05$ eV with regards to its impact on cosmology. The active-sterile mixing angle is $\theta \simeq \sqrt{m/M} = 0.2$ today and decreases like T^{-1} for $T > 0.1$ eV.

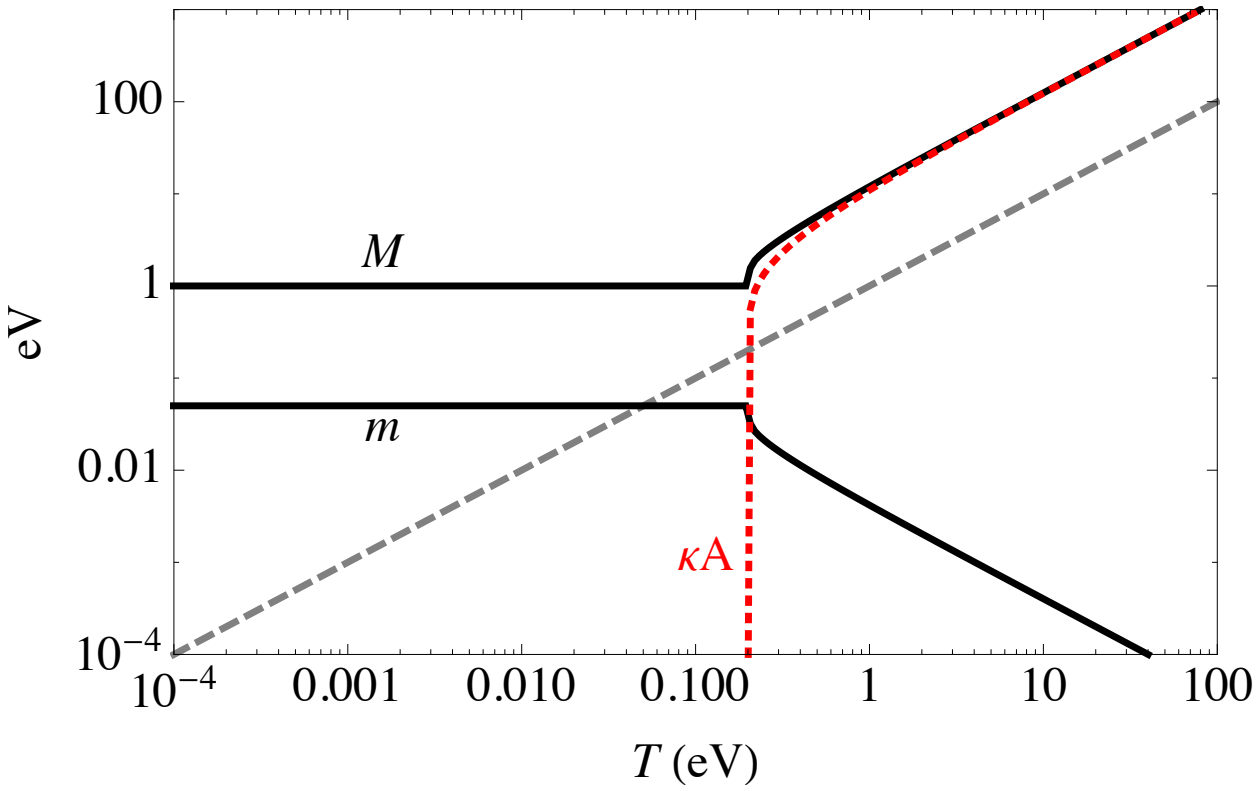

Figure 2.1: Mostly active and mostly sterile neutrino masses, m and M respectively, (solid, black) as functions of the temperature for a logarithmic scalar potential of Eq. (2.4) with $\Lambda = 3.4 \times 10^{-2}$ eV. The Majorana mass depends on the scalar field A as in Eq. (2.6) with $m_0 = 1$ eV and $\kappa = 10^{-6}$. The Dirac mass is taken to be $m_D = 0.22$ eV. Also shown is the value of κA, (dotted, red). For convenience, the gray, dashed line shows where the mass is equal to the temperature.

2.2.2 Including three active neutrinos

Expanding this simple scenario to incorporate three active flavors so that the broad range of neutrino oscillation data can be described is straightforward. The Dirac and Majorana masses become matrices,

$$\mathcal{L}_{\rm mass} = -m_{D\alpha i}\nu_\alpha N_i - m_{Nij}N_iN_j + \text{h.c.}, \tag{2.8}$$

where $\alpha = e, \mu, \tau$ labels the active flavors while i, j label the sterile neutrinos (there must be at least two to generate the solar and atmospheric mass splittings). For definiteness, we use three sterile neutrinos. In the basis where $m_{Nij} = m_{Ni}\delta_{ij}$ is diagonal and taking a Dirac mass matrix of the form

$$m_D = \begin{pmatrix} -\sqrt{\frac{2}{3}}\,\bar{m}_1 & \sqrt{\frac{1}{3}}\,\bar{m}_2 & 0 \\ \sqrt{\frac{1}{6}}\,\bar{m}_1 & \sqrt{\frac{1}{3}}\,\bar{m}_2 & \sqrt{\frac{1}{2}}\,\bar{m}_3 \\ \sqrt{\frac{1}{6}}\,\bar{m}_1 & \sqrt{\frac{1}{3}}\,\bar{m}_2 & -\sqrt{\frac{1}{2}}\,\bar{m}_3 \end{pmatrix} \tag{2.9}$$

leads to light neutrinos, $\hat{\nu}_i$, with masses $m_i = \bar{m}_i^2/m_{Ni}$ and a light neutrino mixing matrix, U, that is approximately tribimaximal.[1] The effective potential in Eq. (2.5) now reads

$$V(A,T) = \Lambda^4 \log\left(1 + \left|\frac{A}{\sigma}\right|\right) + \sum_i \frac{m_i^2(A)\,T^2}{24}, \tag{2.10}$$

where the sum runs over each of the light neutrinos.[2] Allowing the sterile neutrino masses to depend on the scalar via $m_{Ni} = m_{0i} + \kappa_i A$ results in heavy, mostly sterile neutrinos with masses $M_i \propto T$ at large T and $M_i \simeq m_{0i}$ at low temperatures. This pattern of couplings results in three active-sterile mixing angles $\theta_i \simeq \sqrt{m_i/M_i}$. Just as in the simple one-flavor case described above, in the early Universe the light, mostly active neutrinos have masses that scale like T^{-1} while the heavy mostly sterile neutrinos' masses go like the temperature, kinematically blocking their production, rendering them cosmologically unimportant.

---

[1] Deviating from exact tribimaximal mixing to accommodate the data, in particular $U_{e3} \neq 0$, is easy to accomplish by modifying the texture of the Dirac mass matrix slightly.

[2] For now, the temperature-dependent contributions to the effective potential only matter when each of the light neutrinos is relativistic so we do not have to worry about whether the neutrino background is unstable when they go nonrelativistic, as discussed in [75]. We return to this point in § 2.2.3.

The mass splittings $\Delta m^2_{ij} = m^2_i - m^2_j$ can be fixed to have present-day values of $\Delta m^2_{21} = \Delta m^2_{\odot} \simeq 7.5 \times 10^{-5}$ eV^2 and $|\Delta m^2_{31}| = \Delta m^2_{\rm atm} \simeq 2.4 \times 10^{-3}$ eV^2. If we wish to explain the short-baseline reactor anomaly, then we are forced to take $m_1 \simeq m_2 \sim \mathcal{O}(0.01 - 0.1 \text{ eV})$ (and most naturally $M_1 \simeq M_2 \sim 1$ eV) since the anomalies involve either electron neutrino appearance or disappearance and only $\hat{\nu}_1$ and $\hat{\nu}_2$ have appreciable admixtures of ν_e. The third light neutrino, $\hat{\nu}_3$, can either be taken to be much lighter than the other two, which requires $m_1 \simeq m_2 \simeq \sqrt{\Delta m^2_{\rm atm}} \simeq 0.05$ eV, or roughly degenerate with $\hat{\nu}_{1,2}$, with $m_{1,2,3} \sim 0.1$ eV. The mixing angle controlling electron neutrino disappearance is then $\theta_{ee} \simeq \theta_{1,2} \sim 0.1$, as needed to explain the reactor anomaly. Electron (anti)neutrino appearance data is more difficult to fit in this model because the $\nu_\mu \to \nu_e$ probability is suppressed by the typical factor of $\theta^4_{1,2}$ [38, 39] as well as by a further factor of $\theta^2_{13} \ll 1$.

2.2.3 Acceleron as dark energy

In the simple model above, the scalar field A is no longer held away from its true vacuum value. Consequently, it has no connection to dark energy. Here, we describe a way of modifying the model above to allow for one of the light neutrinos to continue holding A, the "acceleron," away from its true vacuum value, allowing for an explanation of the dark energy we observe. Explaining dark energy was the original motivation for the mass-varying neutrino scenarios we have been considering [63, 64]. This dark energy explanation assumes that the true cosmological constant is zero for some reason that does not show up in new particle physics, as in Ref. [76]. We do not address why the true cosmological constant is zero—for a discussion of this problem see review articles such as Refs. [77, 78, 79].

We will begin with the three-flavor model with a logarithmic scalar potential described above, but assume that the A-independent contributions to the sterile neutrino Majorana masses are negligible, $m_{0i} = 0$ so that $m_{Ni} = \kappa_i A$ (as before, we work in a basis where the Majorana mass matrix is diagonal). We use a Dirac mass matrix as given in Eq. (2.9) and will be assuming that $\hat{\nu}_1 \propto 2\nu_e - \nu_\mu - \nu_\tau$ and $\hat{\nu}_2 \propto \nu_e + \nu_\mu + \nu_\tau$ are nearly degenerate (as before we assume a tribimaximal mixing matrix). We now add Majorana masses for the

active neutrinos of the form

$$\mathcal{L}_{\rm mass} \supset -\mu \left[\nu_e \nu_e + \frac{1}{2} \left(\nu_\mu + \nu_\tau \right)^2 \right] + \text{h.c.} \tag{2.11}$$

This gives a common Majorana mass of μ for $\hat{\nu}_1$ and $\hat{\nu}_2$. Such masses could be generated by integrating out another set of Majorana sterile fermions (that do not couple strongly to A). Given a hierarchy between the Dirac masses and the sterile Majorana masses, the heavy neutrino masses are simply $M_i \simeq \kappa_i A$ and the masses of the the light, mostly active neutrinos are $m_1 \simeq m_2 \simeq \left| \mu - \bar{m}_{1,2}^2 / \kappa_{1,2} A \right|$ and $m_3 \simeq \bar{m}_3^2 / \kappa_3 A$. The active-sterile mixing angles are $\theta_i \simeq \bar{m}_i / M_i$.

An important consideration in in this scenario is the instability to collapse which occurs when a neutrino becomes nonrelativistic [80, 75]. These nonrelativistic neutrinos form "nuggets" and are no longer a cosmologically relevant background when computing the effective potential of the acceleron. Hence, they no longer help to "hold up" the acceleron vacuum expectation value (vev). In the Appendix A we show details of the calculation of the temperature at which this instability develops.

Because of this, we work with an inverted hierarchy $m_3 \ll m_{1,2}$; the lightest neutrino is responsible for supporting A today, while the heavier two, which have an appreciable admixture of electron neutrino, provide for oscillations into sterile neutrinos with $\Delta m^2 \simeq 1$ eV^2. In this case, at high temperatures when all of the light neutrinos are relativistic, the sum in the effective potential of Eq. (2.10) runs over $i = 1, 2, 3$ and $\hat{\nu}_1$ and $\hat{\nu}_2$ are dominantly responsible for keeping the acceleron away from its true minimum. Minimizing the potential then leads to $A \propto T^2$. At some point after $\hat{\nu}_1$ and $\hat{\nu}_2$ go nonrelativistic, the sum in Eq. (2.10) only includes $i = 3$. The value of A that minimizes the effective potential is determined by $\hat{\nu}_3$, so that $A \propto T$. We show the masses of the neutrinos as functions of the temperature in Fig. 2.2, setting $\mu = -0.05$ eV, $\bar{m}_{1,2} = 0.1$ eV, $\bar{m}_3 = 0.031$ eV, $\kappa_{1,2} = 1$, $\kappa_3 = 3.3$, and $\Lambda = 9.3 \times 10^{-5}$ eV. As shown in the Appendix A, given these parameters, $\hat{\nu}_{1,2}$ stop supporting the A vev at $T \simeq 1.8 \times 10^{-4}$ eV. Note that due to the presence of a Majorana mass for the active neutrinos, the conclusion of Ref. [81] where a cascade of "nugget" formation occurs

after the heaviest neutrino goes nonrelativistic does not apply.

To get a vacuum energy density $\sim 10^{-11}$ eV^4 requires a very large value for the logarithm in the scalar potential. This could perhaps be most natural in a scenario where a dilaton-like field, ϕ, is the dynamical origin of the A-dependent contribution to the Majorana mass and $A = A_0 \exp(\phi^2/f^2)$. Another possibility is a more conventional quintessence model with an acceleron Compton wavelength on the order of the Hubble scale. In such a model neutrino masses evolve but do not collapse to form nuggets, even when nonrelativistic. In this case the light neutrinos can be quite massive today, of order an eV.[3] The effects of such massive MaVaNs on CMB and structure has been explored in Ref. [82].

2.3 A logarithmic potential and active neutrinos at an eV

We now turn to the question of whether the observed *active* neutrinos can have masses around an eV today.

Neutrinos can free stream over cosmological distances and thus damp perturbations on a scales smaller than the free streaming scale. For standard neutrinos with the sum of their masses $\Sigma m_\nu \sim 1$ eV this effect is observable via suppression of the matter power spectrum on scales smaller than free streaming scale. The larger the neutrino masses the larger the energy density contained in them around matter radiation equality when structures start to grow. Hence, the damping of the matter power spectrum on scales smaller than the free streaming scale is more pronounced as the masses of the neutrinos is increased. Large scale structure surveys which are sensitive the matter power spectrum can therefore put an upper limit on Σm_ν (for details, see, e.g. Ref. [83]).

However, mass-varying neutrinos can act like massless neutrinos during and after matter-radiation equality and become massive at much lower redshifts. Here we construct a phenomenologically viable scenario using the framework described in § 2.2, with a logarithmic scalar potential for the field A. For simplicity let us consider the case of one active and one

[3]The neutrinos' masses locally today in this case would be smaller due to the relative overdensity of neutrinos in our galaxy cluster.

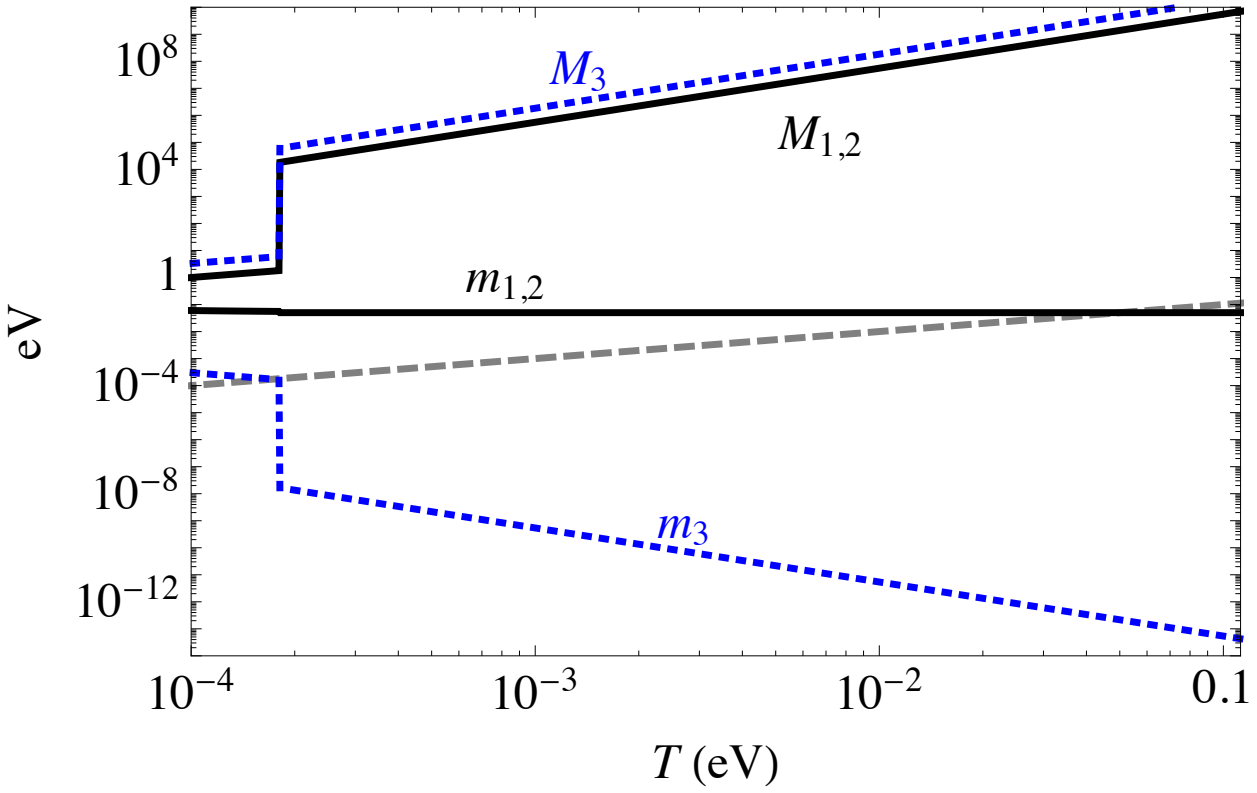

Figure 2.2: Mostly active and mostly sterile neutrino masses, m_i and M_i respectively, as functions of the temperature for a logarithmic scalar potential of Eq. (2.4), with $\Lambda = 9.3 \times 10^{-5}$ eV, in the case where $\hat{\nu}_{1,2}$ have (equal) nonzero, A-independent Majorana masses, $\mu = -0.05$ eV. The sterile neutrino Majorana masses are $m_{Ni} = \kappa_i A$ with $\kappa_{1,2} = 1$, $\kappa_3 = 3.3$. The Dirac masses are $\bar{m}_{1,2} = 0.1$ eV, $\bar{m}_3 = 0.031$ eV. The gray, dashed line shows where the mass is equal to the temperature. $\hat{\nu}_{1,2}$ no longer contribute to the effective A potential when $T \lesssim 1.8 \times 10^{-4}$ eV (see Appendix A for details).

sterile neutrino, leading to an effective potential like that in Eqs. (2.5) and (2.7). Generalizing this, as in § 2.2.2, to three flavors (that are nearly degenerate since we will be describing active neutrinos with a mass around an eV today) is straightforward. We assume that $m_0 = 0$ in Eq. (2.6). At high temperatures when the light neutrino is relativistic, minimizing the potential in Eq. (2.7) leads to a light, mostly active, neutrino of mass $m(T) \simeq \sqrt{12}\Lambda^2/T$ and a heavy, mostly sterile neutrino with mass $M(T) \simeq m_D^2 T/\sqrt{12}\Lambda^2$. As mentioned in the previous section the light neutrinos condense to form "nuggets" after going nonrelativistic and stop supporting the scalar field, which settles to its minimum at $A = 0$. We show in the Appendix A that this occurs when $T \simeq m(T)/10$. The energy density stored in the cosmological neutrinos is now stored in the nuggets which redshift like like matter. The active and sterile neutrinos now form a Dirac fermion of mass m_D which is independent of the temperature and can be much larger than the mass of the light neutrinos when they went nonrelativistic.

In order to illustrate our point let us consider $m_D = 1$ eV and $\Lambda = 10^{-3}$ eV. We plot the light neutrino mass vs. temperature in Fig. 2.3. As can be seen, the neutrino acts effectively massless around matter-radiation equality. After the neutrino becomes nonrelativistic at $T \sim \Lambda$ it stops supporting the acceleron. The sterile and active neutrinos now form a Dirac fermion of mass m_D which is now independent of temperature. This is the mass that is relevant for terrestrial neutrino mass experiments, e.g., searches for endpoints in β-decay spectra. However the relevant mass of the neutrino from the standpoint of experiments which measure the matter power spectrum can be approximated to be the mass when the neutrino becomes nonrelativistic, i.e. $m \sim \Lambda \ll m_D$.

To see this in further detail we show the energy density stored in the neutrinos (and "nuggets" after their formation) as the temperature varies in Fig. 2.4. We also show the energy density of a *constant* 0.1 eV mass neutrino, which is roughly the upper limit on $\sum m_\nu/3$ from cosmological observations. We see that the energy density in the mass-varying neutrino in this case is never greater than that in the constant 0.1 eV neutrino. Indeed, the *temperature-dependent* energy density in the mass varying neutrino is roughly what one

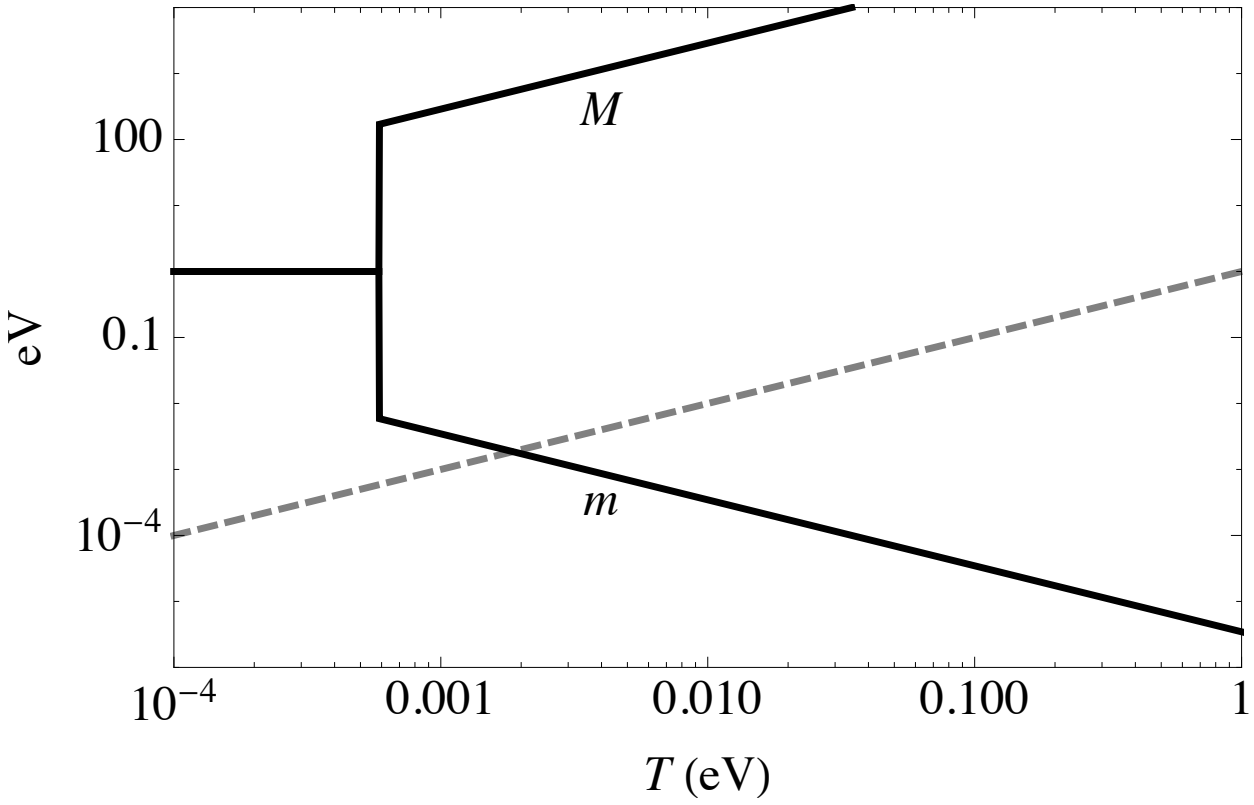

Figure 2.3: The masses of the light, mostly active and heavy, mostly sterile neutrinos, m and M respectively, in a single active flavor scheme as a function of temperature for $m_0 = 0$, $m_D = 1$ eV, and $\Lambda = 10^{-3}$ eV. When $T \simeq m/10$, the light neutrino ceases supporting the A vev and the sterile Majorana mass vanishes. The sterile and active neutrinos then form a Dirac fermion.

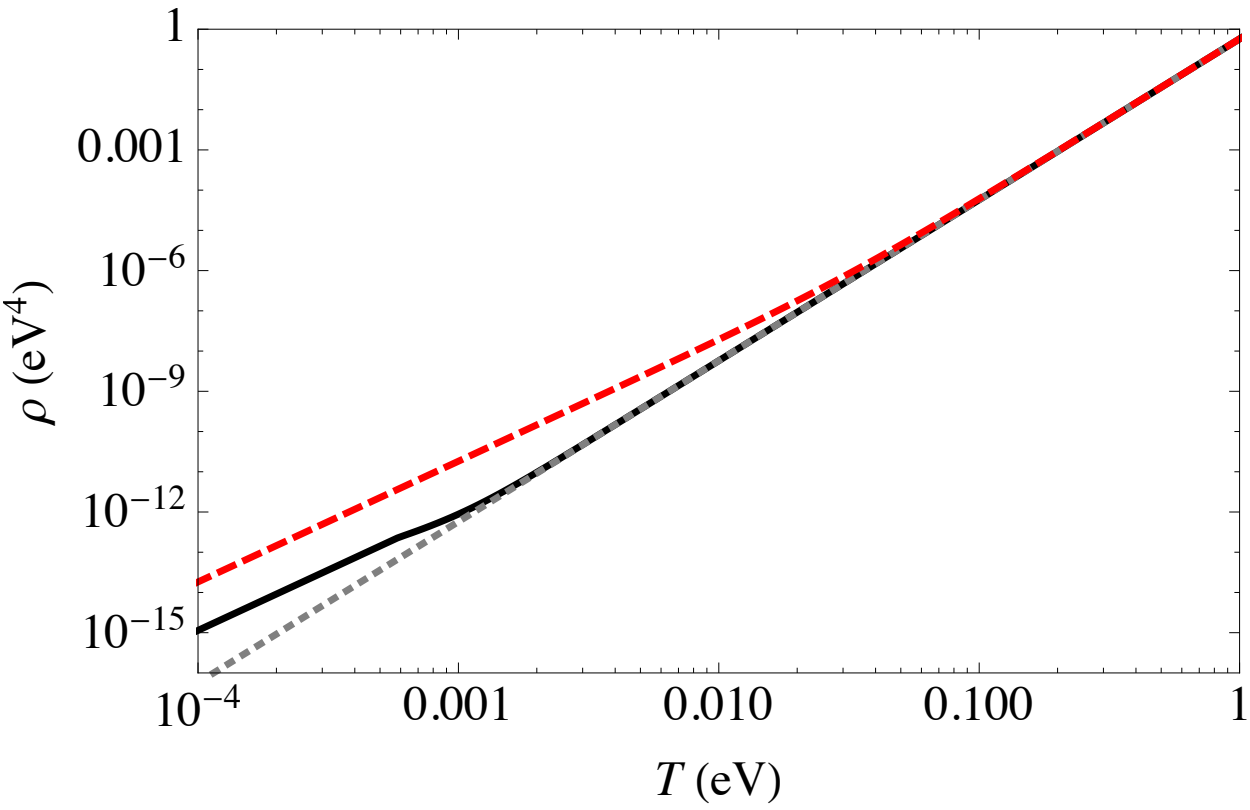

Figure 2.4: The neutrino energy density as a function of temperature for $m_0 = 0$, $m_D = 1$ eV, and $\Lambda = 10^{-3}$ eV (solid, black). Also show are the energy densities for *constant* mass neutrinos of mass 0.1 eV (dashed, red) and zero (dotted, gray).

would find for a constant mass neutrino of mass $\sim \Lambda = 10^{-3}$ eV.

A signal of this mechanism would be detection of an eV scale neutrino mass in tritium beta decay of [43, 44], but with no signature in double beta decay or in searches for massive cosmological neutrinos [45, 46, 47], since the cosmological neutrinos would be clustered and it is unlikely that we would be inside a nugget.

2.4 The Model: SUSY MaVaNs

MaVaNs theories can be made supersymmetric [64, 84], which is well motivated by the necessity of including a light scalar. In this case, however, the scalar potential is constrained to be quadratic in the acceleron field, and not logarithmic as we have so far considered. Dark energy may be obtained via the acceleron-sneutrino coupling, which creates an effective sneutrino potential with a minimum which differs from the vacuum configuration.

Let us begin by briefly describing the supersymmetric MaVaNs theory of a single active neutrino. The superpotential of this theory after electroweak symmetry breaking is

$$W = \kappa\, ann + m_D \nu n, \tag{2.12}$$

where ν, n, and a are the superfields containing the active neutrino, sterile neutrino, and acceleron respectively. Including both SUSY-preserving and -breaking interactions, the scalar potential is

$$\begin{aligned} V_{\text{scalar}} =& {\mu_{\tilde{N}}}^2 \left|\tilde{N}\right|^2 + m_A^2 \left|A\right|^2 + 4\kappa^2 \left|A\right|^2 \left|\tilde{N}\right|^2 \\ &+ \kappa^2 \left|\tilde{N}\right|^4 + \text{const.}, \end{aligned} \tag{2.13}$$

with $\tilde{N}$ the sterile sneutrino and the constant such that the true minimum of the potential is at $V_{\text{scalar}} = 0$. Radiative corrections drive ${\mu_{\tilde{N}}}^2$ to negative values of order $-m_D^2$, which means that $\langle \tilde{N} \rangle = \sqrt{-{\mu_{\tilde{N}}}^2/2\kappa^2} \sim \mathcal{O}\left(m_D/\kappa\right)$ at the true minimum of the potential. As before, the acceleron field is driven to large values at finite temperature due to the contribution to the effective potential from the light neutrino density. If $A > \sqrt{-{\mu_{\tilde{N}}}^2/4\kappa^2} \sim \mathcal{O}\left(m_D/\kappa\right)$ then the sneutrino is trapped at a local minimum with energy density ${\mu_{\tilde{N}}}^4/4\kappa^2 \sim \mathcal{O}\left(m_D^4/\kappa^2\right)$.

The effective potential that determines the finite-temperature value of the acceleron is

$$\begin{aligned} V(A,T) &= m_A^2 \left|A\right|^2 + \frac{m^2(A)\,T^2}{24} \\ &= m_A^2 \left|A\right|^2 + \frac{m_D^4 T^2}{24\kappa^2 \left|A\right|^2}, \end{aligned} \tag{2.14}$$

where we have assumed that the neutrino mass matrix is of the seesaw form. Minimizing this results in

$$A(T) = \frac{m_D}{24^{1/4}} \sqrt{\frac{T}{\kappa m_A}}, \tag{2.15}$$

in contrast to the case of a logarithmic potential where $A \propto T$.

The acceleron mass term receives SUSY-breaking radiative corrections and, in the absence of fine tuning, we expect $m_A^2 \gtrsim \kappa^2 m_D^2$. Therefore, to keep the sneutrino in the false minimum today when $T = T_0 \simeq 10^{-4}$ eV requires that $m_D \lesssim T_0$ in a natural theory.

We now discuss how to extend this treatment to the case of three active neutrinos which means that the couplings κ and m_D are now matrices. As in Ref. [64], a viable set of parameters involves the acceleron vev being held up by the lightest neutrino, which remains relativistic today. To connect with short-baseline anomalies, it is phenomenologically motivated to take an inverted mass hierarchy, so that the smallest neutrino mass is m_3. Like in § 2.2.2, we work in a basis where the matrix $\kappa_{ij} = \kappa_i \delta_{ij}$ is diagonal and the Dirac mass matrix is of the form in Eq. (2.9). We take the Dirac mass corresponding to the lightest neutrino to be $\bar{m}_3 = 10^{-5}$ eV and $\kappa_3 = 10^{-5}$. This gives a present-day dark energy density of the correct order of magnitude $\sim 10^{-11}$ eV^4.

To avoid having to fine-tune away large radiative contributions to the acceleron mass coming from the neutrinos of larger mass, we take $\kappa_{1,2} \ll \kappa_3$. (We will state more precise values for $\kappa_{1,2}$ below.) If this is the end of the story for the neutrino masses, then $\hat{\nu}_{1,2}$ are essentially Dirac fermions containing the active and sterile neutrinos orthogonal to $\hat{\nu}_3$ and $\hat{N}_3$, which does not allow for any mass splitting in this system ~ 1 eV. To fix this we can add an acceleron-independent contribution to the sterile neutrino masses as we did in § 2.2 through the superpotential term $W \supset m_{N_{ij}} n_i n_j$ which leads to terms in the scalar

potential $m_{N\,ij}^2 \tilde{N}_i \tilde{N}_j^*$. If we assume that the terms in this mass matrix involving $i, j = 3$ are suppressed and the nonzero eigenvalues of this matrix are $\mathcal{O}(1\text{ eV})$, then there will be a pair of a sterile neutrinos mass of around an eV, allowing for a oscillations of the active neutrinos with $\Delta m^2 \simeq 1\text{ eV}^2$. Furthermore, the contribution to the scalar potential from $m_{N\,ij}$ pushes $\tilde{N}_{1,2} \to 0$, simplifying the analysis of the scalar potential which is then essentially that of a single sterile state as in Eq. (2.13), involving only the acceleron and $\tilde{N}_3$. Describing atmospheric neutrino oscillations then requires $\bar{m}_1 \simeq \bar{m}_2 \simeq 0.22$ eV so that $m_1 \simeq m_2 \simeq 0.05$ eV.

Because, as we see in Eq. (2.15), $A \propto \sqrt{T}$, the sterile neutrinos are not kinematically forbidden from being produced in the early Universe, unlike the case of the logarithmic potential. This could be in strong conflict with cosmological bounds and furthermore a large sterile neutrino density will affect the acceleron potential, driving the acceleron to small values, ruining this mechanism as an explanation of the dark energy. This can be simply avoided by a Planck-suppressed coupling of the acceleron to electrons, $\mathcal{L} \supset \beta_e (m_e/M_{\rm Pl}) A \bar{e} e$, where β_e is a coupling and $M_{\rm Pl}$ is the Planck mass, as described in Ref. [85]. Fifth force tests limit $|\beta_e| \lesssim 4$. At temperatures above the electron mass, the (mostly) neutrino masses are roughly

$$M_i \simeq 3\text{ MeV}\beta_e \left(\frac{\kappa_i}{10^{-10}}\right)\left(\frac{T}{1\text{ MeV}}\right)^2\left(\frac{10^{-11}\text{ eV}}{m_A}\right)^2. \tag{2.16}$$

As previously mentioned, the acceleron receives quantum corrections and in a natural theory we expect $m_A^2 \gtrsim \sum_i \kappa_i^2 \bar{m}_i^2$. For the values of $\bar{m}_3$ and κ_3 given above, an acceleron mass of around 10^{-11} eV requires a modest 10% fine tuning and limits $\kappa_{1,2} \lesssim \mathcal{O}(10^{-4}\kappa_3) \sim 10^{-9}$. Production of sterile neutrinos at $T \gtrsim$ MeV is therefore suppressed if $\beta_e \sim \mathcal{O}(1)$, which is enough to bring the scenario into agreement with cosmological limits. For further details and constraints, see Ref. [85].

2.5 Conclusions and Outlook

In this chapter we have described several situations involving mass-varying neutrinos that allow for either active neutrinos or sterile neutrinos with a large active-sterile mixing to have masses around an eV and yet still be compatible with strong limits from cosmological observations. Along with "secret" neutrino interactions [53, 54, 55, 56, 57, 59, 48, 60, 61, 62], this possibility illustrates the necessity of combining cosmological probes of neutrino properties with terrestrial experiments. Combining both probes allows us to *test* whether neutrinos have richer structure than expected in ways that cosmological observations or terrestrial experiments alone cannot.

MaVaNs are motivated by attempts to understand dark energy. It is interesting that they can also modify neutrino cosmology to allow recent hints for eV-scale sterile neutrinos to be reconciled with cosmological observations, or for the active neutrinos to have masses within the reach of near future experiments today. In addition, it is worth mentioning that unlike the case of other "secret" neutrino interactions, the (mostly) sterile neutrinos in this scenario with a logarithmic potential are kinematically forbidden from being produced at late times, and therefore do not suffer from the problem that they are produced in late-time collisions, upsetting agreement with cosmological observations [86].

The requirement of a light scalar field for the MaVaNs scenario suggests that this sector could be supersymmetric. Properly supersymmetrizing the theory adds additional constraints and requires introducing very weak couplings of this light field to charged fermions in order to make the sterile neutrinos heavy at early times. Besides cosmological observations and neutrino experiments, these weak couplings offer perhaps the best way of testing the scenario, through, e.g., searches for fifth forces at large distance scales [87] or electron-density–dependent neutrino masses [88, 89].

Interactions between light scalars and active neutrinos can prevent active neutrinos from freely streaming and lead to observable signatures in the CMB [90, 91, 92, 93, 94]. In the scenarios we have considered, the active neutrino-scalar coupling is too small to be constrained

by these considerations. It would be interesting to study such CMB signatures and their complementarity with other terrestrial observables in nonstandard neutrino scenarios.

We have extended earlier work on MaVaNs to take into account the effects of neutrino clustering, to add additional contributions to neutrino mass and additional couplings in the scalar sector. We have been able to exhibit models in which eV mass sterile neutrinos appear in present day neutrino oscillation experiments but do not affect precision cosmology, and in which active neutrinos could have eV scale masses today but not in the early universe.

Neutrino masses, inflation, dark matter, baryogenesis, and dark energy all show that there must be new physics beyond the standard model. We do not know the energy scale, but neutrino masses and dark energy indicate a physical scale of order $10^{-4} - 10^{-2}$ eV. It would be remiss of us to simply adopt theoretical prejudice and assume that such new physics does not involve any new light particles. If there is such new physics, then precision cosmology and laboratory measurements are not necessarily simply different ways of measuring the same neutrino properties. As an illustration of the possibilities, in this chapter we have explored models containing light sterile neutrinos coupled to a light scalar in which laboratory and cosmological measurements which would give seemingly inconsistent results can instead be interpreted as evidence for a new light sector, which could be the origin of dark energy.

Chapter 3

MASS VARYING NEUTRINOS: EFFECT ON COSMOLOGICAL PARAMETERS

The standard model of cosmology (ΛCDM) describes cosmological data rather well. In ΛCDM the energy density of the universe has five components: cold dark matter, baryons, photons, neutrinos, and dark energy . Although neutrinos are assumed to be very light in ΛCDM it is a fairly straightforward extension to consider the case of more massive neutrinos. Since ΛCDM is such a good fit to the observed data, it is hard to concoct a model that changes significantly the evolution of the components of the total energy density at or before recombination. An alternative is to change the behavior of the components after recombination, preferably at late times, so that the CMB spectrum and distance to surface of last scattering are not significantly affected.

The fact that at present times the dark energy density is of the same order of that of dark matter ($\rho_{CDM}/\rho_\Lambda = 1/3$) is called the 'cosmic coincidence problem'. We also have other 'coincidences' in the fact that the other components of energy density i.e. baryons, photons, and neutrinos were also comparable to dark energy within a redshift of a few z. This problem is puzzling because all the different components of the energy density redshift differently. The behavior of dark energy is not known at very high redshifts, but we know it redshifts very slowly at from z = 1 to present times ($\omega \approx$ -1). If we assume that dark energy really is the cosmological constant i.e. ω = -1 throughout history then we have the coincidence problem mentioned above. On the other hand we can make dark energy 'track' one of the other components such as dark matter or baryons until recent times after which dark energy switches to redshifting very slowly. Dark matter and baryons are consistent with redshifting as $1/a^3$ since recombination. We can track baryons even further back to

BBN. Hence it will be hard to postulate a model where dark energy tracks dark matter or baryons until recent times because that will only replace the coincidence problem with the 'why now' problem, i.e. why did the dark energy stop tracking these components only recently. Neutrinos offer more possibilities as the present energy density of neutrinos is not measured. We know that three species of neutrinos were relativistic at BBN until fairly recently, since non relativistic neutrinos act as hot dark matter and tend to erase structure on smaller scales. In ref. [63] it was proposed that dark energy density tracks neutrino energy density, assuming that neutrino mass is not a fixed quantity but rather a dynamical one. If neutrinos couple to a light scalar field scalar field called the acceleron, the scalar field effective potential is a function of the neutrino number density. For a broad range of acceleron potentials the acceleron evolves adiabatically, tracking the minimum of its effective potential, with the neutrino mass also evolving. Depending on the form of the acceleron potential, the neutrino-acceleron fluid together may produce 'dark energy' which can explain the observed acceleration of the universe. Since the effective potential and hence the neutrino mass are a function of the number density, the model is called mass varying neutrinos or MaVaNs.

The aim of the present chapter is to study the impact of MaVaNs on cosmology, particularly the CMB spectrum. This will help us study the viability of MaVaNs as a theory and constrain its parameter space.

The next section discusses MaVaNs, their properties and some relations pertaining to their behavior. For more details and derivations consult [63].

3.1 Introduction

Mass Varying Neutrinos are neutrinos whose mass varies as a function of their number density and hence as a function of the scale factor. In one implementation of the theory the SM neutrinos get their mass from coupling to a sterile neutrino, which in turn gets its mass from the vev of a scalar field the 'acceleron'. As the universe expands the sterile neutrino gets lighter and the SM neutrinos get heavier due to the to the see-saw mechanism. It can be shown [63] that when the neutrinos are non relativistic the effective potential for the

MaVaNs-acceleron fluid is given by

$$V(m_\nu) = m_\nu n_\nu + V_0(m_\nu) \tag{3.1}$$

where V_0 is the acceleron potential. The minimum of this potential is given by

$$V^{'}(m_\nu) = n_\nu + V_0^{'}(m_\nu) \tag{3.2}$$

The equation of state is then given by

$$\omega + 1 = -\frac{\delta log V}{3\delta log a} = \frac{m_\nu n_\nu}{V} = \frac{-m_\nu V_0^{'}(m_\nu)}{V(m_\nu)} \tag{3.3}$$

where we have used Eq. 3.2 to get the second and third equality. If we assume a power law dependence for the acceleron potential as a function of mass with a small exponent ($V_0(m_\nu)$ $\propto$ ${m_\nu}^{-k}$) then we get

$$\omega = \frac{-1}{1+k} \tag{3.4}$$

Assuming that ω scales slowly with the scale factor, using Eq. 3.2 we can show that when the neutrinos are non relativistic

$$m_\nu \propto a^{-3\omega} \tag{3.5}$$

We can also show that when the neutrinos are relativistic their mass scales as follows

$$m_\nu \propto a^{-(3\omega+1)/2} \tag{3.6}$$

If ω = -1 as in the case of a cosmological constant then the SM neutrinos have a mass inversely proportional to their number density when non relativistic.

A potential problem with this theory is that when neutrinos become nonrelativistic an instability may develop where the neutrinos clump on small scales, with the inter clump distance being large compared with the acceleron Compton wavelength, in which case the acceleron field is no longer smooth and no longer acts as dark energy [75]. We assume that such an instability does not develop, which can be arranged either by an acceleron potential which is sufficiently flat, or a semi relativistic neutrino coupled to the acceleron [64].

Thus in this theory the neutrino mass becomes important only during recent times i.e. z $\approx$ few, depending on the present mass of the neutrino. Even if the neutrino mass today is several eV, the neutrinos are nearly massless during recombination and the mass does not directly affect the CMB spectrum. Indirectly, however, if h is held constant, the MaVaNs theory would have a different distance to the last scattering which would change the position of the acoustic peaks. It is therefore necessary to refit the cosmological parameters in the MaVaNs theory in order to obtain accord with the CMB fluctuation spectrum.

In Fig. 3.1 we have plotted comparisons of ρ_ν for ΛCDM and MaVaNs for different neutrino masses to compare how the neutrino energy density should vary in the two theories. In figure 2 we have plotted how neutrinos with the same mass but different ω vary as a function of the scale factor in the MaVaNs theory. It might seem that we are violating the terrestrial bounds on Σm_ν. However studies of gravitational clustering of massive neutrinos in the background of dark matter halos find significant overdensities can occur, thus possibly reducing the neutrino mass as measured by terrestrial experiments [95] relative to the mass influencing larger scale cosmology.

Note that the sterile neutrinos introduced in the MaVaNs theory do not affect cosmology as they are much heavier and out of thermal equilibrium at high redshift. Terrestrial evidence for sterile neutrinos with properties which would otherwise be incompatible with cosmology would be evidence in favor of MaVaNs[85].

Going back to Eq. 3.3 we can see for $\omega \neq$ -1 the dark energy can also vary as a function of the scale factor. We find the quintessence energy density goes as follows in the non relativistic neutrino regime

$$V_0(m_\nu) \propto m_\nu^{-k} \propto a^{-\frac{3k}{1+k}} \tag{3.7}$$

As can be seen for $\omega =$ -1 i.e $k = 0$ V_0 is a constant. But for $\omega \neq$ -1 we get the acceleron potential to depend on the scale factor giving rise to varying dark energy density.

In our implementation of the MaVaNs neutrinos, the neutrinos act like matter after becoming non relativistic and are still influencing the evolution of dark energy.

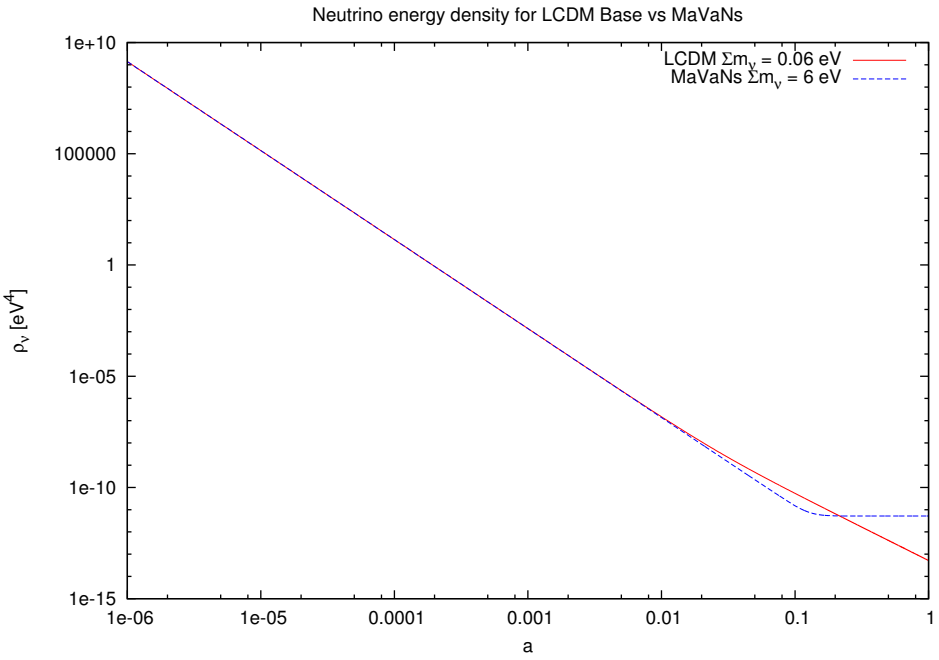

Figure 3.1: Evolution of energy density for neutrinos in ΛCDM as compared to MaVaNs with ω = -1. 'a'= $1/(1+z)$ is the scale factor.

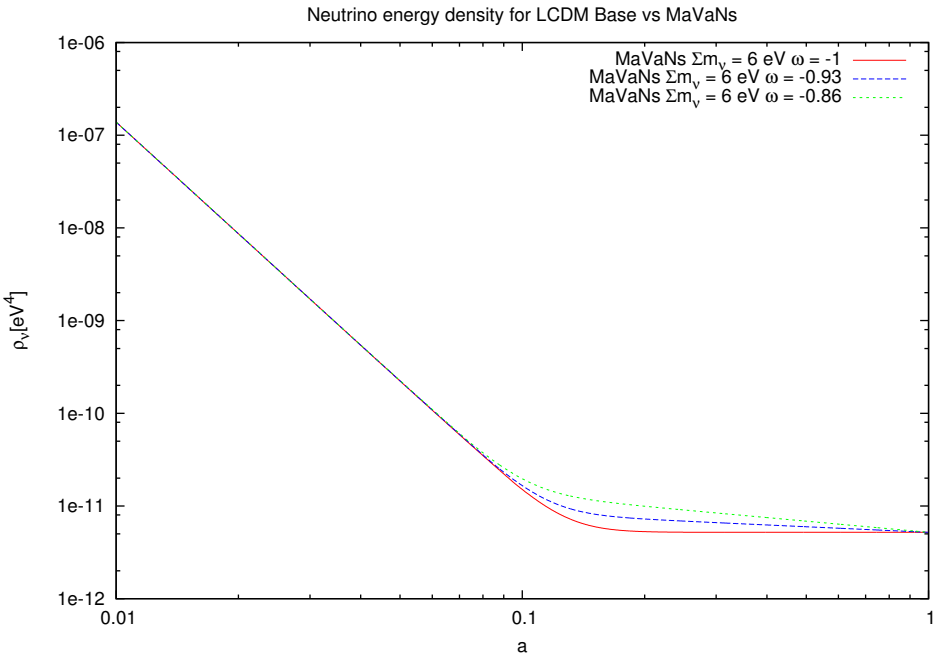

Figure 3.2: Evolution of energy density for MaVaNs neutrinos with $\Sigma m_\nu = 6$ eV but with ω = -1, -0.93, -0.86.

3.2 Implementation of MaVaNs Cosmology

We used the Planck Likelihood calculator for the range $50 \leq l \leq 2500$ to find our base ΛCDM model which was implemented using the publicly available code CMBEASY. We used a Metropolis algorithm to vary $\Omega_m h^2$, $\Omega_b h^2$, h and the scalar amplitude A_s to find our best fit parameters. We however kept $\tau = 0.0925$ and $n_s = 0.9624$ which are the best fit values obtained by Planck[96]. We assumed a flat universe and Ω_Λ was set such that $\Omega_{total} = 1$. We also have $\Sigma m_\nu = 0.06$ eV and $N_{eff} = 3.046$. For our best fit values for the base model, we obtained $\Omega_m h^2 = 0.1385$, $\Omega_b h^2 = 0.02197$, $h = 0.686$ and $\sigma_8 = 0.8237$. These are somewhat different from the best fit values obtained by Planck [96]. We attribute this to the fact that we are using a different code to calculate the CMB anisotropy (CMBEASY as opposed to CAMB) and possibly somewhat different nuisance parameters (see the Appendix A for the list of nuisance parameters). The fact that our best fit model is somewhat different from Planck's best fit model does not affect the main point of the study, which is trying to compare different MaVaNs cosmologies with a base ΛCDM cosmology.

We implemented MaVaNs cosmology by making modifications to CMBEASY. Different MaVaNs cosmologies are parametrized by having different ω and Σm_ν. We found the best fit values for each of the MaVans cosmologies by following the same likelihood minimization procedure above.

For the cases where $\omega \neq -1$ we use the Quintessence class in CMBEASY. Since CMBEASY dosen't have a class that models the MaVaNs potential, the specific potential we use is the inverse power law and we tune the exponent of our power law to give us dark energy density that we would expect from MaVaNs. Although we cannot get an exact MaVaNs like behavior for the quintessence energy density, we demand that they have similar values from $z = 0$ to $z \approx 4$ after which the Dark Energy is subdominant compared to matter. Fig. 3.3 and 3.4 illustrate the fact that the inverse power law is a good approximate fit to what we would expect from MaVaNs.

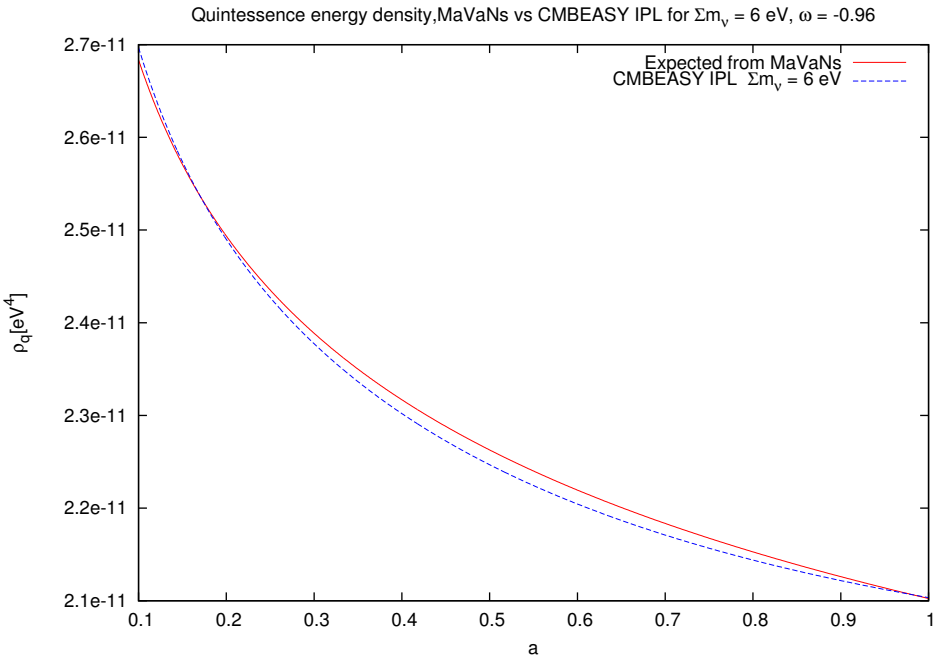

Figure 3.3: Expected quintessence energy density from MaVaNs for ω = -0.96 to that obtained from the inverse power law potential in CMBEASY. The exponent of the power law has been tuned such that the energy densities are very similar until about $a = 1/(1+z) = 0.2$.

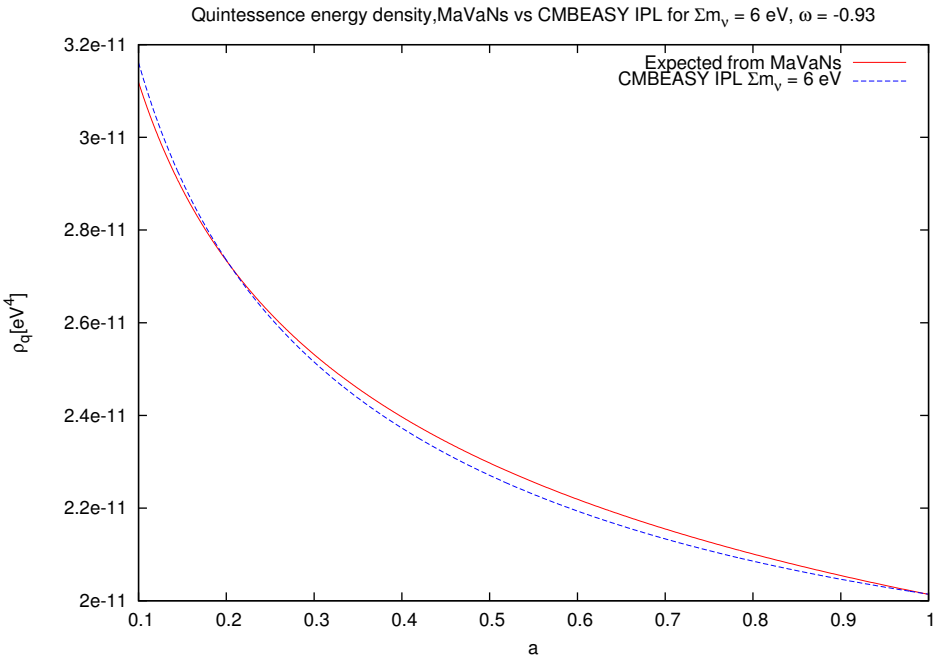

Figure 3.4: Expected quintessence energy density from MaVaNs for ω = -0.93 to that obtained from the inverse power law potential in CMBEASY. The exponent of the power law has been tuned such that the energy densities are very similar until about $a = 1/(1+z) = 0.2$.

3.3 Analysis of MaVaNs Cosmology

To compare the temperature power spectrum of a best fit MaVaNs model to the base ΛCDM model consult Fig. 3.5. As can be clearly seen the two spectra agree everywhere except at very low l, where the base MaVaNs spectrum gives a much larger D_l than the base ΛCDM spectrum. The low l spectrum is plotted in Fig. 3.6.

The low l modes are affected by the late time ISW effect, which is increased because we have neutrinos which are acting like a significant amount of warm dark matter, and therefore less dark energy. We can potentially use this late time ISW effect to put bounds on the current neutrino mass. However we first have to account for the cosmic variance.The cosmic variance of the quadrupole is given by $\Delta D_2 = 0.63 D_2$. The error bars which are mostly due to cosmic variance have been plotted in Fig. 3.6. As can be seen both the ΛCDM and MaVaNs with $\Sigma m_\nu = 6$ lie outside the 1σ error bars. Although it is true that the discrepancy is slightly pronounced for MaVaNs with $\Sigma m_\nu = 6$ as compared to ΛCDM, it still does not contribute significantly more to $\Delta\chi^2$. Moreover, the mechanism that is causing the low l anomaly for ΛCDM, such as running of the spectral tilt, will affect MaVaNs as well making the MaVaNs spectrum for low l and in better concordance with observations. For these reasons we consider $\Sigma m_\nu = 6$ to be an acceptable present day neutrino mass.[1]

We have tabulated our results for the cosmological parameters of various cosmologies in 3.1. Since we are scanning the parameter space over 4 parameters, the criterion for the error bars is that the log likelihood should not be more than 2.38 lower compared to the best fit model. This gives us our 68% bounds. $\Omega_b h^2$ and $\Omega_m h^2$ have not been listed because they were not found to change significantly with the model. This makes sense since the neutrinos in both cosmologies are effectively massless at and before recombination. This implies that recombination must have happened at the same redshift in either theory and hence ρ_b and

[1]Here we have only considered the quadrupole since looking at Planck data the effects of the ISW effect will be most pronounced for $l = 2$. In practice we should consider all multipoles with $l \leq 50$ that we have so far neglected in our likelihood calculations. These have been left for future studies and in principle will help put an upper bound on MaVaNs masses.

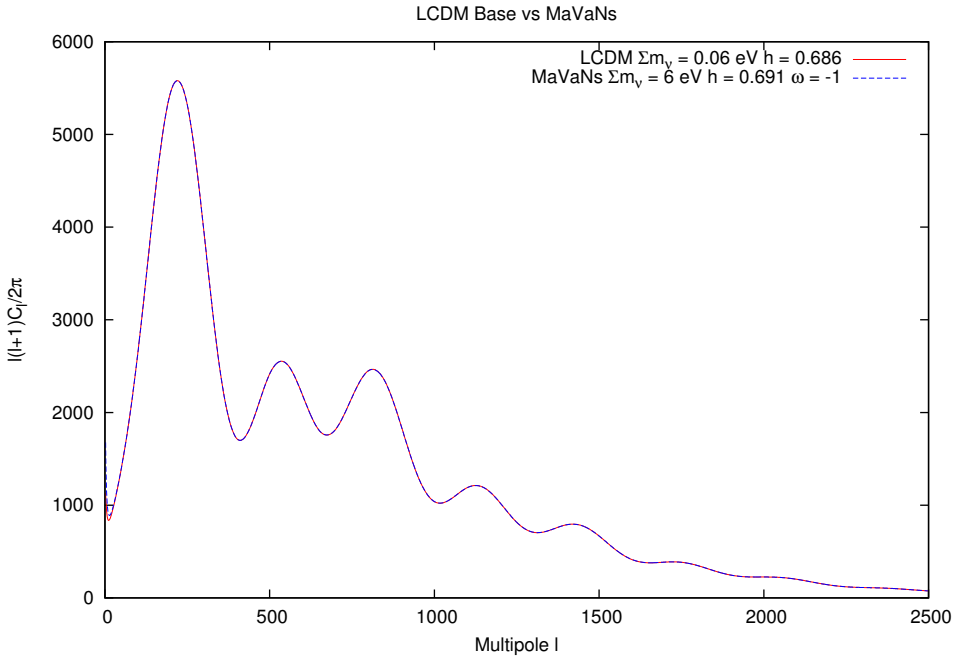

Figure 3.5: The red curve shows the best fit temperature spectrum for our base ΛCDM cosmology.The blue curve show the best fit temperature spectrum for a MaVaNs cosmology with ω = -1 and Σm_ν = 6 eV.As we can see the two curves agree really well for most values of l except for the very low l.

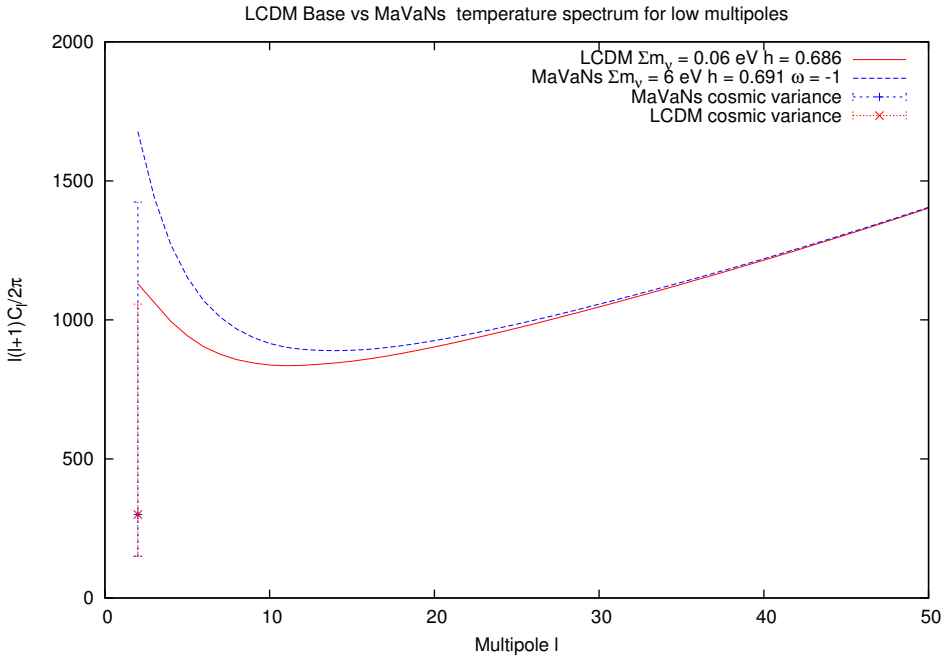

Figure 3.6: This is same as Fig. 3.5 except for low l modes. The red curve shows the best fit temperature spectrum for our base ΛCDM cosmology.The blue curve show the best fit temperature spectrum for a MaVaNs cosmology with ω = -1 and Σm_ν = 6 eV. Their corresponding error bars for the quadrupole are also shown. The two curves are different for $l \leq 10$ but start concurring as we go higher in l.

ρ_m should be the same at recombination and hence throughout history in both cosmologies. This is also what we see in our likelihood fits. The only parameters that change significantly within cosmologies are H_0 and σ_8. H_0 is different between MaVaNs and base ΛCDM since the distance to last scattering is different in both theories for the same H_0 which will result in shifting in the position of the acoustic peaks. Thus H_0 has to be tuned in MaVaNs to get the correct distance to last scattering. The H_0 decreases with increasing ω. For ω = -1, the best fit H_0 is slightly higher than the ΛCDM base model. For ω = -0.93 it is already significantly lower that ΛCDM base model. So as to not increase the tension between CMB measurements of H_0 and other measurements of H_0, ω lower than -0.93 is probably not feasible.

3.3.1 Possible Application to the σ_8 discrepancy in Planck

The Planck Collaboration recently reported their results of the measurement of the anisotropy of the CMB background [96] and found it to be consistent with ΛCDM Cosmology. They reported the measured value of the RMS fluctuations of matter density in linear theory today to be

$$\sigma_8 = 0.834 \pm 0.027(68\%; Planck, \Sigma m_\nu = 0.06eV) \tag{3.8}$$

One can also determine the RMS fluctuations of the matter density by measuring cluster counts as a function of redshift. The Planck Collaboration measured this function from the Sunyaev-Zeldovich (SZ) effect on the CMB photons along whose line of sight the clusters lie. They used a sample of 189 clusters for whom the signal-to-noise ratio was more than seven. They found that the number of clusters in each red shift bin was significantly smaller than what you would expect from ΛCDM cosmology. They measured the RMS value of the matter density fluctuations to be [31]

$$\sigma_8 = 0.77 \pm 0.02 \tag{3.9}$$

in tension with the value derived from the temperature spectrum.

One way to reduce this tension would be to have a higher neutrino mass. However in

Table 3.1: Tabulated below are the values of cosmological parameters for different cosmologies. We do not quote $\Omega_m h^2$ and $\Omega_b h^2$, because they don't change significantly with the cosmology and have a best fit values around 0.0220 and 0.1385 respectively. The quantities in brackets give the best fit parameters.

Cosmology	ω	Σm_ν (eV)	h	σ_8
ΛCDM	-1	0.06	0.6855 ± 0.0125 (0.686)	0.824 ± 0.013 (0.824)
MaVaNs	-1	3.00	0.691 ± 0.013 (0.691)	0.820 ± 0.013 (0.820)
MaVaNs	-1	6.00	0.691 ± 0.012 (0.691)	0.806 ± 0.012 (0.807)
MaVaNs	-0.96	3.00	0.681 ± 0.012 (0.680)	0.8135 ± 0.0125 (0.814)
MaVaNs	-0.96	6.00	0.678 ± 0.014 (0.680)	0.801 ± 0.013 (0.799)
MaVaNs	-0.93	3.00	0.6715 ± 0.0125 (0.672)	0.8075 ± 0.0125 (0.807)
MaVaNs	-0.93	6.00	0.669 ± 0.013 (0.672)	0.793 ± 0.013 (0.792)

ΛCDM cosmology increasing the neutrino mass decreases significantly the value of Hubble's constant in order to get a good fit to the temperature power spectrum which increases the already existing tension between H_0 as measured by Planck and other experiments[96].

In order to resolve this issue we need to be able to change the matter power spectrum without affecting the temperature power spectrum. MaVaNs are a candidate for this purpose since they act as effectively massless during recombination but become massive later acting as warm dark matter. As evidenced by 3.1 using MaVaNs we can get a significant decrease in σ_8 as calculated in linear theory without changing h significantly.

3.4 Conclusion

We have shown when the other cosmological parameters are allowed to vary , a good fit can be obtained to the temperature fluctuation spectrum, even though the neutrino mass and hence the neutrino energy density become important at late times. The only cosmological

parameters affected are H_0 (to match the distance to last scattering) and σ_8. We find that we can obtain a significantly smaller σ_8 in MaVaNs as compared to ΛCDM without changing H_0 very much. Hence MaVaNs are a possible solution to Planck σ_8 discrepancy. Including the low l data in the likelihood calculation will help us put upper bounds on the current neutrino mass. We leave this for future studies.

An interesting corollary to these results is that in MaVaNs theories, CMB data do not constrain possible neutrino mass results in terrestrial experiments. A discrepancy between the neutrino mass as determined from the CMB fits and the neutrino mass determined locally would be strong evidence for MaVaNs.

The σ_8 that we have calculated here has been done in linear theory. Structure formation simulations which include mass varying neutrinos are called for to establish these results conclusively.

Chapter 4

MATTER ANTI-MATTER ASYMMETRY: BARYOGENESIS VIA MESINO OSCILLATIONS

Baryogenesis, the explanation for the asymmetry between matter and antimatter in our universe, is a profound puzzle for particle physics, as well as one of the strongest motivations for extending the standard model (SM). The first proposed solution, by Sakharov in 1967, laid out three conditions for a successful resolution to the puzzle [97]. The first condition, C and CP violation, is satisfied by a CP-violating phase in the CKM matrix of the SM, however the effects of this phase are too suppressed in the early universe to produce a sufficient asymmetry. The second condition, violation of baryon number, is satisfied by anomalous electroweak processes which are sufficiently fast at high temperature to produce baryon number [98, 99, 100, 101, 102], but only if the third condition, departure from thermal equilibrium, is satisfied. The minimal SM with a Higgs boson at 125 GeV does not have any phase transition or sufficiently long-lived heavy particles to produce a sufficient departure from thermal equilibrium for baryogenesis [103, 104, 105, 106, 107, 108].

In most supersymmetric extensions of the standard model, cosmology theory favors a low reheat scale after inflation [109, 110, 111, 112, 113, 114, 115, 116]. Furthermore, in many theories, the absence of observed isocurvature perturbations favors a low inflation scale [116, 117, 118, 119, 120, 121, 8]. A low inflation or reheat scale would imply that the baryogenesis scale must also be low, in some cases as low as an MeV. Although proposals for baryogenesis at scales as low as an MeV exist [122, 123], the time scale at this epoch is relatively long compared to typical particle physics scales, making departure from thermal equilibrium difficult to arrange. Models which do depart from thermal equilibrium at these low scales then produce additional entropy which dilutes the baryon abundance. In addition,

CP violation at these low scales, if large enough to produce enough baryon number to survive the dilution, can easily lead to particle electric dipole moments which are in conflict with experimental bounds. Finally, low energy baryon number violation can lead to rare decays in conflict with observation. It is therefore difficult to produce enough baryons at low energy while satisfying experimental constraints, motivating the exploration of new mechanisms for low scale baryogenesis, particularly ones which enhance the quantum mechanical interference which is necessary for CP violation.

In the SM the CP-violating phase is unphysical if any of the small mixing angles or like-sign quark mass differences vanish. A reparameterization-invariant measure of CP violation [124] in the SM is thus very tiny. Nevertheless, the SM does provide a wealth of large CP-violating asymmetries in the decays of oscillating neutral mesons, illustrating the efficiency of oscillations for enhancing the effects of CP-violating phases. A proposal [125] that a similar enhancement of CP violation could occur during an electroweak phase transition was shown not to work due to the too rapid rate of thermal decoherence [126, 127].

In this paper we present a new baryogenesis mechanism. We show how in an extension of the SM, the particle-antiparticle oscillations of *mesinos* [128, 129] (bound states of a fermion quark and a scalar antiquark or vice versa), when combined with baryon-violating scalar decays, can give rise to baryogenesis. The scalar quark, whose mass is of order a TeV, is produced by the out of equilibrium decays of a long lived heavy neutral fermion, below the QCD hadronization scale but before nucleosynthesis. Both the oscillation rate and the decay rate of the mesinos are rapid when compared with the decoherence time, allowing quantum mechanical interference between particle and anti particle decays to produce substantial CP violation. This mechanism for producing baryons is amusingly similar to the mechanism for CP-violating production of charged leptons in the neutral kaon system. We will illustrate the mechanism in a simplified model which introduces a minimal number of new particles beyond the SM. Our mechanism and the new particles could be part of a supersymmetric extension of the SM with baryon-number–violating R-parity violation.

The organization of the paper is as follows. In Sec. 4.1 we introduce the model, describing

the CP-violating oscillations of the mesino.

4.1 Model and Phenomenon

The ingredients we need for our model are a complex scalar ϕ and n Weyl fermions N_i. ϕ is a color triplet, $\mathrm{SU}(2)_L$ singlet, and carries hypercharge $-1/3$. Each N_i is taken to be a singlet under the SM gauge group. The relevant interactions of these are

$$\mathcal{L} \supset y_{ij}\phi\,\bar{d}_i N_j - \frac{1}{2}m_{Nij}N_i N_j + \alpha_{ij}\phi^*\bar{d}_i\bar{u}_j + \text{c.c.} \tag{4.1}$$

$\bar{u}_i$ and $\bar{d}_i$ are the left handed up and down-type singlet antiquarks, respectively, with the subscript labeling the generation. Another possible baryon-number–violating interaction of ϕ, $\phi\, q_i q_j$, where the q_i are quark doublets, is neglected because we are considering only the interactions that could come from baryon-number–violating interactions in a supersymmetric theory where ϕ is a superpartner of a down-type singlet quark. By rotating and rephasing the N_i we can make the singlet mass matrix m_N real and diagonal. α_{ij} is a 3×3 matrix containing nine complex parameters, with seven phases removable by reparameterizations. The remaining phases in this matrix do not play a role in our baryogenesis mechanism and will be ignored for the rest of the paper. Having exhausted our freedom to rephase the fields, each of the elements in the $3 \times n$ matrix y_{ij} contains a physical, CP-violating imaginary component.

We will see that the simplest version of the model involves three new Weyl fermions, i.e. $n = 3$, which we label in order of their masses, $m_{N_1} < m_{N_2} < m_{N_3}$. The colored scalar is produced in the early Universe by late, out-of-equilibrium decays of N_3. The scalar forms color-singlet bound states with SM quarks, termed mesinos, which undergo particle-antiparticle oscillations and decay. The two lighter singlets provide common intermediate on- and off-shell states for the mesino and antimesino that allow for them to violate CP (and baryon number) in the interference between decays with and without mixing, sourcing the baryon asymmetry of the Universe.

In the following sections we discuss mesino-antimesino oscillation in this model and the

constraints from collider experiments and precision measurements.

4.1.1 Mesino oscillations and decay

At temperatures below the QCD hadronization scale, $T_c \simeq 200$ MeV, if the colored scalars are sufficiently long-lived, they will bind with light SM quarks to form mesinos and antimesinos. In analogy with the naming convention for mesons, we will refer to the (electrically neutral) mesino containing ϕ^* and $q = d, s, b$ as Φ_q with its antiparticle $\bar{\Phi}_q$ containing ϕ and $\bar{q} = \bar{d}, \bar{s}, \bar{b}$.

Φ_q and $\bar{\Phi}_q$ form a pseudo-Dirac fermion and, as discussed in Ref. [130], the system can be described using a two-state Hamiltonian containing dispersive and absorptive parts, just like the case of the neutral mesons,

$$\boldsymbol{H} = \boldsymbol{M} - \frac{i}{2}\boldsymbol{\Gamma}. \tag{4.2}$$

The eigenstates of $\boldsymbol{H}$, with eigenvalues $\omega_{L,H}$, can be given in terms of the flavor eigenstates $|\Phi_q\rangle$ and $|\bar{\Phi}_q\rangle$,

$$|\Phi_{L,H}\rangle = p|\Phi_q\rangle \pm q|\bar{\Phi}_q\rangle, \tag{4.3}$$

with L and H referring to light and heavy. The complex numbers p and q are related by

$$\left(\frac{q}{p}\right)^2 = \frac{\boldsymbol{M}_{12}^* - (i/2)\,\boldsymbol{\Gamma}_{12}^*}{\boldsymbol{M}_{12} - (i/2)\,\boldsymbol{\Gamma}_{12}}. \tag{4.4}$$

The mass and width differences between $|\Phi_L\rangle$ and $|\Phi_H\rangle$ are

$$\Delta m = m_H - m_L = \mathrm{Re}\left(\omega_H - \omega_L\right), \tag{4.5}$$

$$\Delta\Gamma = \Gamma_H - \Gamma_L = -2\mathrm{Im}\left(\omega_H - \omega_L\right), \tag{4.6}$$

with

$$\omega_H - \omega_L = 2\sqrt{\left(\boldsymbol{M}_{12} - \frac{i}{2}\boldsymbol{\Gamma}_{12}\right)\left(\boldsymbol{M}_{12}^* - \frac{i}{2}\boldsymbol{\Gamma}_{12}^*\right)}. \tag{4.7}$$

In the scenario we will study, the mass difference is small compared to the masses of the heavy and light eigenstates,

$$m_H \simeq m_L \simeq \frac{m_H + m_L}{2} \equiv m_{\Phi_q}. \tag{4.8}$$

Furthermore, the mass of the mesino is mostly supplied by the ϕ, $m_{\Phi_q} \simeq m_\phi$. As in the case of meson oscillations, it is often useful to introduce a dimensionless parameter to characterize the oscillation rate,

$$x \equiv \frac{\Delta m}{\Gamma}, \tag{4.9}$$

where $\Gamma = (\Gamma_H + \Gamma_L)/2$ is the average lifetime of the states. $x \gg 1$ indicates that the mesino system oscillates rapidly before decaying while $x \ll 1$ means that the mesino typically decays before oscillating much.

We use $|\Phi_q(t)\rangle$ to label a state at time t that began at $t = 0$ as a pure mesino and $|\bar{\Phi}_q(t)\rangle$ to label one that began as a pure antimesino. These evolve in time according to

$$|\Phi_q(t)\rangle = g_+(t)\,|\Phi_q\rangle - \frac{q}{p} g_-(t)\,|\bar{\Phi}_q\rangle, \tag{4.10}$$

$$|\bar{\Phi}_q(t)\rangle = g_+(t)\,|\bar{\Phi}_q\rangle - \frac{p}{q} g_-(t)\,|\Phi_q\rangle, \tag{4.11}$$

with

$$g_\pm(t) = \frac{1}{2}\left(e^{-im_H t - \frac{1}{2}\Gamma_H t} \pm e^{-im_L t - \frac{1}{2}\Gamma_L t}\right). \tag{4.12}$$

The baryon-number–violating operator $\phi^* \bar{d}_i \bar{u}_j$ and its conjugate in Eq. (4.1) allow for the mesino and antimesino flavor eigenstates to decay to collections of hadrons with baryon number $B = +1$ and $B = -1$, respectively, with amplitudes related by complex conjugation. In terms of the time-independent amplitude for a mesino to decay to a state with $B = +1$, $\mathcal{M}$, the time-dependent amplitudes for initial mesino or antimesino states to decay to $B = \pm 1$ (denoted B and $\bar{B}$) are

$$\begin{aligned}
\langle B|\Phi_q(t)\rangle &= g_+(t)\,\mathcal{M}, \\
\langle \bar{B}|\Phi_q(t)\rangle &= -\frac{q}{p} g_-(t)\,\mathcal{M}^*, \\
\langle B|\bar{\Phi}_q(t)\rangle &= -\frac{p}{q} g_-(t)\,\mathcal{M}, \\
\langle \bar{B}|\bar{\Phi}_q(t)\rangle &= g_+(t)\,\mathcal{M}^*.
\end{aligned} \tag{4.13}$$

Squaring these and integrating over t, we can find the probability that an initial mesino state decays to B and $\bar{B}$,

$$P_{\Phi_q \to B} \propto \int_0^\infty dt \left|\langle B|\Phi_q(t)\rangle\right|^2, \tag{4.14}$$

$$P_{\Phi_q \to \bar{B}} \propto \int_0^\infty dt \left|\langle \bar{B}|\Phi_q(t)\rangle\right|^2, \tag{4.15}$$

and similarly for an initial antimesino. Using these expressions, we write down the baryon asymmetry per mesino-antimesino pair,

$$\epsilon_B = A_B \times \mathrm{Br}_{\Phi_q \to B}, \tag{4.16}$$

where

$$A_B = \frac{P_{\Phi_q \to B} - P_{\Phi_q \to \bar{B}} + P_{\bar{\Phi}_q \to B} - P_{\bar{\Phi}_q \to \bar{B}}}{P_{\Phi_q \to B} + P_{\Phi_q \to \bar{B}} + P_{\bar{\Phi}_q \to B} + P_{\bar{\Phi}_q \to \bar{B}}}. \tag{4.17}$$

and $\mathrm{Br}_{\Phi_q \to B} = \Gamma_{\Phi_q \to B}/\Gamma$ is the (time-independent) branching ratio of a mesino flavor eigenstate to decay into a state with $B = +1$. In terms of the elements of $\boldsymbol{H}$, A_B is

$$A_B = \frac{2\mathrm{Im}\boldsymbol{M}_{12}^* \boldsymbol{\Gamma}_{12}}{\Gamma^2 + 4\left|\boldsymbol{M}_{12}\right|^2}. \tag{4.18}$$

To get a sense of how large the asymmetry ϵ_B can be, we estimate the magnitudes of the elements that appear in it below.

Estimating $\mathbf{M}_{12}$

The leading contributions to $\boldsymbol{M}_{12}$ in the Φ_q-$\bar{\Phi}_q$ system arise from the diagrams in Fig. 4.1, resulting in [129, 128]

$$\boldsymbol{M}_{12} = \sum_i \boldsymbol{M}_{12}(N_i) = \frac{2f_{\Phi_q}^2}{3} \sum_j \frac{y_{qi}^2 m_{N_i}}{m_{N_i}^2 - m_{\Phi_q}^2}, \tag{4.19}$$

where we have written the contribution from each N_i as $\boldsymbol{M}_{12}(N_i)$.

The mesino decay constant f_{Φ_q} can be related to the B meson decay constant [131],

$$f_{\Phi_q} = f_{B_q} \sqrt{\frac{m_b}{m_\phi}} \left(\frac{\alpha_s(m_b)}{\alpha_s(m_t)}\right)^{6/23} \left(\frac{\alpha_s(m_t)}{\alpha_s(m_\phi)}\right)^{6/21}. \tag{4.20}$$

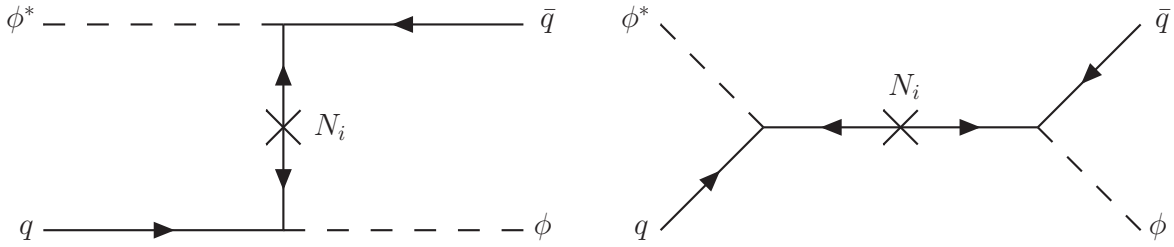

Figure 4.1: Tree level contributions to $\boldsymbol{M}_{12}$.

The cosmology of the model will motivate focusing on the strange mesino; to estimate its decay constant, we use $f_{B_s} = 225$ MeV [132], $\overline{\text{MS}}$ quark masses, $m_b = 4.18$ GeV, $m_t = 160$ GeV [133], and leading order QCD running (the contribution of which is negligible above the top mass in this case), and find

$$f_{\Phi_s} \simeq 21.5 \text{ MeV} \sqrt{\frac{650 \text{ GeV}}{m_\phi}}. \tag{4.21}$$

In what follows, we will take $q = s$, specifying to the case of the strange mesino, Φ_s.

Estimating Γ *and* $\boldsymbol{\Gamma}_{12}$

As mentioned above, the operator $\phi^* \bar{d}_i \bar{u}_j$ in Eq. (4.1) allows for the mesino to decay to a collection of hadrons with $B = +1$ with a rate

$$\Gamma_{\Phi_s \to B} = \frac{1}{16\pi} \sum_{i,j} |\alpha_{ij}|^2 \, m_{\Phi_s} = \frac{\alpha_B^2}{16\pi} m_{\Phi_s}, \tag{4.22}$$

where we assume that we can ignore the masses of the hadrons in the final state in comparison to the mesino's and we have defined $\alpha_B^2 \equiv \sum_{i,j} |\alpha_{ij}|^2$.

In general, the mesinos can also decay to a singlet plus hadrons, $\Phi_q \to N_j + h$ where h labels the hadronic state, through the operator $\phi \bar{d}_i N_j$ with a rate proportional to $|y_{ij}|^2$. This is kinematically allowed for $m_{\Phi_q} > m_{N_j} + m_h$. If h is self-conjugate under C ($h = \pi^0, \pi^+\pi^-, \rho, \dots$) then this is a final state for antimesino decay as well, leading to a nonzero value of $\boldsymbol{\Gamma}_{12}$ and CP violation through Eq. (4.18). This CP asymmetry is suppressed when

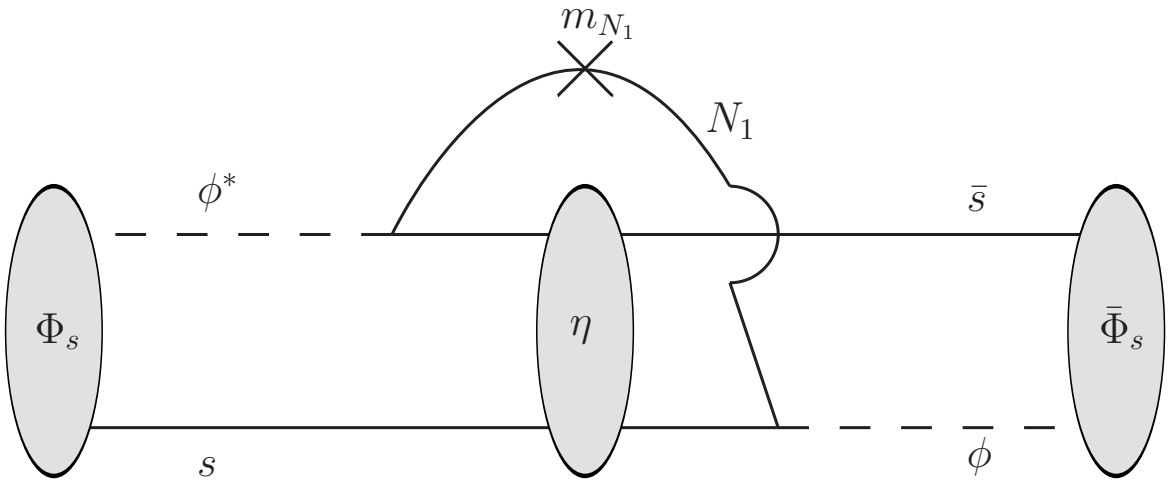

Figure 4.2: 2-body contribution to $\mathbf{\Gamma}_{12}$ from $\Phi_s, \bar{\Phi}_s \to N_1 + \eta$ where η is the lightest meson containing $s\bar{s}$.

$|\mathbf{\Gamma}_{12}|/\Gamma$ is small; for this reason we take only N_1 to be kinematically allowed in the decay of the strange mesino, and set its mass close enough to the mesino's so that single hadron final states dominate the partial width. In this case $|\mathbf{\Gamma}_{12}| \sim \Gamma_{\Phi_s \to N_1}$ and $|\mathbf{\Gamma}_{12}|/\Gamma$ can potentially be unsuppressed.

Assuming that $m_{\Phi_s} \simeq m_{N_i}$, we can approximate $\mathbf{\Gamma}_{12}$ as being dominated by the decays $\Phi_s, \bar{\Phi}_s \to N_1 + \eta$, where η is the lightest pseudoscalar meson composed of $s\bar{s}$, as shown diagrammatically in Fig. 4.2. This results in

$$\mathbf{\Gamma}_{12} \simeq \mathbf{\Gamma}_{12}^{2-\text{body}} \tag{4.23}$$

$$= \frac{y_{s1}^2 m_{N_1}}{16\pi} \left| F\left(m_{N_1}^2\right) \right|^2 \lambda^{1/2} \left(1, \frac{m_{N_1}^2}{m_{\Phi_q}^2}, \frac{m_P^2}{m_{\Phi_q}^2}\right), \tag{4.24}$$

where $\lambda(a,b,c) = a^2 + b^2 + c^2 - 2ab - 2ac - 2bc$ and $F(q^2)$ is the $\Phi_s \to P$ transition form factor at momentum transfer q. We provide estimates of the form factor $F\left(m_{N_1}^2\right)$ in Appendix B. For $m_{\Phi_s} \sim 1$ TeV with a splitting $m_{\Phi_s} - m_{N_1} \sim 1$ GeV, the form factor is $\mathcal{O}(10^{-3} - 10^{-2})$. Defining the mass splitting, $\Delta m_{\phi N_i} \equiv |m_{\Phi_s} - m_{N_i}|$ and assuming that

they are small compared to the mesino mass, the rate to decay to the lightest singlet and the off-diagonal term in the absorptive part of the Hamiltonian are given by

$$\begin{aligned}\Gamma_{\Phi_q\to N_1} \simeq |\boldsymbol{\Gamma}_{12}| \simeq 4\times 10^{-8}\ \text{GeV}\left|\frac{y_{s1}}{0.1}\right|^2 \\ \times\left|\frac{F\left(m_{N_1}^2\right)}{10^{-2}}\right|^2\left(\frac{\Delta m_{\phi N_1}}{1\ \text{GeV}}\right),\end{aligned} \tag{4.25}$$

for a scalar of mass ~ 1 TeV.

For the mesino to hadronize before decaying, the decay rate has to be slow compared to the timescale for hadronization, $\Gamma \ll 1/t_{\text{had}} \sim \Lambda_{\text{QCD}} \sim 200$ MeV. The partial width to N_1 satisfies this condition for any set of parameters we consider. Requiring that the partial width to baryons is smaller than Λ_{QCD} limits $\alpha_B \lesssim 0.1\sqrt{650\ \text{GeV}/m_\phi}$.

Simplifying the asymmetry

In the limit of small mass splittings between Φ_s and N_i, $\Delta m_{\phi N_i} \ll m_\phi$, then the contribution to $\boldsymbol{M}_{12}$ from N_i is approximately

$$\begin{aligned}|\boldsymbol{M}_{12}\left(N_i\right)| \simeq 1.54\times 10^{-6}\ \text{GeV}\left|\frac{y_{si}}{0.1}\right|^2 \\ \times\left(\frac{650\ \text{GeV}}{m_\phi}\right)\left(\frac{1\ \text{GeV}}{\Delta m_{\phi N_i}}\right),\end{aligned} \tag{4.26}$$

choosing to normalize the mass of the scalar above experimental constraints from collider searches (see Sec. 4.2.1 below). Comparing this with Eq. (4.25), we expect that, barring extreme cancellations between contributions from the different singlets, $|\boldsymbol{M}_{12}| \gg \boldsymbol{\Gamma}_{12}, \Gamma_{\Phi_q\to N_1}$.

The asymmetry per mesino pair can be written simply in terms of the oscillation parameter x in this limit. When $|\boldsymbol{\Gamma}_{12}| \ll |\boldsymbol{M}_{12}|$, $x \simeq 2\left|\boldsymbol{M}_{12}\right|/\Gamma$ and

$$\epsilon_B = \frac{x\, r\sin\beta}{1+x^2}\frac{|\boldsymbol{\Gamma}_{12}|}{\Gamma}\text{Br}_{\Phi_q\to B} + \mathcal{O}\left(\left|\frac{\boldsymbol{\Gamma}_{12}}{\boldsymbol{M}_{12}}\right|\right), \tag{4.27}$$

where

$$r \equiv \left|1 - \frac{\boldsymbol{M}_{12}\left(N_1\right)}{\boldsymbol{M}_{12}}\right|,\ 0 < r < 1, \tag{4.28}$$

and the reparameterization-invariant, CP-violating phase is

$$\beta \equiv \arg\left\{\left[\boldsymbol{M}_{12} - \boldsymbol{M}_{12}\left(N_1\right)\right]^* \boldsymbol{\Gamma}_{12}\right\}. \tag{4.29}$$

β is defined this way so as to be generically $\mathcal{O}\left(1\right)$, making use of the fact that $\boldsymbol{\Gamma}_{12}$ and $\boldsymbol{M}_{12}\left(N_1\right)$ have the same phase. If we also make use of the relation between the decay rate to a singlet and the off-diagonal term in $\boldsymbol{\Gamma}$, $|\boldsymbol{\Gamma}_{12}| \simeq \Gamma_{\Phi_q \to N_1} = \Gamma \, \mathrm{Br}_{\Phi_q \to \bar{N}_1}$ then

$$\epsilon_B \simeq \frac{x\, r \sin\beta}{1+x^2} \mathrm{Br}_{\Phi_q \to B} \mathrm{Br}_{\Phi_q \to N_1}. \tag{4.30}$$

The question of whether $|\boldsymbol{M}_{12}|$ is large or small compared to the total mesino decay rate Γ is determined by the partial width to antibaryons, $\Gamma_{\Phi_q \to B}$. If α_B is much smaller than about $10^{-4}\left|y_{s1}\right|\left(650 \text{ GeV}/m_\phi\right)$, then $|\boldsymbol{M}_{12}| \gg \Gamma_{\Phi_q \to B}$ and $x \gg 1$. Then,

$$\epsilon_B \to \frac{r}{x} \sin\beta \, \mathrm{Br}_{\Phi_q \to B} \mathrm{Br}_{\Phi_q \to N_1}. \tag{4.31}$$

In this case, by inspecting Eqs. (4.26) and (4.25), typically $x \lesssim 10^2$, depending on the hierarchy of $|\boldsymbol{\Gamma}_{12}|$ and $\Gamma_{\Phi_q \to B}$. The asymmetry is suppressed by x and a potentially small branching ratio. On the other hand, if $\alpha_B \gg 10^{-4}\left|y_{s1}\right|\left(650 \text{ GeV}/m_\phi\right)$ then $|\boldsymbol{\Gamma}_{12}| \ll |\boldsymbol{M}_{12}| \ll \Gamma_{\Phi_q \to B}$ and $x \ll 1$. The asymmetry becomes

$$\epsilon_B \to x\, r \sin\beta \, \mathrm{Br}_{\Phi_q \to \bar{N}_1}, \tag{4.32}$$

suppressed by the small values of both x and $\mathrm{Br}_{\Phi_q \to \bar{N}_1}$.

The asymmetry is typically largest when $\Gamma_{\Phi_q \to B} \simeq |\boldsymbol{\Gamma}_{12}| \ll |\boldsymbol{M}_{12}|$. In this situation Eq. (4.31) applies and $\epsilon_B \sim 10^{-2} r \sin\beta$. We note that it is possible to achieve an asymmetry as large as $\epsilon_B = 1/8$ if $\Gamma_{\Phi_q \to B} \simeq |\boldsymbol{\Gamma}_{12}| \simeq |\boldsymbol{M}_{12}|$. However, this requires large, unnatural cancellations (at the level of 10^{-2}) between the contributions to $\boldsymbol{M}_{12}$.

4.2 Experimental Constraints

4.2.1 Collider Constraints

In this model the colored scalar can be pair produced in pp and $p\bar{p}$ collisions which then decay to multijet final states. If the dominant decay mode is through the coupling $\alpha_{ij}\phi^* \bar{d}_i \bar{u}_j + \text{h.c.}$,

then ϕ will decay to two hard jets, leading to a four-jet signature. If the decay of ϕ proceeds mostly through N_1, the situation is somewhat more nuanced as we describe below.

In proton-(anti)proton collisions, the $\phi\phi^*$ pair is produced in the lab frame with very little boost in the direction transverse to the beam. The ϕ decays to a very soft light quark with a momentum of $\mathcal{O}\left(\Delta m_{\phi N_1}\right)$ and N_1 that is also essentially at rest in the ϕ rest frame, because of the small mass splitting between the ϕ and N_1. The N_1 decays through an off-shell ϕ to three quarks with a rate

$$\frac{d\Gamma_{N_1}}{dp} \simeq \sum_i \frac{|y_{i1}|^2 \alpha_B^2}{512\pi^3} \frac{p}{m_{N_1}} \left(\frac{m_{N_1} - 2p}{p + \Delta m_{\phi N_1}}\right)^2, \tag{4.33}$$

ignoring the masses of the quarks. p is the momentum of the quark produced in the $N_1 \to \phi \bar{d}_i$ splitting in the N_1 rest frame. Because of the small mass splitting, the momentum of this quark is peaked at small values—in most decays $p \lesssim \sqrt{\Delta m_{\phi N_1} m_{N_1}}$. This means that, for a splitting $\Delta m_{\phi N_1} = 1$ GeV, N_1 masses below ~ 1 TeV result in one of the three quarks in N_1 decays having a transverse momentum in the lab frame of $p_T \lesssim 30$ GeV, making them hard to observe. Therefore, at colliders, ϕ's either decay directly to two hard jets or appear as two hard jets in their decays to N_1.

To use collider searches to set limits, we will focus on the situation where the scalars are produced and decay promptly. At the Large Hadron Collider (LHC) this requires decay lengths $c\tau_\phi, c\tau_{N_1} \lesssim 1$ mm. If the ϕ's decay directly to two quarks this requires $\alpha_B \gtrsim 10^{-7}\sqrt{650 \text{ GeV}/m_\phi}$. If, instead, ϕ decays proceed through N_1, then $(\sum_i |y_{i1}|^2)^{1/2} \gtrsim 10^{-4}$, for a form factor of 10^{-2} and a mass splitting of 1 GeV and $(\sum_i |y_{i1}|^2)^{1/2}\alpha_B \gtrsim 10^{-6}\sqrt{650 \text{ GeV}/m_{N_1}}$. We will see in Sec. 4.2.2 that $|y_{b1}|$ is essentially unconstrained so this last constraint can be taken to be $\alpha_B \gtrsim 10^{-6}\sqrt{650 \text{ GeV}/m_{N_1}}$. The collider limits we will outline are relatively insensitive to the particular values of these couplings so long as they are large enough for prompt decays, given $\phi\phi^*$ production is dominated by QCD. We can also safely assume that these couplings are not so large as to make the width of ϕ large enough to impact the limits.

The requirement of prompt decays at hadron colliders is not a strict condition for the

viability of the model, but merely simplifies our analysis later; a more robust lower bound, weaker on the couplings by $\mathcal{O}(10^6)$, comes from not spoiling Big Bang nucleosynthesis (BBN). Indeed, long-lived particles at colliders have been studied as a probe of baryogenesis, see, e.g., Ref. [134]. In the long-lived case, the lower limits on the particle masses can be quite strong, as high as ~ 1 TeV [134].

A search for squarks decaying to a b and an s quark was undertaken at the LHC by the ATLAS collaboration using 17.4 fb^{-1} of 8 TeV pp collisions [135]. Squarks with masses between 100 GeV and 310 GeV were ruled out at the 95% confidence level (CL). Since they are both color triplet scalars, the production cross section for a $\phi\phi^*$ pair is equal to that of a squark-antisquark pair. Thus, this exclusion would directly apply to our model if the leading α_{ij} were α_{31} or α_{32}, and constrains $m_\phi > 310$ GeV.[1] In addition, ATLAS has searched for the pair production of scalar gluons that each decay to two gluons using 4.6 fb^{-1} collected at 7 TeV [137], finding no excess and setting an upper limit on the cross section for this process. This limit applies to ϕ in the case that it decays to a pair of light flavor quarks, which is the case if the α_{ij}, $i, j = 1, 2$ couplings dominate. Using `NLL-fast` [138, 139, 140, 141, 142] to calculate the cross section to produce a $\phi\phi^*$ pair at next-to-leading order with next-to-leading logarithmic corrections, this search sets the lower limit $m_\phi > 275$ GeV at 95% CL.

The CMS collaboration performed a search with 19.4 fb^{-1} of 8 TeV data, looking for the pair production of resonances that decay to two jets [143]. Colored scalars decaying to a b and a light flavor quark are ruled out at 95% CL for 200 GeV $< m_\phi <$ 385 GeV and those decaying to two light quarks are excluded for 200 GeV $< m_\phi <$ 350 GeV at 95% CL.

Although we expect the ϕ to decay to essentially two hard jets, as explained above, if it decays through N_1, there could be apparent six-jet events from $\phi\phi^*$ production and decay. Searches for three-jet resonances [144, 145, 146] generally have more reach than those for two-jet resonances because of the comparative ease of distinguishing this from backgrounds. In cases where these decays include heavy flavor, limits as high as 600 GeV can be set.

---

[1] A similar limit ~ 300 GeV was derived in Ref. [129] for mesinos oscillating and decaying to a top and a light quark, leading to a same-sign dilepton signal which was constrained by CMS data [136].

In light of this discussion, we consider 600 GeV as a conservative lower bound on the mass of ϕ, deferring a complete study of the collider limits for future work. For this reason, when specifying m_ϕ, we have taken 650 GeV as a benchmark value.

The prospects for future searches for $\phi \to 2j$ are promising, with a study of the 14 TeV LHC indicating that m_ϕ up to 750 GeV could be probed with 300 fb^{-1} and up to 1070 GeV with 1000 fb^{-1} [147]. Such searches would push significantly into the region of parameter space compatible with an explanation of the baryon asymmetry of the Universe, as we will see in Sec. 4.3.

4.2.2 Constraints from Rare Processes

Our model possesses new interactions which violate CP, quark flavor, and baryon number, potentially leading to observable conflicts with Standard Model predictions. In examining the consequences, we note that our model could be part of an R-parity–violating supersymmetric model [148, 149, 150, 151, 152, 153], and we could use some of the existing studies of constraints on such models [154, 155, 156, 157, 158, 159, 160, 161, 162, 163, 164, 165, 166]. The constraints on baryon-number–violating parameters in supersymmetric theories depend on many soft supersymmetry breaking parameters which play no role in baryogenesis. In this section we consider the constraints on the parameters in our more minimal model. Although baryon number is violated, given that that lepton number is conserved,[2] and given that the only fermions lighter than the proton are leptons, the proton is stable. There are stringent constraints on couplings involving the first generation from neutron-antineutron oscillations, and on baryon-violating couplings of the strange quark, from heavy nuclei decays.

Dimension-9 six quark $\Delta B = 2$ operators arise in the low energy effective theory from the diagram shown in Fig. 4.3. The relevant operators are of the form

$$\left(\sum_k \frac{y_{ik} y_{jk}}{M_{N_k}}\right) \frac{\alpha_{lm}\alpha_{no}}{m_\phi^4} \bar{d}_i \bar{d}_j \bar{d}_l \bar{u}_m \bar{d}_n \bar{u}_o \ . \tag{4.34}$$

[2] or conserved mod 2, if there are Majorana neutrino masses

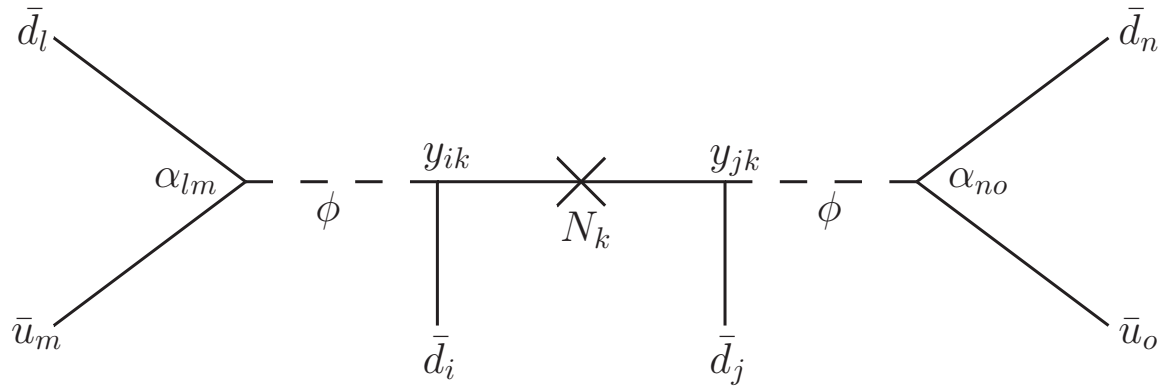

Figure 4.3: Diagram responsible for the dimension-9 $\Delta B = 2$ operator in Eq. (4.34) that leads to neutron-antineutron oscillations.

Constraints on such operators with various color and spin combinations from neutron-antineutron oscillations have been considered in many previous works [167, 168, 169, 170, 171, 163, 164, 152, 153, 172]. An accurate computation of the rate requires perturbative renormalization group scaling and matching to lattice QCD matrix element computations of the various operators [171, 173, 174, 175, 176], and currently still has uncertainties of order 1. Currently the best constraint on the neutron oscillation rate is 2.9×10^{-33} GeV [172]. If we simply estimate the matrix element of

$$\langle \bar{n}|\bar{d}\bar{d}\bar{d}\bar{d}\bar{u}\bar{u}|n\rangle \sim \mathcal{O}(10^{-5}\ \mathrm{GeV}^6)\ , \tag{4.35}$$

which is consistent with the lattice computations, we find

$$\left(\sum_k \frac{y_{dk}^2}{M_{N_k}}\right) \frac{\alpha_{11}^2}{m_\phi^4} < 2.9 \times 10^{-28}\ \mathrm{GeV}^{-5} \tag{4.36}$$

Neglecting the very weakly coupled N_3, and using $M_{N_1} \sim M_{N_2} \sim m_\phi \sim 650\ GeV$ gives

$$\left(y_{d1}^2 + y_{d2}^2\right) \alpha_{11}^2 < \mathcal{O}(10^{-14}). \tag{4.37}$$

The best constraints on operators involving strange quarks arise from limits on dinucleon decay into kaons [153, 123, 165, 177]. Using the rough estimates from Ref. [165] for the

nuclear matrix elements and the experimental bound from Ref. [177] gives a bound on the coefficient of the operator $\bar{s}\bar{s}\bar{d}\bar{d}\bar{u}\bar{u}$ which, for $M_{N_1} \sim M_{N_2} \sim m_\phi \sim 650$ GeV, translates into bounds on combinations of couplings

$$\left(y_{s1}^2 + y_{s2}^2\right) \alpha_{11}^2 < \mathcal{O}(10^{-14}), \tag{4.38}$$

$$\left(y_{d1}^2 + y_{d2}^2\right) \alpha_{12}^2 < \mathcal{O}(10^{-14}), \tag{4.39}$$

$$\left(y_{d1} y_{s1} + y_{d2} y_{s2}\right) \alpha_{12} \alpha_{11} < \mathcal{O}(10^{-14}), \tag{4.40}$$

although the strong interaction and nuclear physics uncertainty in these bounds spans several orders of magnitude. Neutron oscillations and nucleus decay give much weaker constraints on coefficients of operators containing heavier quarks, as the required loops involve weak interactions and small CKM parameters. See, e.g., Ref. [166] for a summary of such constraints in R-parity–violating supersymmetry.

We also need to check that the new sources of flavor violation will not violate the stringent constraints coming from the agreement between theory and experiment in neutral meson oscillation phenomenology. After integrating out ϕ and the N_i, the interactions in Eq. (4.1) will lead to $\Delta F = 2$ flavor-changing operators.The most stringent constraints come from the neutral kaon oscillations.

The relevant $\Delta S = 2$ Hamiltonian that is generated reads [178]

$$\mathcal{H}_{\phi N_i}^{\Delta S=2} = \sum_{i,j} \frac{y_{di}^* y_{dj} y_{si} y_{sj}^*}{2^9\, 3^3\, \pi^2 m_\phi^2} \bar{d}_R^\alpha \gamma^\mu s_R^\alpha\, \bar{d}_R^\beta \gamma_\mu s_R^\beta, \tag{4.41}$$

where α and β are color indices, and we have assumed that $m_\phi \simeq m_{N_i}$. This contributes to the K^0–$\bar{K}^0$ mass difference,

$$\Delta m_K = 2\mathrm{Re}\langle \bar{K}^0 | \mathcal{H}_{\phi N_i}^{\Delta S=2} | K^0 \rangle \tag{4.42}$$

$$= \mathrm{Re} \sum_{i,j} \frac{y_{di}^* y_{dj} y_{si} y_{sj}^*}{2^8\, 3^4\, \pi^2} \frac{m_K f_K^2}{m_\phi^2}, \tag{4.43}$$

with f_K the kaon decay constant. Requiring that this not exceed the measured mass differ-

ence of $(3.484 \pm 0.006) \times 10^{-12}$ MeV [133] leads to a constraint on the couplings,

$$\left(\mathrm{Re} \sum_{i,j} y^*_{di} y_{dj} y_{si} y^*_{sj} \right)^{1/4} < 0.40 \sqrt{\frac{m_\phi}{650 \text{ GeV}}}, \tag{4.44}$$

where we have used $f_K = 155$ MeV [179, 180]. Since the Yukawa couplings are complex, there is also a contribution to CP-violation in the neutral kaon system. This is typically parameterized by

$$\epsilon_K = \frac{\mathrm{Im} \langle \bar{K}^0 | \mathcal{H}^{\Delta S=2} | K^0 \rangle}{\sqrt{2} \Delta m_K}. \tag{4.45}$$

If we assume that the kaon mass difference is saturated by the SM contribution, then the operator in Eq. (4.41) gives a contribution to CP-violation of

$$\epsilon_K = 14 \left(\frac{650 \text{ GeV}}{m_\phi} \right)^2 \mathrm{Im} \sum_{i,j} y^*_{di} y_{dj} y_{si} y^*_{sj}. \tag{4.46}$$

Requiring that this is less than the measured value, $(2.228 \pm 0.011) \times 10^{-3}$ [133], results in a constraint,

$$\left(\mathrm{Im} \sum_{i,j} y^*_{di} y_{dj} y_{si} y^*_{sj} \right)^{1/4} < 0.11 \sqrt{\frac{m_\phi}{650 \text{ GeV}}}. \tag{4.47}$$

Since we expect that the CP-violating phases of the Yukawa couplings have no reason to be suppressed, the limit from ϵ_K is stronger than the one from Δm_K. However, this constraint does not impact the viability of the model; even $\mathcal{O}(1)$ values of $|y_{si}|$ are allowed so long as $|y_{di}| \lesssim \mathcal{O}(10^{-2})$.

Limits from B^0-$\bar{B}^0$ and B_s-$\bar{B}_s$ mixing are no more constraining than from kaon mixing, and values of $|y_{bi}|$ as large as unity are allowed.

Experimental upper bounds on Electric Dipole Moments (EDMs) place strong constraints on new CP-violating physics. For new CP-violating physics at the weak scale, there may be nonstandard contributions to EDMs at one or two loops, which place constraints on combinations of the new couplings and phases. The relevant constraints on R-parity–violating supersymmetry are summarized in Ref. [166], and on supersymmetric models in general in

Ref. [181]. In our minimal model, which does not include new couplings to leptons or to left handed quarks, and which does not require any new couplings to be large, there are no one loop contributions or large two loop contributions to EDMs and no constraints on the CP-violating phases.

4.3 Cosmology and baryon to entropy ratio

The baryon asymmetry of the Universe is quantified by the ratio of the net baryon number to entropy,

$$\eta_B = \frac{n_B}{s}. \tag{4.48}$$

The most precise determination of this quantity comes from measurements of the CMB that fix the baryon density in units of the critical density, Ω_b, which is related to the baryon-to-entropy ratio via $\eta_B = 3.9 \times 10^{-9} \times \Omega_b h^2$. Planck has measured $\Omega_b h^2 = 0.0221 \pm 0.0003$ [96] which gives $\eta_B = (8.6 \pm 0.1) \times 10^{-11}$.

In the minimal version of the model, the colored scalars can be produced at late times, well after they have frozen out, through N_3 decays. Those produced in decays after the universe has cooled below the QCD hadronization temperature $T_c \simeq 200$ MeV bind immediately to form mesinos and antimesinos. The CP-violating oscillations and decays (to antibaryons and baryons) of the (anti)mesinos give rise to a baryon asymmetry. To quantify this asymmetry, we must first determine the number of N_3 present after the universe has cooled below T_c.

There are two processes which control the number density of N_3: annihilation to quarks and scalars and decay to a scalar and quark. The number density of N_3 at time t is then

$$n_{N_3} = n_{N_3}^{\rm relic} e^{-\Gamma_{N_3} t} \left(\frac{a_{\rm relic}}{a_t} \right)^3. \tag{4.49}$$

Here, $n_{N_3}^{\rm relic}$ and $a_{\rm relic}$ are the number density of N_3 and the scale factor, respectively, at T $\approx$ $T \sim m_{N_3}/20$, and a_t is the scale factor at t. Similarly to N_1 and N_2, we assume that N_3 is close in mass to ϕ, $\Delta m_{\phi N_3} \ll m_\phi, m_{N_3}$. Then its decay rate is given by

$$\Gamma_{N_3} \simeq \sum_{q=d,s,b} \frac{y_{q3}^2}{8\pi} \frac{\Delta m_{\phi N_3}^2}{m_{\Phi_q}}. \tag{4.50}$$

We want an appreciable number of N_3 to survive until $T_c \simeq 200$ MeV which corresponds to a time $t_c \sim 10^{-5}$ s assuming standard thermal history. Our thermal history is not standard since we have N_3 decaying and injecting energy into the plasma competing with the cooling of the plasma due to the expansion of the universe. However, as we show below, that does not drastically affect the time vs. temperature relationship. Therefore, to get a respectable number of N_3 to decay after T_c, producing mesinos, we must have $\Gamma_{N_3} \lesssim 1/t_c \sim 10^{-19}$ GeV. For a splitting $\Delta m_{\phi N_3} \sim \mathcal{O}\,(\mathrm{GeV})$, this requires $y_{q3}^2 \lesssim 10^{-15}(m_{N_3}/\mathrm{TeV})$. Since the N_3 annihilation rate is proportional to y_{q3}^4, Yukawa couplings that are this small mean that the annihilation rate was always much smaller than the expansion rate of the Universe. Hence, assuming reheating happened at a high temperature and the N_3 were in equilibrium with the plasma, $n_{N_3}^{\mathrm{relic}} = (3/4)\, n_\gamma$ where n_γ is evaluated at $T = m_{N_3}/20$ and only the decay rate Γ_{N_3} dictates the N_3 number density for $T < T_c$.

We can determine the baryon-to-entropy ratio by co-evolving the N_3 and radiation energy densities,

$$\frac{d\rho_{\mathrm{rad}}}{dt} = -4H\rho_{\mathrm{rad}} + \Gamma_{N_3} m_{N_3} n_{N_3}, \tag{4.51}$$

$$\frac{d\rho_{N_3}}{dt} = -3H\rho_{N_3} - \Gamma_{N_3} m_{N_3} n_{N_3}, \tag{4.52}$$

along with the baryon (minus antibaryon) number density,

$$\frac{dn_B}{dt} = -3Hn_B + \frac{1}{2} A\, \Gamma_{N_3} \epsilon_B n_{N_3}. \tag{4.53}$$

Equations (4.51) and (4.52) describe the radiation and N_3 energy densities, taking into account the expansion of the universe and the fact that the decays of N_3 heat up the plasma. Equation (4.53) describes the evolution of the net baryon number density, which develops a nonzero value due to CP-violating oscillations of mesinos produced by N_3 decays. The factor of $1/2$ appears due to the definition of ϵ_B in Eq. (4.16) as the baryon asymmetry per mesino-antimesino pair. A counts the fraction of mesino states that undergo CP-violating oscillations. In this work, we focus on the strange mesino since, being an isoscalar, it is not decohered by scattering on the pions present in the plasma after confinement, a possibility

in the case of the down mesino that would complicate the analysis. Thus, we take $A = 1/3$, assuming that equal fractions of up, down, and strange mesinos are formed which should be true to $\sim 30\%$, the level of SU(3) flavor breaking observed elsewhere. It is important to keep in mind that in additon to Eq. (4.53), the net baryon number density is subject to the constraint that $n_B = 0$ for $T < T_c$ since scalars produced above the QCD confinement temperature do not hadronize and therefore do not undergo coherent oscillations.

Instead of solving Eqs. (4.51) to (4.53) exactly, we first use the sudden decay approximation to gain an intuitive understanding of the baryon-to-entropy ratio and to obtain simple analytic relations among the parameters of the model. In this approximation, we consider the comoving N_3 number density to be constant until the time $t_{\rm decay} = 1/\Gamma_{N_3}$, after which it is zero. The N_3 decays dump energy into the plasma[3] and produce scalars that, if the plasma temperature at the time of decay is less than T_c, form mesinos that oscillate and decay on time scales short compared to the expansion of the Universe,[4] creating a net baryon asymmetry. We now describe the evolution of the Universe in the context of this approximation.

At very early times, the Universe's energy density is dominated by radiation, until some time $t_{\rm eq} < t_{\rm decay}$ when the energy density in N_3 (matter) is equal to that in radiation. For times $t_{\rm eq} < t < t_{\rm decay}$, the Universe is matter-dominated. After the decays of N_3 at $t_{\rm decay}$, the Universe is again radiation dominated. The temperature of the plasma at the time of matter-radiation equality, $t_{\rm eq}$, is

$$T_{\rm eq} = \frac{45\zeta\left(3\right)}{2\pi^4 g_*\left(T_i\right)} m_{N_3}, \tag{4.54}$$

with $g_*\left(T_i\right)$ the effective number of relativistic degrees of freedom at a temperature $T_i \sim m_{N_3}$

[3]Note that solving Eqs. (4.51) to (4.53) exactly, as we will do below, shows that the plasma temperature does not actually increase during N_3 decay—rather, its cooling rate slows [182]. For this reason we ignore whether N_3 decays "reheat" the plasma to a temperature above T_c, a possibility that would naively spoil hadronization.

[4]At temperatures below T_c, the ϕ-ϕ^* annihilation cross section becomes large, $\mathcal{O}(\Lambda_{\rm QCD}^2)$ [183]. However, the rate for this process is tiny compared to the oscillation and decay rates since it is suppressed by the small ratio of the N_3 to ϕ decay rates, $\Gamma_{\rm ann} \propto n_\phi \sim n_{N_3}\Gamma_{N_3}/\Gamma_\phi$.

when the universe is very hot and radiation dominated. We will use $g_*(T_i) = 116.25$ which takes into account the SM contributions as well as contributions from ϕ and $N_{1,2}$. The time vs. temperature relationship during radiation domination fixes the time at $T_{\rm eq}$,

$$t_{\rm eq} = \sqrt{\frac{45}{2\pi^2 g_*(T_{\rm eq})}}\frac{M_{\rm Pl}}{T_{\rm eq}^2} \tag{4.55}$$

$$= \left(\frac{2\pi^2}{45}\right)^{3/2}\left[\frac{\pi^2}{\zeta(3)}\right]^2 \frac{g_*^2(T_i)}{g_*^{1/2}(T_{\rm eq})}\frac{M_{\rm Pl}}{m_{N_3}^2}, \tag{4.56}$$

where $M_{\rm Pl} = (8\pi G)^{-1/2} = 2.4 \times 10^{18}$ GeV is the Planck mass and $g_*(T_{\rm eq}) \simeq 70$, for $T_{\rm eq}$ of order a few GeV. After $t_{\rm eq}$, assuming $t \gg t_{\rm eq}$ the N_3 and radiation energy densities evolve according to matter domination,

$$\rho_{\rm rad} = \frac{4M_{\rm Pl}^2}{3}\left(\frac{t_{\rm eq}}{t^4}\right)^{2/3}, \ \rho_{N_3} = \frac{4M_{\rm Pl}^2}{3}\frac{1}{t^2}. \tag{4.57}$$

Defining $\xi \equiv \rho_{N_3}(t = t_{\rm decay}^-)/\rho_{\rm rad}(t = t_{\rm decay}^-)$, where $t_{\rm decay}^-$ indicates an infinitesimal time before decay, we find

$$\xi = \left(\frac{t_{\rm decay}}{t_{\rm eq}}\right)^{2/3} \tag{4.58}$$

$$= \left(\frac{45}{2\pi^2}\right)\left[\frac{\zeta(3)}{\pi^2}\right]^{4/3}\left(\frac{g_*(T_{\rm eq})}{g_*^4(T_i)}\right)^{1/3}\left(\frac{m_{N_3}^2}{M_{\rm Pl}\Gamma_{N_3}}\right)^{2/3}. \tag{4.59}$$

The baryon-to-entropy ratio is

$$\eta_B = \frac{n_B\left(t = t_{\rm decay}^+\right)}{s_{\rm rad}\left(t = t_{\rm decay}^+\right)}, \tag{4.60}$$

where $t_{\rm decay}^+$ denotes an infinitesimal time after decay. The net baryon number density is related to the N_3 number density just before decay,

$$n_B\left(t = t_{\rm decay}^+\right) = n_{N_3}\left(t = t_{\rm decay}^-\right) \times \frac{1}{2} A\,\epsilon_B. \tag{4.61}$$

A and ϵ_B are determined solely by the mesino particle physics and factor out of the cosmo-

logical story. We can write η_B in terms of ξ,

$$\eta_B = \frac{\rho_{\rm rad}\left(t^-_{\rm decay}\right)}{s_{\rm rad}\left(t^+_{\rm decay}\right)}\frac{\xi}{m_{N_3}}\frac{A\epsilon_B}{2} \tag{4.62}$$

$$= \frac{3}{4}\frac{T_{\rm rad}\left(t^-_{\rm decay}\right)}{m_{N_3}}\left[\frac{T_{\rm rad}\left(t^-_{\rm decay}\right)}{T_{\rm rad}\left(t^+_{\rm decay}\right)}\right]^3 \xi\,\frac{A\epsilon_B}{2}. \tag{4.63}$$

The ratio of the temperatures before and after decay can be found by using the conservation of energy,

$$\rho_{\rm rad}\left(t^+_{\rm decay}\right) = \rho_{\rm rad}\left(t^-_{\rm decay}\right) + \rho_{N_3}\left(t^-_{\rm decay}\right) \tag{4.64}$$

$$= \rho_{\rm rad}\left(t^-_{\rm decay}\right)(1+\xi), \tag{4.65}$$

which leads to

$$\eta_B = \frac{3}{4}\frac{T_{\rm rad}\left(t^-_{\rm decay}\right)}{m_{N_3}}\frac{\xi}{(1+\xi)^{3/4}}\frac{A\epsilon_B}{2}. \tag{4.66}$$

We can use the expression for the radiation energy density in Eq. (4.57) to find the temperature of the plasma just before decay, $T_{\rm rad}\left(t^-_{\rm decay}\right) \equiv T_{\rm decay}$,

$$T_{\rm decay} \simeq \frac{2}{\sqrt{3}}\left(\frac{\pi^2}{\zeta(3)}\right)^{1/3}\left[\frac{g_*(T_i)}{g_*(T_{\rm decay})}\right]^{1/4}\left(\frac{M_{\rm Pl}^2\Gamma_{N_3}^2}{m_{N_3}}\right)^{1/3} \tag{4.67}$$

$$\simeq \frac{15\sqrt{3}\zeta(3)}{\pi^4}\frac{1}{g_*(T_i)}\frac{m_{N_3}}{\xi}, \tag{4.68}$$

with $g_*(T_{\rm decay}) = 63.75$ the number of relativistic degrees of freedom at this temperature. We ignore here the decrease the number of degrees of freedom below the QCD confinement temperature since it obscures the physics and is numerically unimportant at the level of accuracy of our estimates. Using this expression, we can express the baryon-to-entropy ratio as

$$\eta_B \simeq \frac{45\sqrt{3}\zeta(3)}{8\pi^4}\frac{1}{g_*(T_i)}\frac{1}{(1+\xi)^{3/4}}A\epsilon_B \tag{4.69}$$

$$= 6.1\times10^{-10}\left(\frac{116.25}{g_*(T_i)}\right)\left(\frac{10}{1+\xi}\right)^{3/4} \tag{4.70}$$

$$\times\left(\frac{A}{1/3}\right)\left(\frac{\epsilon_B}{10^{-5}}\right). \tag{4.71}$$

The factor

$$(1+\xi)^{-3/4} = \left[\frac{T_{\rm rad}\left(t^{-}_{\rm decay}\right)}{T_{\rm rad}\left(t^{+}_{\rm decay}\right)}\right]^{3} \tag{4.72}$$

can be thought of as the entropy dilution of the naive baryon-to-entropy ratio due to the N_3 decays heating the plasma.[5]

For a fixed value of m_{N_3}, there is a minimal amount of entropy dilution, i.e. a minimal value of ξ, that can be found by setting the temperature of the plasma at N_3 decay to be equal to the QCD confinement temperature. Using this value of the entropy dilution determines a lower bound on the asymmetry ϵ_B as a function of m_{N_3} such that a baryon-to-entropy ratio of 9×10^{-11} is possible. We plot this lower bound on ϵ_B in Fig. 4.5, as a function of the scalar mass, taking the splitting between N_3 and ϕ to be $\Delta m_{\phi N_3} = 3$ GeV.

To assess whether we can reasonably achieve a baryon-to-entropy ratio in line with the current experimental value of 8.6×10^{-11}, we also show in Fig. 4.5 the asymmetry ϵ_B as a function of m_ϕ, taking $\Delta m_{\phi N_1} = \Delta m_{\phi N_2} = 1$ GeV, $y_{s1} = y_{s2} = 10^{-2} \gg y_{s3}$, for $\alpha_B = 10^{-4}$, 10^{-5}, and 10^{-6}. We see that there exist ranges of parameter choices that allow for scalars with a mass between 300 GeV and 10 TeV to have an asymmetry above the bound, and therefore to account for the measured value of η_B, depending on the choice of Γ_{N_3}. In principle, masses as large as 10^{6-7} GeV can be compatible with the observed baryon asymmetry but scales this large would require a larger ϵ_B, hence a larger amount of fine-tuning. In addition, testing this model and embedding it in a framework that explains the weak scale, like the supersymmetric SM, could become difficult.

We can check the accuracy of our sudden decay approximation by solving Eqs. (4.51) to (4.53) numerically and determining the resulting baryon-to-entropy ratio. In Fig. 4.6, we show the results of a numerical solution of the evolution equations with $m_{N_3} = 650$ GeV and $\Gamma_{N_3} = 10^{-20}$ GeV. The top panel shows the evolution of the plasma temperature in time. As mentioned above, the plasma is not "heated up" by the decay of the N_3's; instead, it cools

[5] Again, we stress that the plasma does not actually heat up in an exact treatment of Eqs. (4.51) to (4.53). See below.

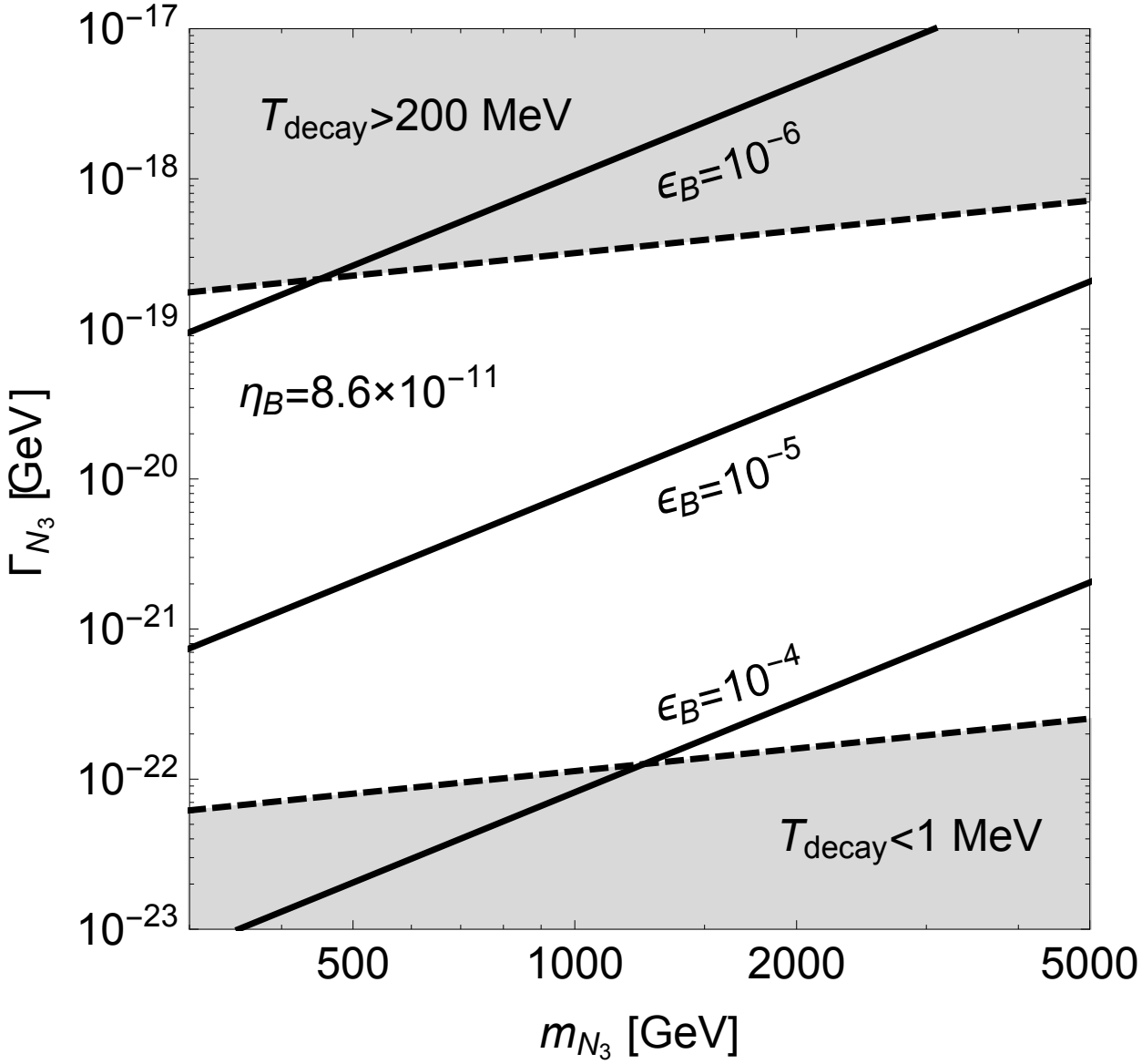

Figure 4.4: Solid lines indicate values of Γ_{N_3} and m_{N_3} that give $\eta_B = 8.6 \times 10^{-11}$ for $\epsilon_B = 10^{-4}, 10^{-5}$, and 10^{-6}, from bottom to top, respectively. The shaded regions lead to a plasma temperature at N_3 decay greater than $T_c \simeq 200$ MeV, in which case mesinos do not form, or a temperature at decay less than 1 MeV, which would spoil BBN. Note that this is calculated within the sudden decay approximation.

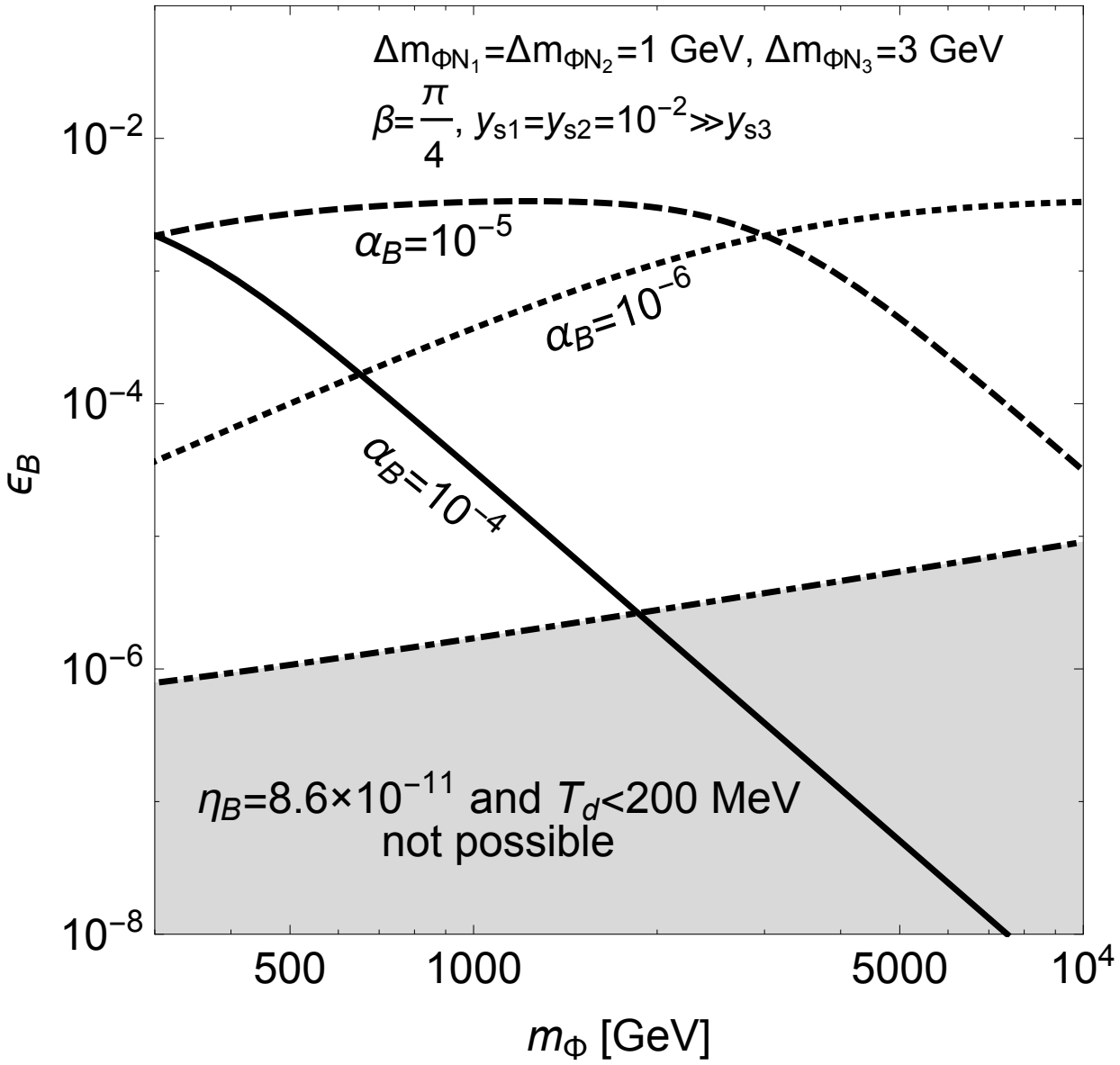

Figure 4.5: The shaded region shows values of ϵ_B and m_ϕ, assuming $\Delta_{\phi N_3} = 3$ GeV, that result in $\eta_B < 8.6 \times 10^{-11}$ for $T_{\rm decay} < T_c \simeq 200$ MeV in the sudden decay approximation. The points above this region can attain the measured value of η_B, depending on the value of Γ_{N_3}. Also shown are the values of ϵ_B when choosing $\Delta_{\phi N_1} = \Delta_{\phi N_2} = 1$ GeV, $y_{s1} = y_{s2} = 10^{-2} \gg y_{s3}$, and $\alpha_B = 10^{-4}$, 10^{-5}, 10^{-6}.

more slowly. The next panel shows the ratio of the N_3 energy density to the radiation energy density, $\rho_{N_3}/\rho_{\rm rad}$, as a function of time. This ratio grows until $\sim 1/\Gamma_{N_3}$ when it decreases to to N_3 decays. The bottom panel shows the net baryon-to-entropy ratio, η_B as it develops from zero at early times to a fixed value at late times for $\epsilon_B = 10^{-4}$, 10^{-5}, and 10^{-6}. We also show the value of η_B calculated for these parameters in the sudden decay approximation. We note that the sudden decay approximation of η_B agrees with the numerical solution of Eqs. (4.51) to (4.53) to within an $\sim \mathcal{O}(1)$ factor for a wide range of values of m_{N_3}, Γ_{N_3}, and ϵ_B. In our numerical solution, we took $g_*(T)$ to be fixed at 63.75 for temperatures less than 4 GeV. Including the change of g_* at the hadronization temperature would not drastically affect our conclusions, and would only obscure the relevant physics.

We note here that the estimate of the baryon asymmetry in this section depended on the assumption that the scalars were produced by the late, out-of-equilibrium decay of a particle that was in thermal equilibrium at very high temperatures. Alternative cosmological histories are certainly possible. For example, the scalars could be produced by the decay of long-lived moduli [116]. Another possibility involves considering a nonthermal parent particle (possibly N_3) that dominates the energy density of the universe. Its decays to scalars reheat the universe and create a baryon asymmetry before the creation of a thermal plasma. Alternative scenarios may, of course, have a quite different relationship between ϵ_B and η_B from the simple one presented here.

4.4 Outlook and Conclusion

We have shown that if there is a scalar quark which lives long enough to hadronize, CP violation in the oscillations of mesinos is possible. If the scalar quark has baryon-number–violating decays, and if it can be produced out of thermal equilibrium in the early universe, such CP violation could be the origin of the matter-antimatter asymmetry of our universe. We presented a mechanism for the out-of-equilibrium production of the scalar quark via the late decays of a very weakly coupled heavy neutral particle, and computed η_B, the ratio of baryon number to entropy, in terms of the relevant parameters of the model. Because η_B

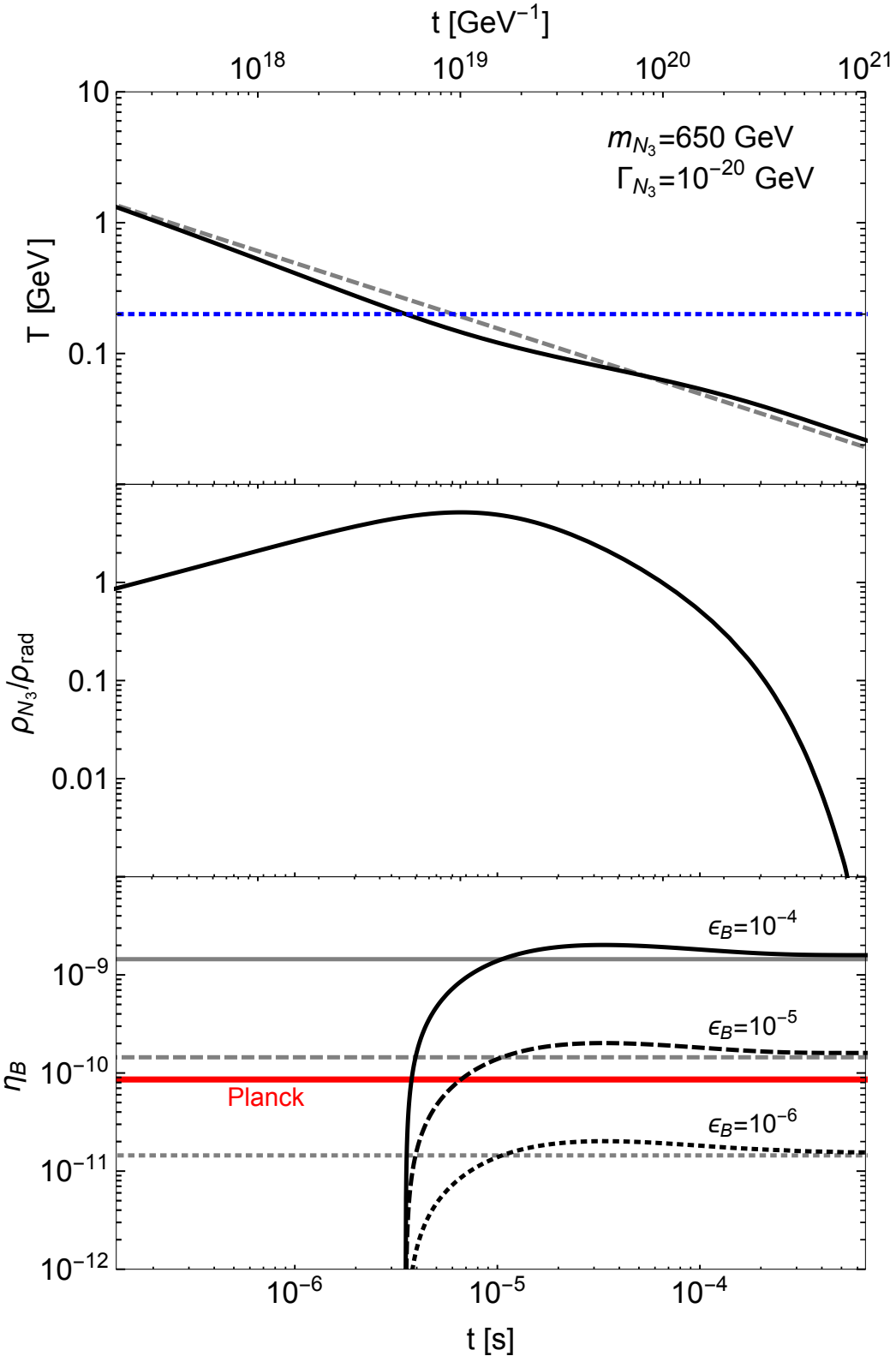
t [GeV^{-1}]
10^{18}
10^{19}
10^{20}
10^{21}
m_{N_3}=650 GeV
Γ_{N_3}=10^{-20} GeV
T [GeV]
10
1
0.1
$\rho_{N_3}/\rho_{\rm rad}$
1
0.1
0.01
ϵ_B=10^{-4}
ϵ_B=10^{-5}
ϵ_B=10^{-6}
Planck
η_B
10^{-9}
10^{-10}
10^{-11}
10^{-12}
10^{-6}
10^{-5}
10^{-4}
t [s]

depends sensitively on the parameters, the viable parameter space of the model is rather well constrained. In particular, obtaining sufficient CP violation requires the existence of a neutral Majorana fermion which is not much lighter than the squark. Such a difficult to explain coincidence hints at an environmental selection principle, which is attractive in light of the observation that the value of η_B in our universe appears to be optimal for creating stars in galaxies which are not so dense as to be unfriendly to advanced life [184].

In order to experimentally test the model one should begin by finding evidence for scalar quarks at the LHC. As discussed in Sec. 4.2.1, existing searches, especially in the case where the decays do not produce significant missing energy, are not very constraining. In our model the squark should decay sometimes into two antiquarks, and sometimes into a quark and a neutral fermion, with the latter decaying into one soft and two hard quarks. The final states are likely to contain at least one third generation quark for the reasons discussed in Sec. 4.2.2. Because successful baryogenesis requires that the neutral fermion not be much lighter than the mesino, the first quark is very soft. Thus the scalar quark should essentially decay into two hard jets (and possibly two very soft quarks). The decays may be prompt or could produce displaced vertices. The LHC reach for the discovery of heavy scalar quarks which decay into jets is projected to reach 1070 GeV [147] with 1000 fb^{-1}. In Ref. [129], Berger, Csaki, Grossman, and Heidenreich proposed looking for same-sign top quarks as evidence for mesino oscillations, assuming that the squark predominantly decays into a top and a strange quark. In our model, same sign tops can be produced without mesino oscillations, as the neutral fermion which is often produced in ϕ decays is equally likely to decay to top and to antitop. Searching for such events containing same sign tops should increase the reach for searching for scalar quarks and significantly constrain the model. Note that this signature will be CP-violating, but the small asymmetry between top and antitop will be too challenging to measure at the LHC.

We also point out that a slight extension to the model would allow for asymmetric dark matter (for a review, see, e.g., [185, 186]) to be incorporated. If the operator mediating ϕ decays to baryons, $\alpha_{ij}\phi^* \bar{d}_i \bar{u}_j$, were modified to the dimension-5 operator $\alpha_{ij}\phi^* \bar{d}_i \bar{u}_j (\chi/M)$

where χ is a complex scalar and M is the relevant scale, the model would possess a $\mathbb{Z}_2$ symmetry under which χ, ϕ, and N_i are odd. This would render χ stable if it were the lightest of these particles. Then the oscillations and decays of the mesinos would produce a χ-χ^* asymmetry along with the baryon-antibaryon asymmetry. The χ mass in this model would be fixed to be ~ 5 GeV since the number densities of dark and baryonic matter would be equal. The signature of ϕ production at a hadron collider would now include missing energy, pushing up the lower bound on the allowed mass.

BIBLIOGRAPHY

[1] David Griffiths. *Introduction to elementary particles.* 2008.

[2] M. Srednicki. *Quantum field theory.* Cambridge University Press, 2007.

[3] Brian C. Odom, D. Hanneke, B. D'Urso, and G. Gabrielse. New Measurement of the Electron Magnetic Moment Using a One-Electron Quantum Cyclotron. *Phys. Rev. Lett.*, 97:030801, 2006. [Erratum: Phys. Rev. Lett.99,039902(2007)].

[4] J. M. Pendlebury et al. Revised experimental upper limit on the electric dipole moment of the neutron. *Phys. Rev.*, D92(9):092003, 2015.

[5] R. D. Peccei and Helen R. Quinn. CP Conservation in the Presence of Instantons. *Phys. Rev. Lett.*, 38:1440–1443, 1977.

[6] Steven Weinberg. A New Light Boson? *Phys. Rev. Lett.*, 40:223–226, 1978.

[7] Jihn E. Kim. Weak Interaction Singlet and Strong CP Invariance. *Phys. Rev. Lett.*, 43:103, 1979.

[8] Pierre Sikivie. Axion Cosmology. *Lect. Notes Phys.*, 741:19–50, 2008. [,19(2006)].

[9] Stephen P. Martin. A Supersymmetry primer. 1997. [Adv. Ser. Direct. High Energy Phys.18,1(1998)].

[10] Nima Arkani-Hamed, Savas Dimopoulos, and G. R. Dvali. The Hierarchy problem and new dimensions at a millimeter. *Phys. Lett.*, B429:263–272, 1998.

[11] Lisa Randall and Raman Sundrum. A Large mass hierarchy from a small extra dimension. *Phys. Rev. Lett.*, 83:3370–3373, 1999.

[12] Lisa Randall and Raman Sundrum. An Alternative to compactification. *Phys. Rev. Lett.*, 83:4690–4693, 1999.

[13] Michael J. Dugan, Howard Georgi, and David B. Kaplan. Anatomy of a Composite Higgs Model. *Nucl. Phys.*, B254:299–326, 1985.

[14] Peter W. Graham, David E. Kaplan, and Surjeet Rajendran. Cosmological Relaxation of the Electroweak Scale. *Phys. Rev. Lett.*, 115(22):221801, 2015.

[15] H. N. Brown et al. Precise measurement of the positive muon anomalous magnetic moment. *Phys. Rev. Lett.*, 86:2227–2231, 2001.

[16] P. A. R. Ade et al. Planck 2015 results. XIII. Cosmological parameters. *Astron. Astrophys.*, 594:A13, 2016.

[17] Scott Dodelson. *Modern Cosmology.* Academic Press, Amsterdam, 2003.

[18] Vera C. Rubin and W. Kent Ford, Jr. Rotation of the Andromeda Nebula from a Spectroscopic Survey of Emission Regions. *Astrophys. J.*, 159:379–403, 1970.

[19] Lam Hui, Jeremiah P. Ostriker, Scott Tremaine, and Edward Witten. Ultralight scalars as cosmological dark matter. *Phys. Rev.*, D95(4):043541, 2017.

[20] Simeon Bird, Ilias Cholis, Julian B. Muñoz, Yacine Ali-Haïmoud, Marc Kamionkowski, Ely D. Kovetz, Alvise Raccanelli, and Adam G. Riess. Did LIGO detect dark matter? *Phys. Rev. Lett.*, 116(20):201301, 2016.

[21] Scott Dodelson and Lawrence M. Widrow. Sterile-neutrinos as dark matter. *Phys. Rev. Lett.*, 72:17–20, 1994.

[22] Xiang-Dong Shi and George M. Fuller. A New dark matter candidate: Nonthermal sterile neutrinos. *Phys. Rev. Lett.*, 82:2832–2835, 1999.

[23] Adam G. Riess et al. Observational evidence from supernovae for an accelerating universe and a cosmological constant. *Astron. J.*, 116:1009–1038, 1998.

[24] S. Perlmutter et al. Measurements of Omega and Lambda from 42 high redshift supernovae. *Astrophys. J.*, 517:565–586, 1999.

[25] Andrei D. Linde. A New Inflationary Universe Scenario: A Possible Solution of the Horizon, Flatness, Homogeneity, Isotropy and Primordial Monopole Problems. *Phys. Lett.*, B108:389–393, 1982.

[26] Steven Weinberg. *Cosmology.* 2008.

[27] M. Fukugita and T. Yanagida. Baryogenesis Without Grand Unification. *Phys. Lett.*, B174:45–47, 1986.

[28] P. A. R. Ade et al. Planck 2015 results. XX. Constraints on inflation. *Astron. Astrophys.*, 594:A20, 2016.

[29] J. Billard, L. Strigari, and E. Figueroa-Feliciano. Implication of neutrino backgrounds on the reach of next generation dark matter direct detection experiments. *Phys. Rev.*, D89(2):023524, 2014.

[30] Max Tegmark et al. Cosmological parameters from SDSS and WMAP. *Phys. Rev.*, D69:103501, 2004.

[31] P. A. R. Ade et al. Planck 2013 results. XX. Cosmology from Sunyaev–Zeldovich cluster counts. *Astron. Astrophys.*, 571:A20, 2014.

[32] Th. A. Mueller et al. Improved Predictions of Reactor Antineutrino Spectra. *Phys. Rev.*, C83:054615, 2011.

[33] Patrick Huber. On the determination of anti-neutrino spectra from nuclear reactors. *Phys. Rev.*, C84:024617, 2011. [Erratum: Phys. Rev.C85,029901(2012)].

[34] Mario A. Acero, Carlo Giunti, and Marco Laveder. Limits on nu(e) and anti-nu(e) disappearance from Gallium and reactor experiments. *Phys. Rev.*, D78:073009, 2008.

[35] Carlo Giunti and Marco Laveder. Statistical Significance of the Gallium Anomaly. *Phys. Rev.*, C83:065504, 2011.

[36] A. Aguilar-Arevalo et al. Evidence for neutrino oscillations from the observation of anti-neutrino(electron) appearance in a anti-neutrino(muon) beam. *Phys. Rev.*, D64:112007, 2001.

[37] A. A. Aguilar-Arevalo et al. Improved Search for $\bar{\nu}_\mu \to \bar{\nu}_e$ Oscillations in the MiniBooNE Experiment. *Phys. Rev. Lett.*, 110:161801, 2013.

[38] Joachim Kopp, Pedro A. N. Machado, Michele Maltoni, and Thomas Schwetz. Sterile Neutrino Oscillations: The Global Picture. *JHEP*, 05:050, 2013.

[39] M. C. Gonzalez-Garcia, Michele Maltoni, and Thomas Schwetz. Global Analyses of Neutrino Oscillation Experiments. *Nucl. Phys.*, B908:199–217, 2016.

[40] M. G. Aartsen et al. Searches for Sterile Neutrinos with the IceCube Detector. *Phys. Rev. Lett.*, 117(7):071801, 2016.

[41] G. H. Collin, C. A. Argüelles, J. M. Conrad, and M. H. Shaevitz. First Constraints on the Complete Neutrino Mixing Matrix with a Sterile Neutrino. 2016.

[42] V. N. Aseev et al. An upper limit on electron antineutrino mass from Troitsk experiment. *Phys. Rev.*, D84:112003, 2011.

[43] R. G. Hamish Robertson. KATRIN: an experiment to determine the neutrino mass from the beta decay of tritium. In *Proceedings, Community Summer Study 2013: Snowmass on the Mississippi (CSS2013): Minneapolis, MN, USA, July 29-August 6, 2013*, 2013.

[44] P. J. Doe et al. Project 8: Determining neutrino mass from tritium beta decay using a frequency-based method. In *Proceedings, Community Summer Study 2013: Snowmass on the Mississippi (CSS2013): Minneapolis, MN, USA, July 29-August 6, 2013*, 2013.

[45] Steven Weinberg. Universal Neutrino Degeneracy. *Phys. Rev.*, 128:1457–1473, 1962.

[46] S. Betts et al. Development of a Relic Neutrino Detection Experiment at PTOLEMY: Princeton Tritium Observatory for Light, Early-Universe, Massive-Neutrino Yield. In *Proceedings, Community Summer Study 2013: Snowmass on the Mississippi (CSS2013): Minneapolis, MN, USA, July 29-August 6, 2013*, 2013.

[47] Andrew J. Long, Cecilia Lunardini, and Eray Sabancilar. Detecting non-relativistic cosmic neutrinos by capture on tritium: phenomenology and physics potential. *JCAP*, 1408:038, 2014.

[48] Maria Archidiacono, Stefano Gariazzo, Carlo Giunti, Steen Hannestad, Rasmus Hansen, Marco Laveder, and Thomas Tram. Pseudoscalar - sterile neutrino interactions: reconciling the cosmos with neutrino oscillations. 2016.

[49] Shaun A. Thomas, Filipe B. Abdalla, and Ofer Lahav. Upper Bound of 0.28eV on the Neutrino Masses from the Largest Photometric Redshift Survey. *Phys. Rev. Lett.*, 105:031301, 2010.

[50] Signe Riemer-Sorensen et al. The WiggleZ Dark Energy Survey: Cosmological neutrino mass constraint from blue high-redshift galaxies. *Phys. Rev.*, D85:081101, 2012.

[51] Gong-Bo Zhao et al. The clustering of galaxies in the SDSS-III Baryon Oscillation Spectroscopic Survey: weighing the neutrino mass using the galaxy power spectrum of the CMASS sample. *Mon. Not. Roy. Astron. Soc.*, 436:2038–2053, 2013.

[52] J. L. Feng et al. Planning the Future of U.S. Particle Physics (Snowmass 2013): Chapter 4: Cosmic Frontier. In *Proceedings, Community Summer Study 2013: Snowmass on the Mississippi (CSS2013): Minneapolis, MN, USA, July 29-August 6, 2013*, 2014.

[53] Steen Hannestad, Rasmus Sloth Hansen, and Thomas Tram. How Self-Interactions can Reconcile Sterile Neutrinos with Cosmology. *Phys. Rev. Lett.*, 112(3):031802, 2014.

[54] Basudeb Dasgupta and Joachim Kopp. Cosmologically Safe eV-Scale Sterile Neutrinos and Improved Dark Matter Structure. *Phys. Rev. Lett.*, 112(3):031803, 2014.

[55] Torsten Bringmann, Jasper Hasenkamp, and Jörn Kersten. Tight bonds between sterile neutrinos and dark matter. *JCAP*, 1407:042, 2014.

[56] Ninetta Saviano, Ofelia Pisanti, Gianpiero Mangano, and Alessandro Mirizzi. Unveiling secret interactions among sterile neutrinos with big-bang nucleosynthesis. *Phys. Rev.*, D90(11):113009, 2014.

[57] Xiaoyong Chu, Basudeb Dasgupta, and Joachim Kopp. Sterile neutrinos with secret interactions?lasting friendship with cosmology. *JCAP*, 1510(10):011, 2015.

[58] John F. Cherry, Alexander Friedland, and Ian M. Shoemaker. Short-baseline neutrino oscillations, Planck, and IceCube. 2016.

[59] Maria Archidiacono, Steen Hannestad, Rasmus Sloth Hansen, and Thomas Tram. Cosmology with self-interacting sterile neutrinos and dark matter - A pseudoscalar model. *Phys. Rev.*, D91(6):065021, 2015.

[60] Zurab G. Berezhiani and Rabindra N. Mohapatra. Reconciling present neutrino puzzles: Sterile neutrinos as mirror neutrinos. *Phys. Rev.*, D52:6607–6611, 1995.

[61] Luca Vecchi. Light sterile neutrinos from a late phase transition. 2016.

[62] Yasaman Farzan and Steen Hannestad. Neutrinos secretly converting to lighter particles to please both KATRIN and the cosmos. *JCAP*, 1602(02):058, 2016.

[63] Rob Fardon, Ann E. Nelson, and Neal Weiner. Dark energy from mass varying neutrinos. *JCAP*, 0410:005, 2004.

[64] Rob Fardon, Ann E. Nelson, and Neal Weiner. Supersymmetric theories of neutrino dark energy. *JHEP*, 03:042, 2006.

[65] K. Enqvist, K. Kainulainen, and Mark J. Thomson. Stringent cosmological bounds on inert neutrino mixing. *Nucl. Phys.*, B373:498–528, 1992.

[66] Riccardo Barbieri and A. Dolgov. Bounds on Sterile-neutrinos from Nucleosynthesis. *Phys. Lett.*, B237:440–445, 1990.

[67] Kimmo Kainulainen. Light Singlet Neutrinos and the Primordial Nucleosynthesis. *Phys. Lett.*, B244:191–195, 1990.

[68] P. Di Bari. Update on neutrino mixing in the early universe. *Phys. Rev.*, D65:043509, 2002.

[69] Kevork N. Abazajian. Telling three from four neutrinos with cosmology. *Astropart. Phys.*, 19:303–312, 2003.

[70] A. D. Dolgov. Neutrinos in cosmology. *Phys. Rept.*, 370:333–535, 2002.

[71] A. D. Dolgov and F. L. Villante. BBN bounds on active sterile neutrino mixing. *Nucl. Phys.*, B679:261–298, 2004.

[72] Marco Cirelli, Guido Marandella, Alessandro Strumia, and Francesco Vissani. Probing oscillations into sterile neutrinos with cosmology, astrophysics and experiments. *Nucl. Phys.*, B708:215–267, 2005.

[73] Scott Dodelson, Alessandro Melchiorri, and Anze Slosar. Is cosmology compatible with sterile neutrinos? *Phys. Rev. Lett.*, 97:041301, 2006.

[74] A. D. Dolgov. Cosmology and Neutrino Properties. *Phys. Atom. Nucl.*, 71:2152–2164, 2008.

[75] Niayesh Afshordi, Matias Zaldarriaga, and Kazunori Kohri. On the stability of dark energy with mass-varying neutrinos. *Phys. Rev.*, D72:065024, 2005.

[76] Sidney R. Coleman. Why There Is Nothing Rather Than Something: A Theory of the Cosmological Constant. *Nucl. Phys.*, B310:643–668, 1988.

[77] Sean M. Carroll, William H. Press, and Edwin L. Turner. The Cosmological constant. *Ann. Rev. Astron. Astrophys.*, 30:499–542, 1992.

[78] Sean M. Carroll. The Cosmological constant. *Living Rev. Rel.*, 4:1, 2001.

[79] T. Padmanabhan. Cosmological constant: The Weight of the vacuum. *Phys. Rept.*, 380:235–320, 2003.

[80] G. J. Stephenson, Jr., J. Terrance Goldman, and B. H. J. McKellar. Neutrino clouds. *Int. J. Mod. Phys.*, A13:2765–2790, 1998.

[81] Christopher Spitzer. Stability in MaVaN Models. 2006.

[82] Akshay Ghalsasi and Ann E. Nelson. Effects of Mass Varying Neutrinos on Cosmological Parameters as determined from the Cosmic Microwave Background. *Phys. Rev.*, D90(4):045002, 2014.

[83] Julien Lesgourgues and Sergio Pastor. Neutrino mass from Cosmology. *Adv. High Energy Phys.*, 2012:608515, 2012.

[84] Ryo Takahashi and Morimitsu Tanimoto. Model of mass varying neutrinos in SUSY. *Phys. Lett.*, B633:675–680, 2006.

[85] Neal Weiner and Kathryn M. Zurek. New matter effects and BBN constraints for mass varying neutrinos. *Phys. Rev.*, D74:023517, 2006.

[86] Alessandro Mirizzi, Gianpiero Mangano, Ofelia Pisanti, and Ninetta Saviano. Collisional production of sterile neutrinos via secret interactions and cosmological implications. *Phys. Rev.*, D91(2):025019, 2015.

[87] E. G. Adelberger, Blayne R. Heckel, and A. E. Nelson. Tests of the gravitational inverse square law. *Ann. Rev. Nucl. Part. Sci.*, 53:77–121, 2003.

[88] David B. Kaplan, Ann E. Nelson, and Neal Weiner. Neutrino oscillations as a probe of dark energy. *Phys. Rev. Lett.*, 93:091801, 2004.

[89] Kathryn M. Zurek. New matter effects in neutrino oscillation experiments. *JHEP*, 10:058, 2004.

[90] Alexander Friedland, Kathryn M. Zurek, and Sergei Bashinsky. Constraining Models of Neutrino Mass and Neutrino Interactions with the Planck Satellite. 2007.

[91] Anders Basboll, Ole Eggers Bjaelde, Steen Hannestad, and Georg G. Raffelt. Are cosmological neutrinos free-streaming? *Phys. Rev.*, D79:043512, 2009.

[92] Tristan L. Smith, Sudeep Das, and Oliver Zahn. Constraints on neutrino and dark radiation interactions using cosmological observations. *Phys. Rev.*, D85:023001, 2012.

[93] Francis-Yan Cyr-Racine and Kris Sigurdson. Limits on Neutrino-Neutrino Scattering in the Early Universe. *Phys. Rev.*, D90(12):123533, 2014.

[94] Maria Archidiacono and Steen Hannestad. Updated constraints on non-standard neutrino interactions from Planck. *JCAP*, 1407:046, 2014.

[95] Shwetabh Singh and Chung-Pei Ma. Neutrino clustering in cold dark matter halos : Implications for ultrahigh-energy cosmic rays. *Phys. Rev.*, D67:023506, 2003.

[96] P. A. R. Ade et al. Planck 2013 results. XVI. Cosmological parameters. *Astron. Astrophys.*, 571:A16, 2014.

[97] A. D. Sakharov. Violation of CP Invariance, c Asymmetry, and Baryon Asymmetry of the Universe. *Pisma Zh. Eksp. Teor. Fiz.*, 5:32–35, 1967. [Usp. Fiz. Nauk161,61(1991)].

[98] V. A. Kuzmin, V. A. Rubakov, and M. E. Shaposhnikov. On the Anomalous Electroweak Baryon Number Nonconservation in the Early Universe. *Phys. Lett.*, B155:36, 1985.

[99] Peter Brockway Arnold and Larry D. McLerran. Sphalerons, Small Fluctuations and Baryon Number Violation in Electroweak Theory. *Phys. Rev.*, D36:581, 1987.

[100] Peter Brockway Arnold and Larry D. McLerran. The Sphaleron Strikes Back. *Phys. Rev.*, D37:1020, 1988.

[101] Peter Brockway Arnold, Dam Son, and Laurence G. Yaffe. The Hot baryon violation rate is O (alpha-w**5 T**4). *Phys. Rev.*, D55:6264–6273, 1997.

[102] Guy D. Moore. Sphaleron rate in the symmetric electroweak phase. *Phys. Rev.*, D62:085011, 2000.

[103] Peter Brockway Arnold and Olivier Espinosa. The Effective potential and first order phase transitions: Beyond leading-order. *Phys. Rev.*, D47:3546, 1993. [Erratum: Phys. Rev.D50,6662(1994)].

[104] Michael Dine, Robert G. Leigh, Patrick Y. Huet, Andrei D. Linde, and Dmitri A. Linde. Towards the theory of the electroweak phase transition. *Phys. Rev.*, D46:550–571, 1992.

[105] W. Buchmuller, Z. Fodor, T. Helbig, and D. Walliser. The weak electroweak phase transition. *Annals Phys.*, 234:260–299, 1994.

[106] K. Farakos, K. Kajantie, K. Rummukainen, and Mikhail E. Shaposhnikov. 3-D physics and the electroweak phase transition: Perturbation theory. *Nucl. Phys.*, B425:67–109, 1994.

[107] K. Kajantie, M. Laine, K. Rummukainen, and Mikhail E. Shaposhnikov. The Electroweak phase transition: A Nonperturbative analysis. *Nucl. Phys.*, B466:189–258, 1996.

[108] F. Csikor, Z. Fodor, and J. Heitger. Endpoint of the hot electroweak phase transition. *Phys. Rev. Lett.*, 82:21–24, 1999.

[109] Heinz Pagels and Joel R. Primack. Supersymmetry, Cosmology and New TeV Physics. *Phys. Rev. Lett.*, 48:223, 1982.

[110] Steven Weinberg. Cosmological Constraints on the Scale of Supersymmetry Breaking. *Phys. Rev. Lett.*, 48:1303, 1982.

[111] John R. Ellis, Dimitri V. Nanopoulos, and M. Quiros. On the Axion, Dilaton, Polonyi, Gravitino and Shadow Matter Problems in Supergravity and Superstring Models. *Phys. Lett.*, B174:176, 1986.

[112] John R. Ellis, G. B. Gelmini, Jorge L. Lopez, Dimitri V. Nanopoulos, and Subir Sarkar. Astrophysical constraints on massive unstable neutral relic particles. *Nucl. Phys.*, B373:399–437, 1992.

[113] T. Moroi, H. Murayama, and Masahiro Yamaguchi. Cosmological constraints on the light stable gravitino. *Phys. Lett.*, B303:289–294, 1993.

[114] Renata Kallosh, Lev Kofman, Andrei D. Linde, and Antoine Van Proeyen. Gravitino production after inflation. *Phys. Rev.*, D61:103503, 2000.

[115] M. Bolz, A. Brandenburg, and W. Buchmuller. Thermal production of gravitinos. *Nucl. Phys.*, B606:518–544, 2001. [Erratum: Nucl. Phys.B790,336(2008)].

[116] Tom Banks, David B. Kaplan, and Ann E. Nelson. Cosmological implications of dynamical supersymmetry breaking. *Phys. Rev.*, D49:779–787, 1994.

[117] Andrei D. Linde. GENERATION OF ISOTHERMAL DENSITY PERTURBATIONS IN THE INFLATIONARY UNIVERSE. *JETP Lett.*, 40:1333–1336, 1984. [Pisma Zh. Eksp. Teor. Fiz.40,496(1984)].

[118] Michael S. Turner. Windows on the Axion. *Phys. Rept.*, 197:67–97, 1990.

[119] Andrei D. Linde. Axions in inflationary cosmology. *Phys. Lett.*, B259:38–47, 1991.

[120] David H. Lyth and Ewan D. Stewart. Constraining the inflationary energy scale from axion cosmology. *Phys. Lett.*, B283:189–193, 1992.

[121] Patrick Fox, Aaron Pierce, and Scott D. Thomas. Probing a QCD string axion with precision cosmological measurements. 2004.

[122] Mark Claudson, Lawrence J. Hall, and Ian Hinchliffe. COSMOLOGICAL BARYON GENERATION AT LOW TEMPERATURES. *Nucl. Phys.*, B241:309, 1984.

[123] Savas Dimopoulos and Lawrence J. Hall. Baryogenesis at the MeV Era. *Phys. Lett.*, B196:135, 1987.

[124] C. Jarlskog. Commutator of the Quark Mass Matrices in the Standard Electroweak Model and a Measure of Maximal CP Violation. *Phys. Rev. Lett.*, 55:1039, 1985.

[125] Glennys R. Farrar and M. E. Shaposhnikov. Baryon asymmetry of the universe in the minimal Standard Model. *Phys. Rev. Lett.*, 70:2833–2836, 1993. [Erratum: Phys. Rev. Lett.71,210(1993)].

[126] M. B. Gavela, P. Hernandez, J. Orloff, and O. Pene. Standard model CP violation and baryon asymmetry. *Mod. Phys. Lett.*, A9:795–810, 1994.

[127] Patrick Huet and Eric Sather. Electroweak baryogenesis and standard model CP violation. *Phys. Rev.*, D51:379–394, 1995.

[128] Uri Sarid and Scott D. Thomas. Mesino - anti-mesino oscillations. *Phys.Rev.Lett.*, 85:1178–1181, 2000.

[129] Joshua Berger, Csaba Csaki, Yuval Grossman, and Ben Heidenreich. Mesino Oscillation in MFV SUSY. *Eur.Phys.J.*, C73(4):2408, 2013.

[130] Seyda Ipek, David McKeen, and Ann E. Nelson. CP Violation in Pseudo-Dirac Fermion Oscillations. *Phys. Rev.*, D90(7):076005, 2014.

[131] Aneesh V. Manohar and Mark B. Wise. Heavy quark physics. *Camb. Monogr. Part. Phys. Nucl. Phys. Cosmol.*, 10:1–191, 2000.

[132] Heechang Na, Chris J. Monahan, Christine T. H. Davies, Ron Horgan, G. Peter Lepage, and Junko Shigemitsu. The B and B_s Meson Decay Constants from Lattice QCD. *Phys. Rev.*, D86:034506, 2012.

[133] K.A. Olive et al. Review of Particle Physics. *Chin.Phys.*, C38:090001, 2014.

[134] Yanou Cui and Brian Shuve. Probing Baryogenesis with Displaced Vertices at the LHC. *JHEP*, 02:049, 2015.

[135] ATLAS Collaboration Public Note. *ATLAS-CONF-2015-026,.*

[136] Serguei Chatrchyan et al. Search for new physics in events with same-sign dileptons and b jets in pp collisions at $\sqrt{s} = 8$ TeV. *JHEP*, 03:037, 2013. [Erratum: JHEP07,041(2013)].

[137] Georges Aad et al. Search for pair-produced massive coloured scalars in four-jet final states with the ATLAS detector in proton-proton collisions at $\sqrt{s} = 7$ TeV. *Eur. Phys. J.*, C73(1):2263, 2013.

[138] W. Beenakker, R. Hopker, M. Spira, and P.M. Zerwas. Squark and gluino production at hadron colliders. *Nucl. Phys. B*, 492:51–103, 1997.

[139] A. Kulesza and L. Motyka. Threshold resummation for squark-antisquark and gluino-pair production at the LHC. *Phys. Rev. Lett.*, 102:111802, 2009.

[140] A. Kulesza and L. Motyka. Soft gluon resummation for the production of gluino-gluino and squark-antisquark pairs at the LHC. *Phys. Rev. D*, 80:095004, 2009.

[141] Wim Beenakker, Silja Brensing, Michael Kramer, Anna Kulesza, Eric Laenen, et al. Soft-gluon resummation for squark and gluino hadroproduction. *JHEP*, 0912:041, 2009.

[142] W. Beenakker, S. Brensing, M.n Kramer, A. Kulesza, E. Laenen, et al. Squark and Gluino Hadroproduction. *Int.J.Mod.Phys.*, A26:2637–2664, 2011.

[143] Vardan Khachatryan et al. Search for pair-produced resonances decaying to jet pairs in proton proton collisions at $\sqrt{s}$=8 TeV. *Phys. Lett.*, B747:98–119, 2015.

[144] Georges Aad et al. Search for pair production of massive particles decaying into three quarks with the ATLAS detector in $\sqrt{s} = 7$ TeV pp collisions at the LHC. *JHEP*, 12:086, 2012.

[145] Georges Aad et al. Search for massive supersymmetric particles decaying to many jets using the ATLAS detector in pp collisions at $\sqrt{s} = 8$ TeV. *Phys. Rev.*, D91(11):112016, 2015.

[146] Serguei Chatrchyan et al. Searches for light- and heavy-flavour three-jet resonances in pp collisions at $\sqrt{s} = 8$ TeV. *Phys. Lett.*, B730:193–214, 2014.

[147] Daniel Duggan, Jared A. Evans, James Hirschauer, Ketino Kaadze, David Kolchmeyer, Amit Lath, and Matthew Walker. Sensitivity of an Upgraded LHC to R-Parity Violating Signatures of the MSSM. 2013.

[148] Pierre Fayet. Supergauge Invariant Extension of the Higgs Mechanism and a Model for the electron and Its Neutrino. *Nucl. Phys.*, B90:104–124, 1975.

[149] D. V. Volkov and V. P. Akulov. Is the Neutrino a Goldstone Particle? *Phys. Lett.*, B46:109–110, 1973.

[150] Lawrence J. Hall and Mahiko Suzuki. Explicit R-Parity Breaking in Supersymmetric Models. *Nucl. Phys.*, B231:419, 1984.

[151] Graham G. Ross and J. W. F. Valle. Supersymmetric Models Without R-Parity. *Phys. Lett.*, B151:375, 1985.

[152] F. Zwirner. Observable Delta B=2 Transitions Without Nucleon Decay in a Minimal Supersymmetric Extension of the Standard Model. *Phys. Lett.*, B132:103–106, 1983.

[153] Riccardo Barbieri and A. Masiero. Supersymmetric Models with Low-Energy Baryon Number Violation. *Nucl. Phys.*, B267:679, 1986.

[154] Sally Dawson. R-Parity Breaking in Supersymmetric Theories. *Nucl. Phys.*, B261:297, 1985.

[155] Savas Dimopoulos and Lawrence J. Hall. Lepton and Baryon Number Violating Collider Signatures from Supersymmetry. *Phys. Lett.*, B207:210, 1988.

[156] Linda M. Carpenter, David E. Kaplan, and Eun-Jung Rhee. Reduced fine-tuning in supersymmetry with R-parity violation. *Phys. Rev. Lett.*, 99:211801, 2007.

[157] Jared A. Evans and Yevgeny Kats. LHC Coverage of RPV MSSM with Light Stops. *JHEP*, 04:028, 2013.

[158] Christopher Brust, Andrey Katz, Scott Lawrence, and Raman Sundrum. SUSY, the Third Generation and the LHC. *JHEP*, 03:103, 2012.

[159] Gian Francesco Giudice, Ben Gripaios, and Raman Sundrum. Flavourful Production at Hadron Colliders. *JHEP*, 08:055, 2011.

[160] Csaba Csaki, Yuval Grossman, and Ben Heidenreich. MFV SUSY: A Natural Theory for R-Parity Violation. *Phys. Rev.*, D85:095009, 2012.

[161] Yang Bai, Andrey Katz, and Brock Tweedie. Pulling Out All the Stops: Searching for RPV SUSY with Stop-Jets. *JHEP*, 01:040, 2014.

[162] B. C. Allanach and S. A. Renner. Large Hadron Collider constraints on a light baryon number violating sbottom coupling to a top and a light quark. *Eur. Phys. J.*, C74(1):2707, 2014.

[163] John R. Ellis, G. Gelmini, C. Jarlskog, Graham G. Ross, and J. W. F. Valle. Phenomenology of Supersymmetry with Broken R-Parity. *Phys. Lett.*, B150:142, 1985.

[164] Vernon D. Barger, G. F. Giudice, and Tao Han. Some New Aspects of Supersymmetry R-Parity Violating Interactions. *Phys. Rev.*, D40:2987, 1989.

[165] J. L. Goity and Marc Sher. Bounds on $\Delta B = 1$ couplings in the supersymmetric standard model. *Phys. Lett.*, B346:69–74, 1995. [Erratum: Phys. Lett.B385,500(1996)].

[166] R. Barbier et al. R-parity violating supersymmetry. *Phys. Rept.*, 420:1–202, 2005.

[167] Tzee-Ke Kuo and S. T. Love. Neutron Oscillations and the Existence of Massive Neutral Leptons. *Phys. Rev. Lett.*, 45:93, 1980.

[168] Sumathi Rao and Robert Shrock. $n \leftrightarrow \bar{n}$ Transition Operators and Their Matrix Elements in the MIT Bag Model. *Phys. Lett.*, B116:238, 1982.

[169] A. D. Dolgov and F. R. Urban. Baryogenesis by R-parity violating top quark decays and neutron-antineutron oscillations. *Nucl. Phys.*, B752:297–315, 2006.

[170] K. Babu et al. Neutron-Antineutron Oscillations: A Snowmass 2013 White Paper. 2013.

[171] M. Ozer. NEUTRON ANTI-NEUTRON OSCILLATIONS AND RENORMALIZATION EFFECTS FOR DELTA B = 2 SIX QUARK OPERATORS. *Phys. Rev.*, D26:3159–3166, 1982.

[172] K. Abe et al. The Search for $n - \bar{n}$ oscillation in Super-Kamiokande I. *Phys. Rev.*, D91:072006, 2015.

[173] Michael I. Buchoff, Chris Schroeder, and Joseph Wasem. Neutron-antineutron oscillations on the lattice. *PoS*, LATTICE2012:128, 2012.

[174] D. G. Phillips, II et al. Neutron-Antineutron Oscillations: Theoretical Status and Experimental Prospects. *Submitted to: Phys. Rept.*, 2014.

[175] Michael I. Buchoff and Michael Wagman. Neutron-Antineutron Operator Renormalization. *PoS*, LATTICE2014:290, 2015.

[176] Michael I. Buchoff and Michael Wagman. Perturbative Renormalization of Neutron-Antineutron Operators. 2015.

[177] M. Litos et al. Search for Dinucleon Decay into Kaons in Super-Kamiokande. *Phys. Rev. Lett.*, 112(13):131803, 2014.

[178] F. Gabbiani, E. Gabrielli, A. Masiero, and L. Silvestrini. A Complete analysis of FCNC and CP constraints in general SUSY extensions of the standard model. *Nucl.Phys.*, B477:321–352, 1996.

[179] S. Durr, Z. Fodor, C. Hoelbling, S.D. Katz, S. Krieg, et al. The ratio FK/Fpi in QCD. *Phys.Rev.*, D81:054507, 2010.

[180] E. Follana, C.T.H. Davies, G.P. Lepage, and J. Shigemitsu. High Precision determination of the pi, K, D and D(s) decay constants from lattice QCD. *Phys.Rev.Lett.*, 100:062002, 2008.

[181] Maxim Pospelov and Adam Ritz. Electric dipole moments as probes of new physics. *Annals Phys.*, 318:119–169, 2005.

[182] Robert J. Scherrer and Michael S. Turner. Decaying Particles Do Not Heat Up the Universe. *Phys. Rev.*, D31:681, 1985.

[183] Junhai Kang, Markus A. Luty, and Salah Nasri. The Relic abundance of long-lived heavy colored particles. *JHEP*, 0809:086, 2008.

[184] Max Tegmark, Anthony Aguirre, Martin Rees, and Frank Wilczek. Dimensionless constants, cosmology and other dark matters. *Phys. Rev.*, D73:023505, 2006.

[185] Kalliopi Petraki and Raymond R. Volkas. Review of asymmetric dark matter. *Int. J. Mod. Phys.*, A28:1330028, 2013.

[186] Kathryn M. Zurek. Asymmetric Dark Matter: Theories, Signatures, and Constraints. *Phys. Rept.*, 537:91–121, 2014.

[187] T. S. van Albada, J. N. Bahcall, K. Begeman, and R. Sancisi. Distribution of dark matter in the spiral galaxy NGC 3198. *Astrophys. J.*, 295:305–313, August 1985.

[188] V. L. Chernyak and A. R. Zhitnitsky. Asymptotic Behavior of Exclusive Processes in QCD. *Phys. Rept.*, 112:173, 1984.

Appendix A

INSTABILITY IN MAVANS

As pointed out in Ref. [75], there is a inherent instability in the neutrino-acceleron fluid when the neutrinos go nonrelativistic. The end result of the instability is that the neutrinos condense to form "neutrino nuggets" which then redshift like matter. To see this easily, one can treat the neutrino-acceleron fluid hydrodynamically. Let us do an illustrative back of the envelope calculation to demonstrate the instability. The accurate result from the full Boltzmann calculation is given by A.4.

To simply illustrate the instability, let us first assume that there is just one light neutrino and that its mass is inversely proportional to the scalar field, $m \propto 1/A$. We will generalize to the case of more than one active neutrino flavor and other functional forms for the light neutrino mass below. When the neutrinos are nonrelativistic, the effective potential from Eqs. (2.2) and (2.3) is

$$V(A,T) = \Lambda^4 \log\left|\frac{\sigma'}{m}\right| + m\, n_\nu, \tag{A.1}$$

where σ' is a scale and n_ν is the light neutrino number density. Minimizing this potential with respect to A gives

$$n_\nu = -\frac{\partial V_0}{\partial m} \simeq \frac{\Lambda^4}{m}, \tag{A.2}$$

so that the light neutrino energy density is roughly constant, $\rho_\nu \simeq m\, n_\nu \simeq \Lambda^4$.

Now we calculate the speed of sound of the neutrino-acceleron fluid. The fluid's pressure is $P = -\rho_a + w_\nu \rho_\nu$ where $\rho_a = V_0$ is the energy density stored in the acceleron field and w_ν is the neutrino's equation of state parameter. Since the neutrino is nonrelativistic, $w_\nu \simeq 0$. The energy density of the fluid is given by $\rho = \rho_\nu + \rho_a$. The speed of sound is related to the

rate of change of the pressure and energy density,

$$c_s^2 = \frac{\dot{P}}{\dot{\rho}} \simeq -\frac{\dot{\rho_a}}{\dot{\rho_a}} = -1, \tag{A.3}$$

where we have used the fact that ρ_ν is approximately constant. Because density perturbations evolve in time as $e^{-ic_s t}$, an imaginary component to c_s signals an instability, and we see that the neutrino-acceleron fluid is unstable when the neutrinos are nonrelativistic.

A more sophisticated picture can be obtained from a kinetic theory treatment where the speed of sound is determined by [75]

$$\begin{aligned} c_s^2 = \frac{1}{m}\frac{\partial V_0}{\partial m}\left(\frac{\partial^2 V_0}{\partial m^2}\right)^{-1} \times \\ \left[1 + \frac{\langle p^2 \rangle}{T^2}\left(c_s^2 + c_s^{-2} - 2\right)\left(\frac{T}{m}\right)^2 + O\left(\frac{T}{m}\right)^4\right]. \end{aligned} \tag{A.4}$$

Again, the fluid becomes unstable when the speed of sound, as found by this relationship, develops an imaginary component. Below, we use this expression to determine the temperature at which the neutrino-acceleron fluid becomes unstable for the scenarios considered in §§ 2.2.3 and 2.3.

In § 2.2.3 the heavier, mostly active neutrinos $\hat{\nu}_1$ and $\hat{\nu}_2$ get contributions to their masses from the active Majorana mass μ which are independent of acceleron vev as well as contributions that depend on the acceleron vev. Taking $m_1 \simeq m_2 \equiv m$, we rewrite the logarithmic part of the acceleron potential in terms of the neutrino mass as

$$V(A,T) = V_0 + m\, n_\nu = \Lambda^4 \log\left|\frac{\mu_0}{m+\mu}\right| + m\, n_\nu. \tag{A.5}$$

Here, n_ν is the sum of the number densities of the two nearly degenerate neutrinos $\hat{\nu}_{1,2}$. This gives

$$\frac{1}{m}\frac{\partial V_0}{\partial m}\left(\frac{\partial^2 V_0}{\partial m^2}\right)^{-1} = -\frac{1}{m}\frac{\bar{m}_{1,2}^2}{\kappa_{1,2} A}. \tag{A.6}$$

Minimizing the effective potential implies that

$$\frac{\bar{m}_{1,2}^2}{\kappa_{1,2} A} \simeq \frac{2\pi^2}{3\zeta(3)}\frac{\Lambda^4}{T^3}. \tag{A.7}$$

Λ is determined by the present-day mass of the lightest neutrino and temperature, $\Lambda^4 = m_3^2(T_0)\,T_0^2/12$ and we can approximate m with $|\mu|$. Thus, we can write Eq. (A.4) as

$$\begin{aligned} c_s^2 &= -\frac{\pi^2}{18\zeta(3)}\frac{m_3^2(T_0)\,T_0^2}{|\mu|\,T^3}\times \\ &\quad\left[1+12.9\left(c_s^2+c_s^{-2}-2\right)\left(\frac{T}{m}\right)^2+O\left(\frac{T}{m}\right)^4\right] \\ &= -0.23\times\frac{m_3^2(T_0)\,T_0^2}{|\mu|^4}\left(\frac{m}{T}\right)^3\times \\ &\quad\left[1+12.9\left(c_s^2+c_s^{-2}-2\right)\left(\frac{T}{m}\right)^2+O\left(\frac{T}{m}\right)^4\right]. \end{aligned} \tag{A.8}$$

For the parameter values specified in § 2.2.3 we get the temperature at which the nuggets are formed to be $T \simeq 2\times 10^{-4}$ eV.

A similar calculation can be done for the scenario described in § 2.3. In that case there is no active Majorana mass and

$$\frac{1}{m}\frac{\partial V_0}{\partial m}\left(\frac{\partial^2 V_0}{\partial m^2}\right)^{-1} = -1. \tag{A.9}$$

As before, Eq. (A.4) can then be solved to determine when nuggets form. We find that this occurs at the temperature $T \simeq m/10$.

Appendix B

FORM FACTOR ESTIMATION

In this appendix, we detail our estimation of the mesino-meson transition form factor which enters the two-body contribution to $\mathbf{\Gamma}_{12}$. We specialize to the $\Phi_s \to \eta N_1$ case that we considered above.

We begin by expressing the form factor using an operator product expansion (see, e.g., Ref. [188] for a description of the formalism),

$$F\left(q^2\right) = \int \overline{dx}\,\overline{dy}\,\langle \eta\left(p'\right)|\bar{s}^i_\alpha s^k_\gamma|0\rangle C^{ijkl}_{\alpha\beta\gamma\delta}\langle 0|\phi^j \bar{s}^l_\delta|\Phi_{s\beta}\left(p\right)\rangle. \tag{B.1}$$

p is the mesino momentum and $p' = p + q$ is the meson momentum—a transition involving an on-shell N_1 has $q^2 = m^2_{n_1}$. $C^{ijkl}_{\alpha\beta\gamma\delta}$ is the short-distance Wilson coefficient calculated perturbatively. Greek subscripts are Lorentz indices and Latin superscripts are color indices. We use the shorthand $\int \overline{dx} = \int_0^1 dx_1 \int_0^1 dx_2 \delta(1 - x_1 - x_2)$ and similarly for $\overline{dy}$. x_1 is the momentum fraction of the squark in the mesino and x_2 is that of the light quark. $y_{1,2}$ are the momentum fractions of the quark and antiquark in the meson. We expand the bilinear operators in terms of operators of definite quantum numbers using the meson and mesino momentum distributions,[1]

$$\langle \eta\left(p'\right)|\bar{s}^i_\alpha s^k_\gamma|0\rangle = \frac{\delta^{ik}}{N_c}\left(-\frac{1}{4}\right)\left(\not{p}'\gamma^5\right)_{\alpha\gamma}\phi^*_\eta\left(y_1, y_2\right) + \ldots, \tag{B.2}$$

$$\langle 0|\phi^j \bar{s}^l_\delta|\Phi_{s\beta}\left(p\right)\rangle = \frac{\delta^{jl}}{N_c}\delta_{\beta\delta}\phi_{\Phi_s}\left(x_1, x_2\right) + \ldots\ , \tag{B.3}$$

where the distribution amplitudes ϕ_η and ϕ_{Φ_s} are normalized so that

$$\int \overline{dy}\phi_\eta\left(y_1, y_2\right) = f_\eta, \quad \int \overline{dx}\phi_{\Phi_s}\left(x_1, x_2\right) = f_{\Phi_s}, \tag{B.4}$$

[1] We ignore the $u\bar{u}$ and $d\bar{d}$ quark components of η, an approximation that is valid given the overall uncertainty of the calculation.

Figure B.1: Leading diagrams responsible for the $\Phi_s \to \eta N_1$ transition. Dashed lines are ϕ lines and solid lines are s or $\bar{s}$ lines. Curly lines are gluons. Shaded dots represent the ϕ-s-N_1 coupling.

where f_η and f_{Φ_s} are the meson and mesino decay constants.

At leading order there are two diagrams that contribute to the Wilson coefficient, shown in Fig. B.1, which give

$$C^{ijkl}_{\alpha\beta\gamma\delta} = (ig_s)^2 \left(-\frac{i}{k^2}\right) (\gamma_\rho)_{\gamma\delta} (t^a)^{ij} (t^a)^{kl} \times \left[\gamma^\rho \frac{i \not{\Delta}_1}{\Delta_1^2} P_L - \frac{i (x_1 p + \Delta_2)^\rho}{\Delta_2^2 - m_\phi^2} P_L\right]_{\alpha\beta}. \tag{B.5}$$

$\Delta_1 = p' - x_2 p$ and $\Delta_2 = p - y_2 p'$ are the momenta of the virtual quark and squark in the two diagrams and k is the gluon momentum. Using these, the form factor becomes

$$F\left(q^2\right) = \pi \alpha_s \frac{\mathrm{tr}\left(t^a t^a\right)}{N_c^2} \times \int \overline{dx}\, \overline{dy}\, \phi_M\left(x_1, x_2\right) \phi_P^*\left(y_1, y_2\right) \frac{\tilde{C}}{k^2}, \tag{B.6}$$

with

$$\tilde{C} = \frac{1}{\Delta_1^2} \mathrm{Tr}\left(\not{p}' \gamma^5 \gamma^\rho \not{\Delta}_1 P_L \gamma_\rho\right) - \frac{1}{\Delta_2^2 - m_\phi^2} \mathrm{Tr}\left(\not{p}' \gamma^5 P_L \left(x_1 \not{p} + \not{\Delta}_1\right)\right) \tag{B.7}$$

$$= \frac{4 p' \cdot \Delta_1}{\Delta_1^2} + \frac{2 p' \cdot (x_1 p + \Delta_1)}{\Delta_2^2 - m_\phi^2}. \tag{B.8}$$

We will use simple forms for the distribution functions,

$$\phi_\eta\left(y_1, y_2\right) = 6 f_\eta\, y_1 y_2, \tag{B.9}$$

$$\phi_{\Phi_s}\left(x_1, x_2\right) = f_{\Phi_s}\delta\left(x_2 - \frac{\Lambda_{\rm QCD}}{m_{\Phi_s}}\right). \tag{B.10}$$

where $\Lambda_{\rm QCD} \sim 300$ MeV is the QCD scale. The meson distribution function is motivated by the requirement that the quark and antiquark momentum distributions be symmetric—it can also be shown to be the asymptotic meson distribution amplitude. The mesino distribution function encodes the fact that the light quark carries a momentum fraction m_q/m_{Φ_s} where $m_q \sim \Lambda_{\rm QCD}$ is a constituent quark mass.

Integrating over the mesino momentum distribution takes

$$\frac{4p'\cdot\Delta_1}{\Delta_1^2} \to -2 + \mathcal{O}\left(\frac{\Lambda_{\rm QCD}}{m_{\Phi_s}}\right), \tag{B.11}$$

$$\begin{aligned}\frac{2p'\cdot\left(x_1 p + \Delta_1\right)}{\Delta_2^2 - m_\phi^2} \to{}& \frac{m_{\Phi_s}^2 - q^2}{m_{\Phi_s}^2 - m_\phi^2 - y_2\left(m_{\Phi_s}^2 - q^2\right)} \\ &+ \mathcal{O}\left(\frac{\Lambda_{\rm QCD}}{m_{\Phi_s}}\right),\end{aligned} \tag{B.12}$$

and

$$k^2 \simeq -\Lambda_{\rm QCD} m_{\Phi_s} y_2\left(1 - \frac{q^2}{m_{\Phi_s}^2}\right) + \mathcal{O}\left(\frac{\Lambda^2}{m_{\Phi_s}^2}\right). \tag{B.13}$$

Because of the factor of $1/k^2$ in the Wilson coefficient, the form factor is enhanced in the region where q^2 approaches $m_{\Phi_s}^2$ giving the form factor a $1/\left(m_{\Phi_s}^2 - q^2\right)$ scaling. After integrating over the meson momentum distribution, (B.12) gives a logarithmic correction to the scaling which we can ignore. We therefore take $\tilde{C} \simeq -2$, finding

$$F\left(q^2\right) \simeq \frac{3\left(N_c^2 - 1\right)}{N_c^2}\pi\alpha_s \frac{f_\eta f_{\Phi_s}}{\Lambda_{\rm QCD} m_{\Phi_s}} \frac{1}{1 - q^2/m_{\Phi_s}^2} \tag{B.14}$$

$$= \frac{8\pi\alpha_s}{3}\frac{f_\eta f_{\Phi_s}}{\Lambda_{\rm QCD} m_{\Phi_s}} \frac{1}{1 - q^2/m_{\Phi_s}^2}. \tag{B.15}$$

Using $\alpha_s \simeq 0.3$, appropriate for the mass splitting between Φ_s and N_1 of ~ 1 GeV that we have in mind, $\Lambda_{\rm QCD} \simeq 300$ MeV, a value of the η decay constant derived from the $\eta \to \gamma\gamma$

rate ($f_\eta = 130$ MeV), and the mesino decay constant from Eq. (4.21), this gives, for the production of a physical N_1,

$$F\left(m_{N_1}^2\right) \simeq 1.2 \times 10^{-2} \sqrt{\frac{650 \text{ GeV}}{m_{\Phi_s}}} \left(\frac{1 \text{ GeV}}{\Delta m_{\Phi N_1}}\right). \tag{B.16}$$

Being an estimate of an exclusive process in QCD, this calculation has considerable uncertainty, and represents the largest contribution to the overall uncertainty in our estimate of the baryon-to-entropy ratio. However, it captures the essential physics: this rate is enhanced when the singlet mass is close to the mass of the mesino. This is because the quark produced in the $\phi \to N_1 s$ splitting has a smaller momentum in this regime, allowing it to more easily bind with the spectator quark to form a meson. Similar behavior is observed in the B meson system, where the semileptonic transition form factor in $B \to \pi \ell \nu$ decays grows as the $\ell\nu$ mass approaches m_B.

Note that the overall normalization of the form factor, for a fixed $|\mathbf{\Gamma}_{12}|$, is degenerate with the value of $|y_{s1}|$.

VITA

Akshay Ghalsasi was born in Mumbai, India and raised in the city of Pune which is about 150 km east of Mumbai. He finished his high school in 2007.

In August 2007 he moved to University of Illinois Urbana-Champaign to pursue his undergraduate degree in physics. He graduated magna cum laude in 2011 from University of Illinois. The same year he came to University of Washington Seattle to pursue graduate studies in physics. He finished his graduate studies in 2017 which are the subject of this thesis.